ΕΘΝΙΚΟ ΜΕΤΣΟΒΙΟ ΠΟΛΥΤΕΧΝΕΙΟ

Εργαστήριο Ατμοκινητήρων & Λεβήτων

Τομέας Θερμότητας της Σχολής Μηχανολόγων Μηχανικών

ΔΙΠΛΩΜΑΤΙΚΗ ΕΡΓΑΣΙΑ

Αξιολόγηση συναρτήσεων μεταφοράς θερμότητας και πτώσης πίεσης σε πλακοειδείς εναλλάκτες

Assessment of heat transfer and pressure drop correlations for plate heat exchangers

Του Φοιτητή

Φώσκολου Χαρίλαου

Επιβλέπων

Καρέλλας Σωτήριος, Αναπληρωτής Καθηγητής,

Σχολή Μηχανολόγων Μηχανικών, ΕΜΠ

Αθήνα, Ιούλιος 2019

Abstract

Heat exchangers are one of the most common components in power, heating and cooling applications. Large share in the heat exchangers market is occupied by plate heat exchangers thanks to their relative low cost and high heat transfer coefficient. Hence, the accurate design of the plate heat exchangers is of crucial importance. This study focused on the review for specific case studies of the proposed heat transfer and pressure drop correlations for evaporation, condensation and single phase flow. As expected, the results of the analysis revealed that there is a huge deviation among the proposed in literature correlations on both the heat transfer and the pressure drop estimation, with a number of correlations failing to provide realistic results when extrapolated either in terms of the working range or the considered working fluid. The key outcome of this study is a detailed mapping of the most well-known correlations in comparison to each other for various working fluids and working conditions, to allow a reader to choose the proper correlation for each respective case study.

Περίληψη

Οι εναλλάκτες θερμότητας αποτελούν τις πιο ευρέως χρησιμοποιούμενες συσκευές σε συστήματα παραγωγής ηλεκτρισμού, θερμότητας και ψύξης. Μεγάλο κομμάτι της αγοράς εναλλακτών θερμότητας καταλαμβάνουν οι πλακοειδείς εναλλάκτες λόγω του σχετικά χαμηλού τους κόστους και του μεγάλου συντελεστή μεταφοράς θερμότητας. Ως εκ τούτου, ο προσεκτικός και ακριβής σχεδιασμός των πλακοειδών εναλλακτών θερμότητας είναι μείζονος σημασίας. Η συγκεκριμένη μελέτη εστιάζει στην διερεύνηση, για ένα πλήθος σεναρίων λειτουργίας, των προτεινόμενων στη βιβλιογραφία εμπειρικών σχέσεων μεταφοράς θερμότητας και πτώσης πίεσης για ροή που ατμοποιείται, ροή που υφίσταται συμπύκνωση και μονοφασική ροή. Όπως αναμενόταν, τα αποτελέσματα της ανάλυσης αναδεικνύουν μεγάλες αποκλίσεις ανάμεσα στις προτεινόμενες σχέσεις τόσο για τη μεταφορά θερμότητας όσο και για την πτώση πίεσης, με ορισμένες εξισώσεις να αδυνατούν να εμφανίσουν έστω ρεαλιστικά αποτελέσματα σε σενάρια εκτός του πεδίου ορισμού τους ή/και για διαφορετικό από το εργαζόμενο μέσο με το οποίο αναπτύχθηκαν. Βασικό αποτέλεσμα της παρούσας μελέτης είναι η λεπτομερής χαρτογράφηση των προβλέψεων των κυριότερων σχέσεων μεταφοράς θερμότητας και πτώσης πίεσης και η σύγκριση μεταξύ τους για έναν αριθμό διαφορετικών εργαζόμενων μέσων και συνθηκών λειτουργίας, που θα επιτρέψει στον αναγνώστη να εκλέξει την κατάλληλη σχέση ανάλογα με την περίπτωση που μελετά.

Preface

I would like to thank my supervisor, Assistant Proffessor Dr. Sotirios Karellas and PhD Candidate Mr. Tryfonas Roumpedakis for their involvement and assistance throughout the completion of my thesis. I would also like to thank my mother and my brother, as well as my whole family and friends, for their support and their inspiration throughout my studies.

Table of Contents

List of Figures

List of Tables

Nomenclature

A	*Surface*	$[m^2]$
a	*Heat transfer coefficient*	$[W\ m^{-2}K^{-1}]$
A_p	*Heat transfer surface with corrugation*	$[m^2]$
a_{pl}	*Plate amplitude*	$[m]$
A_{ref}	*Heat transfer surface without corrugation*	$[m^2]$
Bd	*Bond number*	-
Bo	*Boiling number*	-
B_p	*Horizontal plate length*	$[m]$
Co	*Convection number*	-
c_p	*Specific heat capacity*	$[J\ kg^{-1}\ K^{-1}]$
D_h	*Hydraulic diameter*	$[m]$
D_p	*Port diameter*	$[m]$
F	*Radiation emission properties constant*	-
f	*Friction number*	-
Fr	*Froude number*	-
G	*Mass velocity*	$[kg\ m^{-2}\ s^{-1}]$
g	*Gravity constant*	$[m\ s^{-2}]$
Ga	*Galileo number*	-
h	*Convective heat transfer coefficient*	$[W\ m^{-2}]$
h_{fg}	*Latent heat of vaporization*	$[J\ kg^{-1}]$
j	*Heat transfer coefficients in Wanniarachchi correlation*	$[W\ m^{-2}\ K^{-1}]$
Ja	*Jacob number*	-
k	*Thermal conductivity coefficient*	$[W\ m^{-1}]$
L_p	*Vertical plate length*	$[m]$
M	*Molecular number*	-
$\dot{m}$	*Mass flowrate*	$[kg\ s^{-1}]$
N_{cp}	*Number of channels per pass in plate heat exchanger*	-
N_p	*Number of passes in plate heat exchanger*	-
Nu	*Nusselt number*	-
p	*Pressure*	$[bar]$
Pr	*Prandtl number*	-
Q	*Heat transfer rate*	$[W]$
q_{flux}	*Heat flux*	$[W\ m^{-2}]$
Re	*Reynolds number*	-
R_f	*Fouling resistance*	$[K\ m^2\ W^{-1}]$
T	*Temperature*	$[K]$
t_{plate}	*Plate thickness*	$[m]$
U	*Overall heat transfer coefficient*	$[W\ m^{-2}]$

v	Velocity	$[m\ s^{-1}]$
We	*Webber number*	-
x	*Quality*	-
X_{tt}	*Lockhart–Martinelli parameter*	-
X_{vv}	*Lockhart–Martinelli parameter*	-

Greek symbols

β	*Chevron angle*	$[°]$
γ	*Latent heat of vaporization*	$[Jkg^{-1}]$
δ	*Surface roughness*	$[m]$
Δh_{LG}	*Latent heat of vaporization*	$[Jkg^{-1}]$
Δp	*Pressure loss*	$[bar]$
ΔT_{lm}	*Logarithmic mean temperature*	$[K]$
ε	*Arithmetic mean roughness*	$[\mu m]$
Λ	*Corrugation pitch*	$[m]$
λ	*Thermal conductivity*	$[W\ m^{-1}\ K^{-1}]$
μ	*Dynamic viscosity*	$[kg\ m^{-1}\ s^{-1}]$
ξ	*Darcy friction factor*	-
ξ_0	*Friction factor for longitudinal flow*	-
ξ_1	*Friction factor for wavy longitudinal flow*	-
ρ	*Density*	$[kg\ m^{-3}]$
σ	*Surface tension*	$[Nm^{-1}]$
σ_b	*Boltzmann's constant*	-
Φ	*Enlargement factor*	-
φ	*Chevron angle*	$[°]$
ω	*Accentric factor*	-

Subscripts/superscripts

bulk	*Bulk*
c	*Cold*
cb	*Convective boiling*
ch	*Channel*
cs	*Cold side*
condensation	*Referring to the condensation zone*
conv	*Convective*
crit	*Critical*
desup	*Desuperheater*
eq	*Equivalent*
evap	*Evaporator*
g	*Vapor*
guess	*Guess value*
h	*Hot*
hs	*Hot side*

in	*Inlet*
l (Wanniarachchi)	*Laminar*
l	*Saturated liquid*
lo	*Liquid only*
m	*Mean*
mod	*Modified*
nb	*Nucleate boiling*
nucl	*Nucleate*
out	*Outlet*
pl	*Plate*
port	*Port*
pre	*Preheating zone*
red	*Reduced*
req	*Required*
sat	*Saturated*
shear	*Shear*
subc	*Subcooling*
suph	*Superheater*
t	*Turbulent*
tot	*Total*
tp	*Two- phase*
w	*Wall*

Chapter 1. Introduction

1.1. Heat transfer

Energy can be transferred between a system and its surroundings via heat and work. This section focuses on the analysis of heat transfer and heat exchangers, which are the means to accomplish this energy transfer.

Heat transfer is defined as the process occurring in one or more medium, due to temperature difference, where thermal energy is transferred from hot to cold.

When the thermal energy is transferred within and across a solid medium or a fluid due to a temperature gradient the type of heat transfer is called conduction. In liquids and gases, molecules having higher kinetic energies and higher temperatures collide with the lower kinetic energy molecules and part of this energy is transferred, raising the temperature of the latter. In solids free flow electrons and lattice waves caused by the vibrational motions of the molecules at relatively fixed positions, lead to a similar heat transfer within the medium[1].

To describe this phenomenon along the x-direction Fourier's law is applied, which states:

$$q_x = -k \cdot \frac{dT}{dx} \qquad (1.1)$$

where k is the thermal conductivity and is a transport property of the medium through which heat is conducted. Heat flows in the positive direction of the x-axis hence $\frac{dT}{dx}$ is negative, as shown in Fig. 1.1.

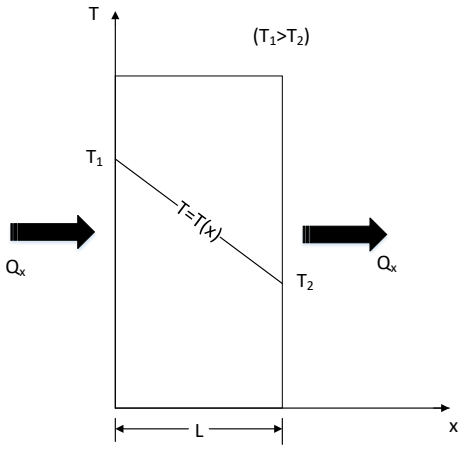

Fig. 1.1. Conductive heat transfer schematic

The second heat transfer mechanism is called convection, and takes place when there is a temperature difference between a solid surface and a fluid flowing over it. This type of heat transfer consists of two sub-mechanisms:

- Conduction at the solid surface.
- Advection near the solid surface by the macroscopic motion of the fluid.

There can be distinguished two types of convection:

1. Forced convection: The fluid is forced to flow over the surface with the use of external means such as fans, pumps, etc.
2. Free(Natural) convection: The flow motion is caused by buoyancy forces.

Near the solid surface, a region is assumed at which the velocity of the fluid equals zero (no slip condition), therefore heat is transferred between the fluid and the surface by conduction. The flow region adjacent to the wall in which the viscous effects are significant is called boundary layer. The fluid velocity along the boundary layer reaches a finite value (Fig. 1.2).The contribution of advection due the fluid motion arises with the growth of the boundary layer in the flow direction. The conducted heat into this layer is swept downstream and is eventually transferred to the fluid outside the boundary layer[1].

Similarly, there is a region in which the fluid temperature varies from T_s (at the surface) to T_∞ (finite, outer flow). This region is called thermal boundary layer.

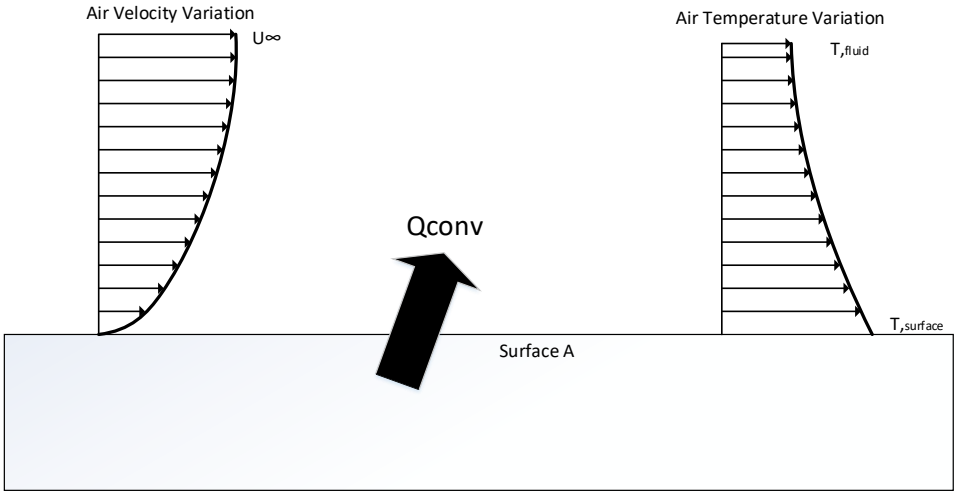

Fig. 1.2. Convective heat transfer schematic.

Convective heat transfer over a surface area A is expressed through Newton's law of cooling:

$$Q_{conv} = h \cdot A \cdot \Delta T \qquad (1.2)$$

where h is the convective heat transfer coefficient related to the thermal conductivity of the fluid, and the temperature gradient, and ΔT is the temperature difference between the surface and the fluid (reference temperature).

The third type of heat transfer is radiation. Radiation is a result of electromagnetic waves and a material's capability to absorb part of the radiation received and re-emit a part of it. In contrast to the two aforementioned types of heat transfer, radiation does not require a transfer medium and is even more efficient under vacuum conditions.

Thermal radiation is emitted in a specific band of wavelength from 0.1 to 100 μm[1]. The radiant energy emitted by an ideal radiator (blackbody) according to Boltzmann's law is equal to:

$$E_b = \sigma_b \cdot A \cdot T^4 \qquad (1.3)$$

where σ is the Boltzmann's constant, A is the surface area, and T is the absolute surface temperature. Since equation (1.3) refers to an ideal radiator, it has to be modified to be applicable for real bodies which emit radiation at a lower rate compared to a blackbody:

$$E = \varepsilon \cdot \sigma_b \cdot A \cdot T^4 \ [W] \qquad (1.4)$$

where ε is the emissivity of the radiating body and is practically the ratio of the emission rate from a real body to that from a blackbody at the same temperature. Hence, by definition the emissivity of a blackbody equals to 1 and that of a real body is always less than 1 ($0 < \varepsilon < 1$).

Thus, assuming two bodies (solid or gas), with respective temperatures $T_{s,1}$and $T_{s,2}$ ($T_{s,1} > T_{s,2}$), the radiation heat flow between these them is equal to:

$$Q = F \cdot \sigma_b \cdot A \cdot \left({T_{s,1}}^4 - {T_{s,2}}^4\right) \qquad (1.5)$$

where F includes the emission properties of the two bodies depending also on their dimensions and geometries.

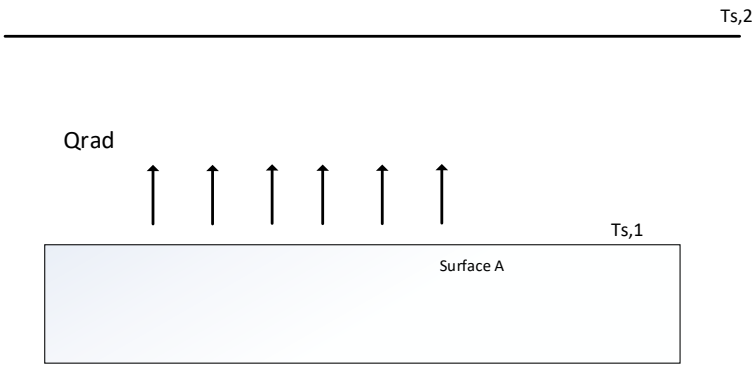

Fig. 1.3.Radiation heat transfer schematic

1.2. Heat Exchangers

The device mostly used to transfer heat between two or more fluids, or between a solid surface and a fluid, at different temperatures is called a heat exchanger. Examples of industries using heat exchangers include process, power, transportation, air-conditioning and many more.

Heat exchangers consist of sub-components such as a core or a matrix and usually have no moving parts. The core contains the surface, in which the heat transfer takes place, and fluid distribution elements such as pipes (inlet, outlet). The area of this surface is critical for the efficiency of the heat transfer and can be enhanced with the implementation of fins. Inside the heat exchangers all three heat transfer types take place. A primary categorization can be made based on the nature of the heat transfer, by means of either being direct, e.g. via a separating wall, or indirect with intermittent heat exchange (e.g. energy storage).

Heat exchangers can also be classified based on the number of fluids, the surface compactness, their design characteristics and flow arrangements, or the dominant heat transfer mechanisms. Another important classification is according to heat transfer surface to volume ratios: (compact/ non- compact heat exchangers)[2].

The most common industrial heat exchangers are listed below:

- Shell and tube heat exchangers
- Plate heat exchangers
- Finned tube heat exchangers
- Plate fin heat exchangers
- Micro-channel heat exchangers

Those five types of heat exchangers differ in their design and applications mainly due to different working range and performance characteristics including their heat transfer surface to volume ratio, pressure drop, cost and materials.

1.2.1 Shell and tube heat exchangers

Shell and tube heat exchangers are indirect, cross-flow heat exchangers. The main components include tubes, baffles, shell, front head, rear head, tube sheets and nozzles. These components are selected according to the temperature range of the involved streams, their pressure, the properties of the working fluids, fouling, cost and the specific requirements of the application. This type of heat exchangers is used in high temperature and high pressure conditions and is the most frequently used in industries including power, food and chemical, consisting of a bundle of tubes inside a cylindrical shell[3, 4]. A schematic of the two stream flows inside a shell and tube heat exchanger is presented in Fig 1.4.

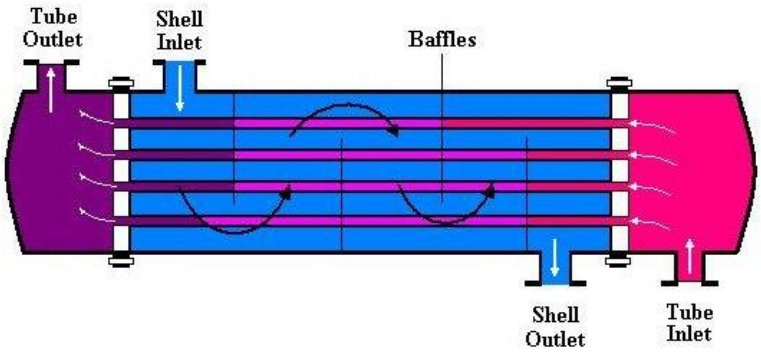

Fig. 1.4. Schematic of a shell and tube heat exchanger [5]

Main characteristics of the shell and tube heat exchangers include the following [2]:

- Versatility in a high range of applications (in terms of heat load and operating conditions)
- High maximum allowable operating pressure

- Relatively simple construction
- Robustness and reliability
- Low pressure drop
- Relatively high specific costs per heat transfer area: 550 $/m^2 [6]
- Typical U values range (depending on the fluids): 50-300 W/m^{2}K[6]

1.2.2 Plate heat exchangers

Plate heat exchangers are also widely used in industries including food processing, petroleum refineries, power and chemical industries. They can be used instead of shell and tube heat exchangers when there are low- and medium operating pressures and consist of a number of corrugated metal plates in mutual contact, each having two inlet and two outlet ports with seals to direct the two fluid flows, which do not mix as the flow passages are formed by adjacent plates so that the two streams exchange heat while passing through alternate panels. These plates are clamped together and combine to a frame that includes these fluid connections[2, 7].

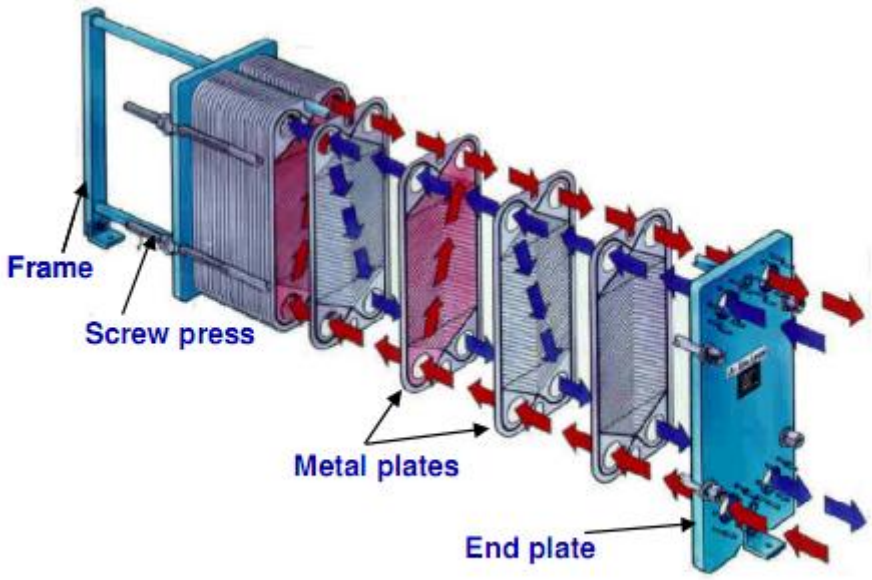

Fig. 1.5. Schematic of a gasketed plate heat exchanger layout and its streamlines

The number and size of the plates are determined by the operating conditions such as flow rate, fluids' properties, maximum allowable pressure drop and temperature profiles of the two streams. The spacing between the adjacent plates is a few millimeters. Each medium and the adjacent plates are gasketed (vented to atmosphere), eliminating the possibility of cross- contamination of the two fluids.

The main characteristics of the plate heat exchangers include[2]:

- Compact design, suitable for applications with space restrictions
- Smaller operating range (in terms of temperature, pressure)
- Higher pressure drops

- For gasketed plate heat exchangers (Fig. 1.5) only: modular design, allowing for modification of the number of plates
- Low specific costs
- Low maintenance
- Typical U values range: 3500-7000 W/m^{2}K [2]

Another variation of this conventional gasketed plate heat exchanger in answer to the need for a more compact solution is the brazed plate heat exchanger. It is also constructed of a series of corrugated metal plates but without the gaskets, tightening bolts, frame, or carrying and guide bars. The steel plates are brazed together in a vacuum forming a pressure-resistant unit which can achieve higher pressures and temperatures. This structure makes the units less expendable, but their main advantage is their compact size.

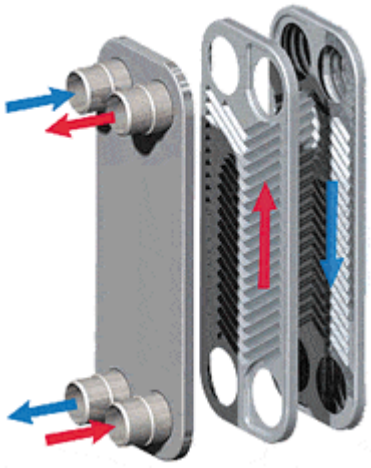

Fig. 1.6. Schematic of a brazed plate heat exchanger layout and its streamlines

1.2.3 Finned tube heat exchangers

Finned tube heat exchangers are also widely used in industry especially in applications on which one stream is in higher pressure and has higher heat transfer coefficient compared to the other. This mostly occurs to liquid- gas heat exchangers, since liquids tend to have higher heat transfer coefficients.

This type of heat exchangers consists of tubes in various shapes, mostly round or rectangular, which have fins enhancing the heat transfer surface. The fins based on the application can be attached either on the outer, the inner surface or both sides of the tubes' walls. In the most usual arrangement, liquid is flowing inside the tubes while gas at lower pressures flows across the finned tubes, and is mostly used in air-conditioning and refrigeration applications as condensers and evaporators.

The fins on the tubes can be categorized as follows:

- Normal fins on individual tubes: a geometry more rugged and less compact than continuous fin geometry. The most prevalent individually finned tubes are with circular, helical or annular enhanced geometries. They are mostly made of copper

aluminum or steel and are arranged in line or staggered, depending on the properties of gas flow and desired heat transfer rates.

- Longitudinal fins on individual tubes: a geometry mostly used in condensing and highly viscous fluid applications.
- Continuous fins on a tube array: mostly used in cooling applications and as vehicular radiators. Tubes are mechanically bonded with the fins, reducing the construction cost, but limiting the operating temperature.

The core of the heat exchanger must be designed carefully, taking in to account fin spacing which can increase fouling while the construction is more sensitive and less compact. Also the proper selection of the surface is important, using both qualitative, such as heat transfer requirements, flow resistance and fouling characteristics, and quantitative, by comparing various heat exchangers' performances and choosing the most fitting, criteria[2].

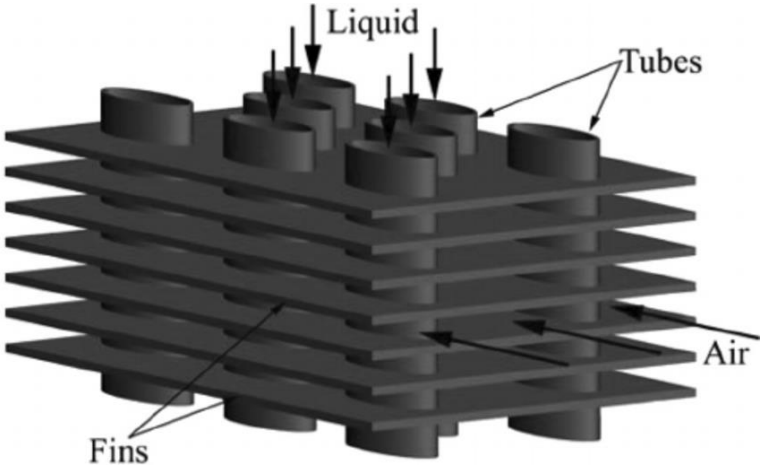

Fig. 1.7. Schematic of a finned tube heat exchanger [8]

1.2.4 Plate fin heat exchangers

Plate-fin heat exchangers are compact devices, consisting of flat "parting" sheets and fin corrugations used mostly in gas-to-gas heat transfer applications and in cryogenic, aerospace and oil industries. Fluids flow between the parting sheets along the corrugations, which act as secondary heat exchange surfaces while providing mechanical support (*Fig 1.8*).

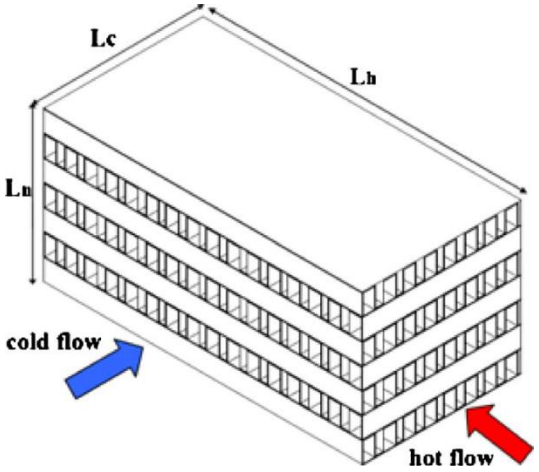

Fig. 1.8. Schematic of a plate-fin heat exchanger [9]

Fins can be manufactured in many different geometries such as plain, straight uninterrupted fins in the flow direction, which generally result to lower heat transfer coefficients. Fins are usually wavy or have off-set strips, resulting in thinner boundary layers and therefore in higher heat transfer coefficients[2].

Their main characteristics include:

- Compact design
- High thermal effectiveness
- Low weight per unit of volume
- Wide range of temperatures with the proper selection of materials
- Allow for multiple streams heat transfer in a single unit
- Complex and energy intensive construction
- Pressure drop issues

1.2.5 Micro-channel heat exchangers

Microchannel is a modern type of heat exchanger which has flow passages as small as 1 mm [10] achieving very high heat transfer surface densities. These devices are generally lighter and even more compact than the aforementioned heat exchangers, and are able to achieve higher heat transfer rates. One more important advantage is the use of aluminum for its construction, reducing the cost and the weight, contributing to copper substitution. The advancement in micromachining allowed the use of metals for the construction of these heat exchangers, where micro-scale flow passages are created on thin metal foils, which are then welded or soldered together, into crossflow type exchangers.

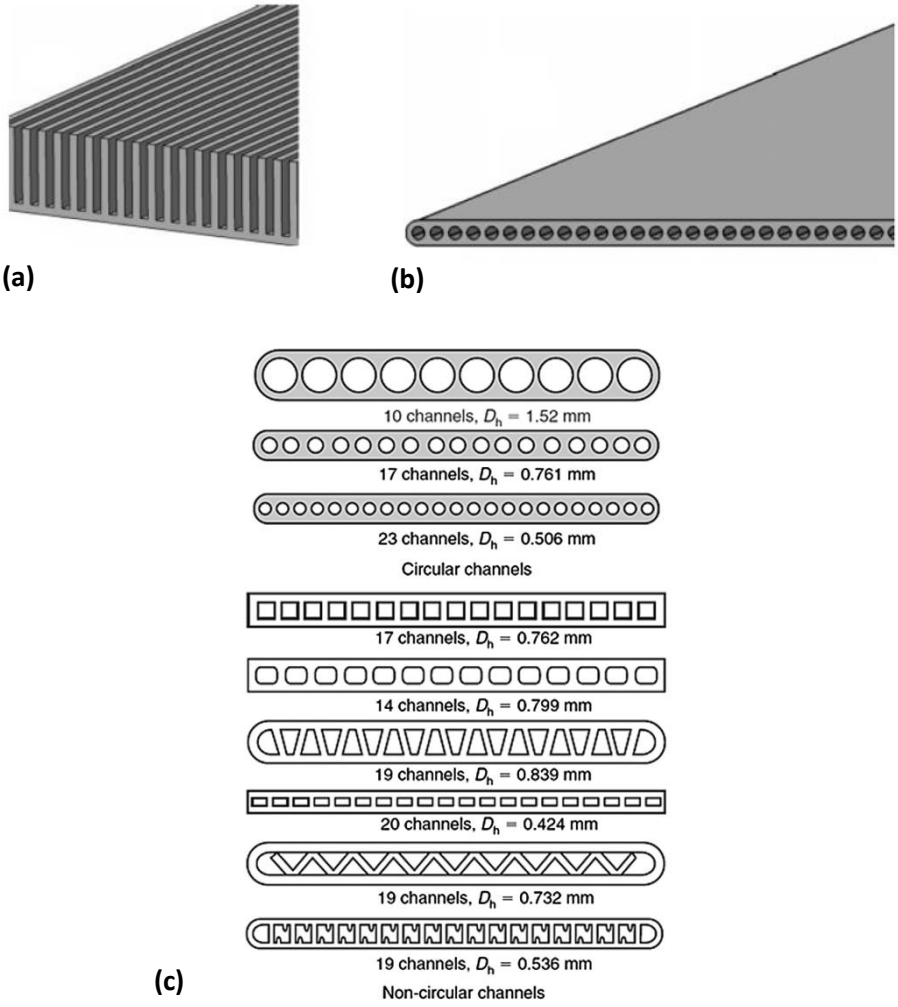

Fig. 1.9. Schematic of possible microchannel heat exchangers configurations[10]

Microchannel heat exchangers have been greatly used for cooling electrical hardware and are gradually expanding their field of applications in larger scale cooling applications.

Currently the research's main focus is the difference in flow characteristics in the channels, compared to conventional heat exchangers, due to reduced scale. Effects like flow compressibility, viscous forces and drag coefficient are intensified because of the reduced size and structural differences [11, 12].

1.3. Thesis scope

As already discussed, the heat exchangers is a widely applied component involved in almost all power, heating and cooling applications. Among several types of heat exchangers, plate heat exchangers have a large share of the global market, thanks to their relative low cost, their high energy density and their large availability. Thus the proper selection of the design procedure and hence the study and evaluation of the proposed in literature heat transfer correlations for plate heat exchangers is of crucial importance for the accurate design of a power, heating and/or cooling system. Within this scope, this study aims to provide a precise accounting towards the following issues:

- Which is the range of prediction for commonly applied heat transfer correlations for evaporation, condensation and single phase flow in plate heat exchangers?
- How the nature of the working fluid is affecting the calculated heat transfer coefficient?
- How much is the dependence of each proposed correlation on the Reynolds number?
- How accurate is the extrapolation of the proposed correlations?
- Which is the range of the predicted values for the proposed correlations of the plate's pressure drop?
- How is the nature of the working fluid and the Reynolds number affecting the pressure drop prediction for each proposed correlation?

Chapter 2. Plate heat exchanger modelling

In the following sections, the procedure of the plate heat exchanger's modelling is presented. Three models were developed for the plate heat exchanger configuration: an evaporator, a condenser and single phase heat exchanger. Various heat transfer correlations will be used in these calculations, which will be presented in the following chapters.

2.1. Evaporator Modelling

The calculation of the required geometry of the plate heat exchanger- evaporator to achieve the required heat duty is essential. Hence, for the initialization of these calculations, the two inlet streams (working fluid, pressure, temperature and mass flow rate) as well as the exit condition of the cold stream (nominal point) are required as input data. If the outlet condition of the primary stream is assumed, the outlet of the secondary- hot- stream can be determined by applying a simple energy balance.

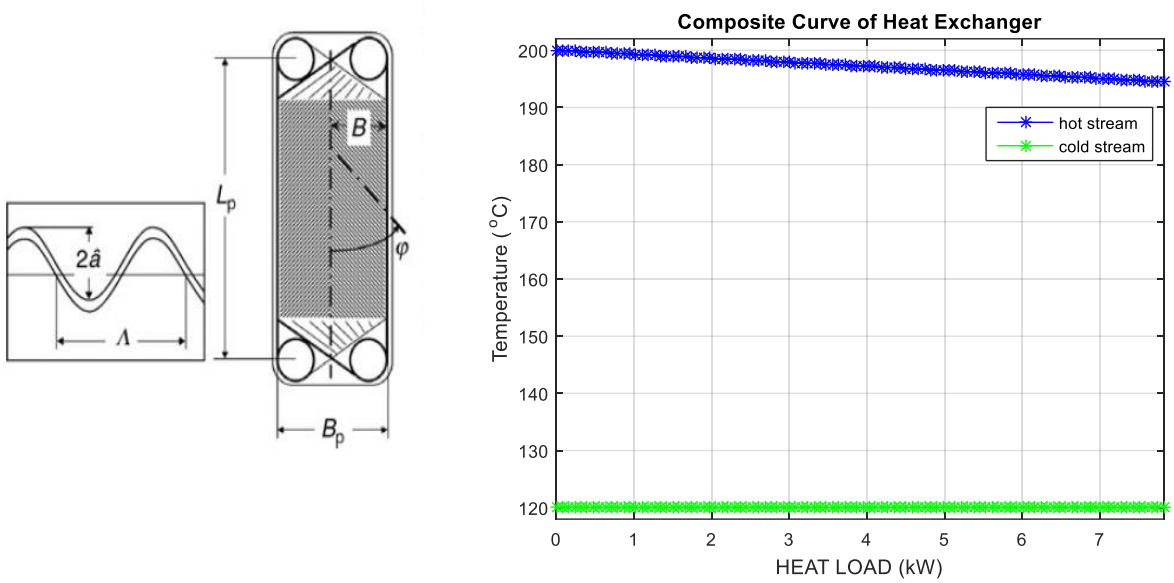

Fig. 2.1. (a) Schematic of a plate with key dimensions (b) a composite curve for an example of evaporation zone (hot stream: Therminol D12, cold stream: r245fa)

In order to evaluate whether a specific number of plates are sufficient for the investigated heat transfer duty, both the plain surface of a single plate as well as its enhanced surface due to the existence of corrugations are required.

$$A_{ref} = B_p \cdot L_p \qquad (2.1)$$

$$A_p = A_{ref} \cdot \Phi \qquad (2.2)$$

With Φ the enlargement factor, calculated by the following expression:

$$\Phi = \frac{1}{6}\left(1 + \sqrt{1+X^2} + 4\sqrt{1+\frac{X^2}{2}}\right) \qquad (2.3)$$

$$X = \frac{2\pi\alpha_{pl}}{\Lambda} \qquad (2.4)$$

The hydraulic diameter is calculated by the following expression:

$$D_h = \frac{4\alpha_{pl}}{\Phi} \quad (2.5)$$

And the mass velocity per stream is calculated as following:

$$G_{hs,ch} = \frac{\dot{m}_{hs}}{N_{cp} \cdot A_{ch}} \quad (2.6)$$

$$G_{cs,ch} = \frac{\dot{m}_{cs}}{N_{cp} \cdot A_{ch}} \quad (2.7)$$

With N_{cp}, the number of channels per pass, $\dot{m}_{hs}$, the total mass flow rate of the hot side and $\dot{m}_{cs}$, the total mass flow rate of the cold side and A_{ch}, the channel surface, which is equal to:

$$A_{ch} = 2\alpha_{pl} \cdot B_p \quad (2.8)$$

For the heat transfer calculations the heat exchanger was subdivided into three zones, as shown in Fig. 2.1. The preheating zone was the first to be calculated. Based on the exit stream results, the evaporation zone was afterwards calculated, and eventually the superheating zone was defined. The preheating and superheating zones were solved using a single element approach based on single-phase analysis. On the contrary, the evaporation zone was discretized in 10 consecutive elements, since the heat transfer rate is highly varying with the quality. Within each element, an equal increase of the cold stream's quality was assumed. The analysis of each zone follows:

2.1.1 Preheating zone

Since the preheating zone is solved as a single element, for the cold stream, the inlet conditions of the preheating zone were equal to those of the entire heat exchanger, while the outlet conditions corresponded to the saturated liquid. The hot stream inlet for this zone is calculated with an energy balance, since the pressures for the two streams were regarded equal to the heat exchanger's input values, and the (hot stream) outlets were the same as for the whole heat exchanger, and were also known.

Having calculated the mean temperature of the preheating zone on each side, $\bar{T}_{hs,pre}$ and $\bar{T}_{cs,pre}$, the plate's mean temperature is given:

$$\bar{T}_{pl,pre} = \frac{\bar{T}_{hs,pre} + \bar{T}_{cs,pre}}{2} \quad (2.9)$$

The mean temperature of the wall is also calculated, on each side:

$$\bar{T}_{wall,hs} = \frac{\bar{T}_{hs,pre} + \bar{T}_{pl,pre}}{2} \quad (2.10)$$

$$\bar{T}_{wall,cs} = \frac{\bar{T}_{cs,pre} + \bar{T}_{pl,pre}}{2} \quad (2.11)$$

Then the logarithmic mean temperature ΔT_{lm} is equal to:

$$\Delta T_{lm} = \frac{\left(T_{hs,in,pre} - T_{cs,out,pre}\right) - \left(T_{hs,out,pre} - T_{cs,in,pre}\right)}{\ln\left(\frac{T_{hs,in,pre} - T_{cs,out,pre}}{T_{hs,out,pre} - T_{cs,in,pre}}\right)} \quad (2.12)$$

The last step was the calculation of the Prandtl and Reynolds numbers on the cold and hot side, respectively. The Prandtl number for the cold stream is calculated indirectly using Refprop's database for the corresponding mean condition in the preheating zone:

$$Re_{hs} = \frac{G_{hs,ch} * D_h}{\mu_{hs}} \quad (2.13)$$

$$Pr_{hs} = \frac{\mu_{hs} * c_{p,hs}}{\lambda_{hs}} \quad (2.14)$$

$$Re_{cs} = \frac{G_{cs,ch} * D_h}{\mu_{cs}} \quad (2.15)$$

The heat transfer coefficient of the hot side is calculated as follows:

$$a_{hs,pre} = \frac{Nu_{hs} * \lambda_{hs}}{D_h} \quad (2.16)$$

The correlation for the Nusselt number, Nu_{hs}, to be used will be eventually selected in the next chapters.

For the cold side, the heat transfer coefficient is calculated as follows:

$$a_{cs,pre} = \frac{Nu_{cs} * \lambda_{cs}}{D_h} \quad (2.17)$$

Finally, the preheating zone overall heat transfer coefficient is calculated by the following equation:

$$U_{pre} = \frac{1}{\frac{1}{a_{hs}} + \frac{1}{a_{cs}} + \frac{t_{plate}}{\lambda_{wall}} + R_{f,cs} + R_{f,hs}} \quad (2.18)$$

Where $R_{f,cs}$ and $R_{f,hs}$ are the fouling resistances of the two sides of the stream. The heat transfer surface is easily calculated:

$$A_{req,pre} = \frac{\dot{Q}_{pre}}{\Delta T_{lm} * U_{pre}} \quad (2.19)$$

Regarding the pressure drop, $\Delta p_{hs,pre}$, of the hot side stream the equations will also be shown and evaluated in the following chapters.

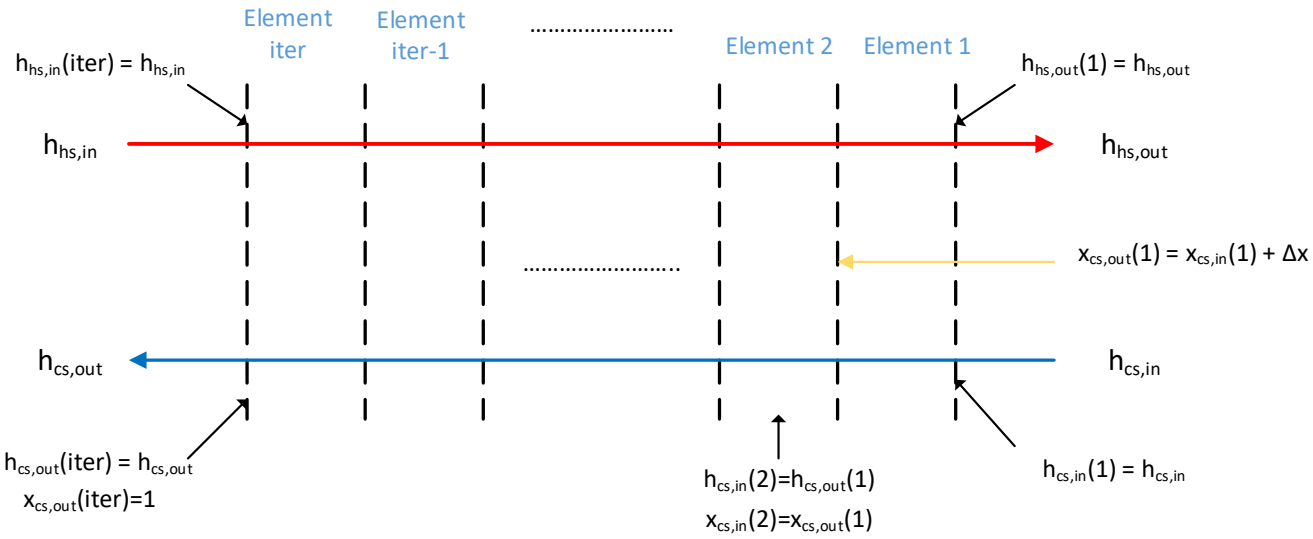

Fig. 2.2. Discretization of the plate in the evaporation zone

2.1.2 Evaporation zone

For the initialization of the evaporating zone, as shown in Fig. 2.2, the following conditions are considered:

$$h_{cs,in}(1) = h_{cs,out,pre}$$

$$h_{hs,out}(1) = h_{hs,in,pre}$$

The hot stream's inlet enthalpy of each element *m* is determined using an energy balance:

$$h_{hs,in}(m) = h_{hs,out}(m) + \frac{\dot{m}_c}{\dot{m}_h}\left[h_{cs,out}(m) - h_{cs,in}(m)\right] \qquad (2.20)$$

The first step includes the calculation of the temperatures for each element using Refprop's database and then, using equation (2.12), the mean logarithmic as well as the actual temperature differences are calculated. Similarly, the Prandtl and Reynolds numbers are calculated for each element *m* through equations (2.13- 2.15). Since the cooling process of the hot side is single phase, equation (2.16) combined with the appropriate single phase Nusselt correlation gives the heat transfer coefficient of each element *m*, $a_{hs,evap}(m)$.

On the other hand, the cold side demands two phase heat transfer analysis, therefore the appropriate Nusselt number, $Nu_{cs}(m)$, equations must be chosen, which will also be a subject of the next chapters. By calculating the Nusselt number the cold side heat transfer coefficient is calculated:

$$a_{cs,evap}(m) = \frac{Nu_{cs}(m) * \lambda_{cs,L}}{D_h} \qquad (2.21)$$

Finally, the overall heat transfer coefficient of the evaporation zone equals:

$$U_{evap}(m) = \frac{1}{\frac{1}{a_{hs,evap}(m)} + \frac{1}{a_{cs,evap}(m)} + \frac{t_{plate}}{\lambda_{wall}} + R_{f,cs} + R_{f,hs}} \quad (2.22)$$

Then, the heat transfer surface required is calculated as follows:

$$A_{req,evap}(m) = \frac{\dot{Q}_{evap}(m)}{\Delta T_{lm} * U_{evap}(m)} \quad (2.23)$$

As mentioned above, the two phase pressure drop for the cold side, $\Delta p_{cs,evap}(m)$, will be calculated using various equations, which will be examined in the following chapters.

2.1.3 Superheating zone

In the superheating zone the heat transfer is single phase, hence the calculations are similar to the preheating zone. Consequently, by implementing the inlet and outlet conditions for the superheating zone on equations (2.9-2.18), the heat transfer coefficients of both sides, $a_{hs,suph}$ and $a_{cs,suph}$, can be determined. Therefore, the overall heat transfer coefficient equals:

$$U_{suph} = \frac{1}{\frac{1}{a_{hs,suph}} + \frac{1}{a_{cs,suph}} + \frac{t_{plate}}{\lambda_{wall}} + R_{f,cs} + R_{f,hs}} \quad (2.24)$$

Finally, the required heat transfer surface is calculated using the following equation:

$$A_{req,suph} = \frac{\dot{Q}_{suph}}{\Delta T_{lm} * U_{suph}} \quad (2.25)$$

The pressure drops for the hot and the cold side will be calculated using various equations, which will be mentioned in the following chapters.

2.1.4 Overall Calculations

After evaluating the heat transfer and pressure drop for the preheating, evaporation and superheating zones, the total heat transfer surface needed to accomplish the defined heat duty, can be calculated as the sum of all the aforementioned parts:

$$A_{req,tot} = A_{req,pre} + \sum_{m=1}^{iter} A_{req,evap}(m) + A_{req,suph} \quad (2.26)$$

Whereas the pressure drop for the two streams are:

$$\Delta p_{cs,tot} = \Delta p_{cs,port} + \Delta p_{cs,pre} + \sum_{m=1}^{iter} \Delta p_{cs,evap}(m) + \Delta p_{cs,suph} \quad (2.27)$$

$$\Delta p_{hs,tot} = \Delta p_{hs,port} + \Delta p_{hs,pre} + \sum_{m=1}^{iter} \Delta p_{hs,evap}(m) + \Delta p_{hs,suph} \quad (2.28)$$

Where the pressure drop at the ports, Δp_{port}, equals (Shah and Focke 1988):

$$\Delta p_{port} = 0.75 \left(\frac{G^2}{\rho_m} \right) \qquad (2.29)$$

To determine the size of the evaporator, an initial guess is made regarding the number of plates, N_t, of the heat exchanger, which increases until the total surface is higher than the required $A_{req,tot}$. The pressure drop of each streams sets an upper limit for the loop to end. This method is visualized in the following figure (Fig. 2.3):

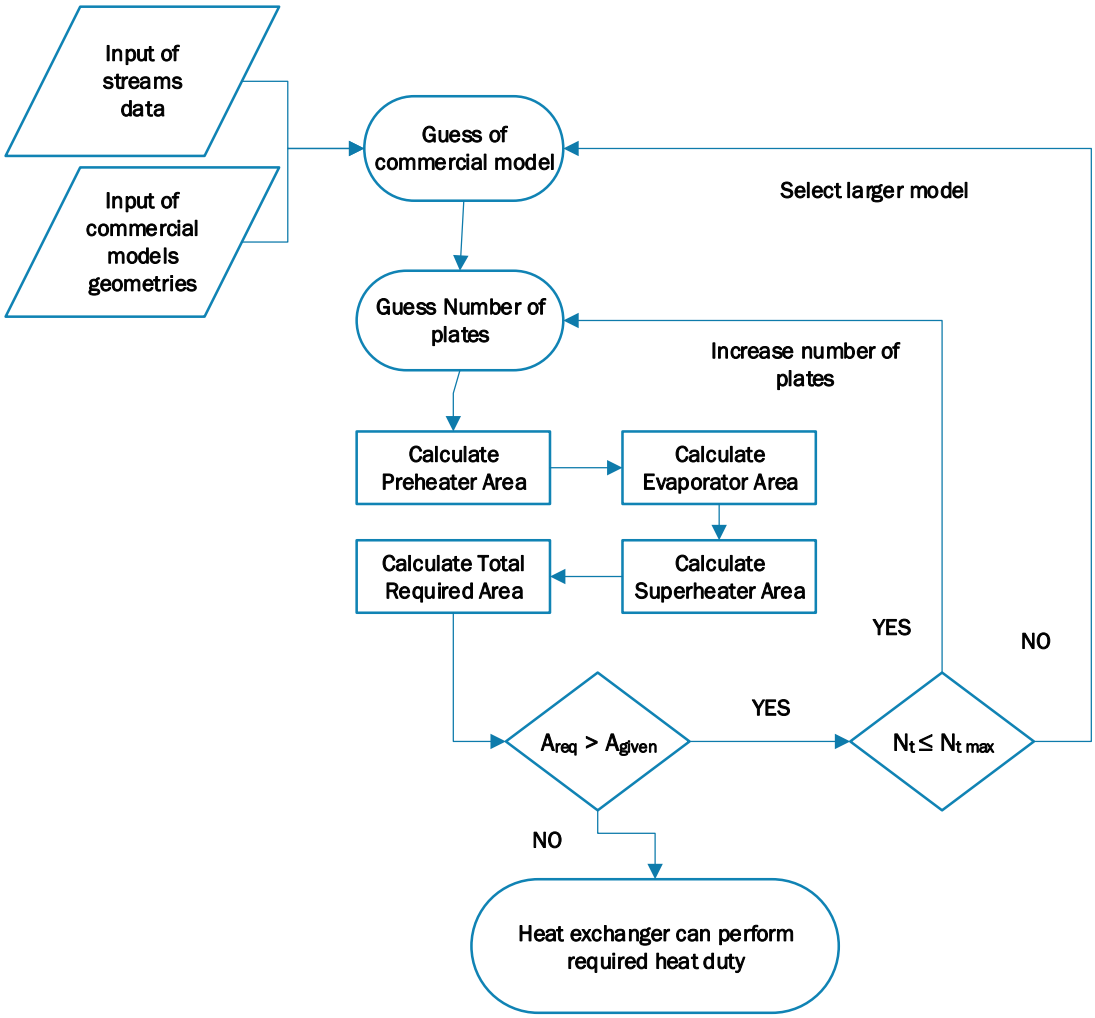

Fig. 2.3. Flow chart of the evaporator sizing process

2.2. Condenser Modelling

Similarly to the evaporator modelling, the condenser is divided in three zones. The first one is the desuperheating zone, whose exit results are inserted in the condensation zone analysis. Finally, the subcooling zone is designed. In a similar manner with the evaporator, the single phase heat transfer is solved as a single element, while the condensation zone is separated in 10 elements. Equal decrease of the stream's quality is assumed in each of the 10 elements. The figure below (Fig. 2.4) presents an overview of the three heat transfer

zones for a case study. Once again the properties of both streams are acquired from the Refprop database and the analysis uses the calculations in equations (2.1-2.8).

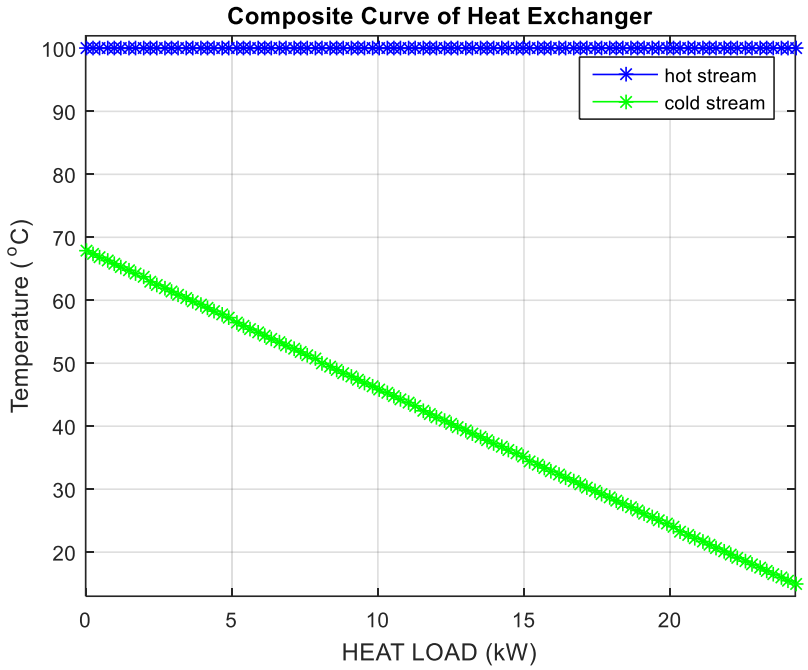

Fig. 2.4. Condensation zone for a heat transfer overview example (hot stream: Cyclopen, cold stream: Ammonia)

2.2.1 Desuperheating zone

As abovementioned the desuperheating zone is solved as a single element. Hence, the inlet of the hot stream matches that of the whole condenser. The outlet conditions equaled to saturated vapor. Moreover, the cold side's outlet of the whole heat exchanger and the desuperheating zone coincide. Therefore, the inlet of the cold stream is also defined with the use of an energy balance. Similarly to the evaporator the Prandtl number was calculated with the use of Refprop, while the Reynolds number are determined by the equations (2.13) and (2.15). The Nusselt number and the equations for the pressure drop will be listed in the next chapters. Finally, with the use of the equations (2.18) and (2.19) the overall heat transfer coefficient as well as the surface area required to perform the heat duty are defined.

2.2.2 Condensation zone

The condensation zone is discretized in a similar way to the evaporation zone abovementioned in 10 consecutive elements. Each element, *m*, is considered to have an equal decrease of quality of the hot stream, therefore the inlet and outlet conditions of the hot side are easily calculated. For the cold side the outlet of the condensation zone is deemed equal to the inlet of the desuperheating zone, hence known. The inlet enthalpy of each element, *m*, of the cold side is defined with the use of an energy balance:

$$h_{cs,in}(m) = h_{cs,out}(m) - \frac{\dot{m}_h}{\dot{m}_c}\left[h_{hs,in}(m) - h_{hs,out}(m)\right] \qquad (2.30)$$

By calculating the enthalpies of each element, the first step is the calculation of the temperatures for each element using Refprop's database and then using equation (2.12) the mean logarithmic as well as the actual temperature differences are calculated. Similarly, the Prandtl and Reynolds numbers are given for each element *m* through equations (2.13- 2.15). Since the cooling process of the hot side is single phase, equation (2.16) combined with various Nusselt equations gives the heat transfer coefficient of each element *m*, $a_{cs,condensation}(m)$.

At the same time, for the hot side, since two phase heat transfer analysis is required, the appropriate Nusselt number equations $Nu_{hs}(m)$ will be chosen in the following chapters. The heat transfer coefficient of each element, *m*, equals:

$$a_{hs,condensation}(m) = \left(\frac{\lambda}{D_h}\right) Nu_{hs}(m) \qquad (2.31)$$

Finally, with the use of equations (2.22) and (2.23), the overall heat transfer coefficient, $U_{condensation}$, as well as the required condensation surface, $A_{condensation}$, are calculated. For the pressure drop of each side, equations and formulas will be presented in the following chapters.

2.2.3 Subcooling zone

The subcooling zone is solved like the desuperheating zone, by applying the inlet and outlet conditions on equations (2.9-2.17), since single phase heat transfer takes place on both the cold and the hot side. Consequently, the heat transfer coefficients, $a_{hs,subc}$ and $a_{cs,subc}$, are calculated. Furthermore, with the use of equation (2.18) and (2.19) the overall heat transfer coefficient, U_{subc}, and the required surface, A_{subc} , are defined. As mentioned above, for the Nusselt number, as well as the pressure drop, various equations will be presented in the next chapter.

2.2.4 Overall calculations

Having specified the heat transfer and pressure drop for each part of the condenser, the overall required surface to achieve the heat duty equals:

$$A_{req,tot,cond} = A_{req,desup} + \sum_{m=1}^{iter} A_{req,condensation}(m) + A_{req,subc} \qquad (2.32)$$

The pressure drop of the two streams are:

$$\Delta p_{cs,tot,cond} = \Delta p_{cs,port} + \Delta p_{cs,desup} + \sum_{m=1}^{iter} \Delta p_{cs,condensation}(m) + \Delta p_{cs,subc} \qquad (2.33)$$

$$\Delta p_{hs,tot,cond} = \Delta p_{hs,port} + \Delta p_{hs,desup} + \sum_{m=1}^{iter} \Delta p_{hs,condensation}(m) + \Delta p_{hs,subc} \qquad (2.34)$$

The sizing method is similar to the one used for the evaporator. A heat exchanger model is guessed, while, the number of plates, N_t, are increasing, until the total surface of the plate heat exchanger is larger than the required, $A_{req,tot}$. Once again, an upper limit of the pressure drop within each stream is set, for the iterations to end.

2.3. Single phase heat exchanger

Since the heat transfer taking place on both streams at this part, is single phase, the analysis used will be similar to the one abovementioned for the preheating and the superheating zones of the evaporator, and the desuperheating and subcooling zones of the condenser, respectively. Hence, the single phase heat exchanger will be solved as a single element.

A pinch point of 6 K can be assumed, thus by having already defined the inlet conditions of the heat exchanger, the cold stream exit can be heated up to temperature which equals the hot stream inlet minus the 6 K of the pinch point. Since the cold stream heat capacity is higher than the hot stream's value, the pinch point will be spotted at the exit of the hot stream form the heat exchanger, where the temperature change will be greater, as shown in Fig. 2.5. With the hot stream's outlet conditions known, and the use of an energy balance, the outlet of the cold stream can be calculated.

The Prandtl numbers for both streams were defined with the use of Refprop, while the Reynolds numbers were given by equations (2.13) and (2.15). The Nusselt numbers like abovementioned will be calculated with equations which will be shown in the following chapters. Finally, with the use of equations (2.18) and (2.19), the overall heat transfer coefficient and the required surface area, are calculated respectively. Due to the fact, that the single phase heat exchanger's heat duty is smaller than the evaporator's and the condenser's, smaller commercial plate heat exchangers are considered in the script.

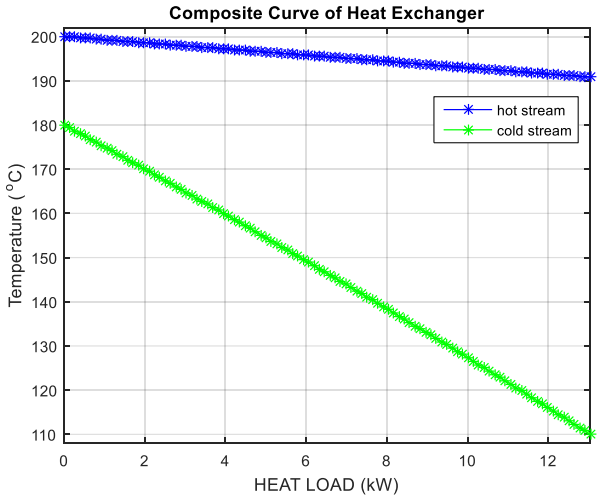

Fig. 2.5. Composite curve for an example of a single phase heat exchanger (hot stream: Therminol D12, cold stream: Cyclohexane)

2.4. Geometrical characteristics of evaluated commercial plate heat exchangers

Below there are the geometrical data of the plate heat exchangers, used in the heat transfer analysis:

Table 2-1. Basic plate geometrical characteristics used for the heat transfer analysis

Property	Number of passes, N_p	Plate thickness (mm)	Chevron angle, φ (°)	Pitch (mm)	Plate amplitude, a_{pl} (mm)	Corrugation pitch, Λ (mm)
Value	1	0.7	60	2.7	1	7

Table 2-2. Geometrical data of the considered plate heat exchangers for the evaporation phase

Model	D_p(m)	L_p(m)	B_p(m)	Min-Max Number of plates	Max flow (kg/s)
AC30EQ	0.02	0.269	0.095	4-120	8.8
AC70X	0.02	0.466	0.111	4-124	14
AC112	0.02	0.519	0.191	10-300	51
CB200	0.04	0.624	0.324	10-230	128

Table 2-3. Geometrical data of the considered plate heat exchangers for the condensation phase

Model	D_p(m)	L_p(m)	B_p(m)	Min-Max Number of plates	Max flow (kg/s)
CB10	0.013	0.154	0.0735	4-60	4.1
CB20	0.019	0.270	0.0940	10-110	8.8
CB30	0.019	0.250	0.113	4-150	14

Chapter 3. Heat transfer correlations

In this chapter the heat transfer correlations for the determination of the heat transfer coefficient will be presented in correspondence to the previous chapter's heat transfer analysis for the single phase, heat transfer, evaporation and condensation, respectively, using a number of working fluids and flow regimes.

3.1. Evaporation

The Nusselt correlation used in the hot side of the plate heat exchanger in equation (2.16) is Donowski's equation listed in Table 3-3 with the single phase heat transfer correlations.

For the cold side the Nusselt number used in equation (2.17) and (2.21) is calculated using various correlations shown in Table 3-1.

The correlations shown in Table 3-1 are introduced to the evaporator's modeling, which was presented at Chapter 2.1 and the heat transfer coefficient for the cold side is calculated.

The analysis is carried out using three different vaporizing fluids: R245ca, R1234ze and Cyclopentane. For each fluid the heat transfer coefficient is calculated for various Reynolds numbers, to take in to account the flow's turbulence influence on the heat transfer prediction by each correlation. For the first set of calculations, of each fluid, the parameters are set as default, with the mass flow of the cold side $m_c = 0.07\ kg/sec$ and the hot side mass flow $m_h = 0.5\ kg/sec$. The inlet temperatures are set at 150 °C for the cold side and at 200 °C for the hot side. Three more calculations are carried out, varying the mass flows to increase the Reynolds number to 500, 1000 and 3000. Below the calculations results are presented in heat transfer coefficient ($a\left[\frac{W}{m^2K}\right]$)- Quality ($x$) diagrams. In the case of R1234ze, the inlet temperatures for the cold and the hot side were decreased by 50°C respectively. The key conclusions are summarized below:

- Palmer's equation's results are normalized for qualities above 0.2 ($x > 0.2$).
- Khan's equation's results are relatively constant to the changes of Re
- Almalfi's results are proportional to the Re number
- Park and Kim's results are inversely proportioned to the Re number
- The curvature observed in Koyama's and Arima's results, which could be caused by the use of the Lockhart- Martinelli parameter
- Lee's correlation uses two equations in its calculation, resulting in some discontinuities.
- For high Reynolds numbers Ayub's correlation tends to overpredict the heat transfer coefficient
- Vakili's and Koyama's correlations produce similar results in the turbulent region.
- Taboas' and Arima's results seem to be unaffected by the increase of the Reynolds number.

With the use of Cyclopen:

- Hsieh,Lin and Huang's correlations produce similar results in the laminar region

- Yan and Lin and Longo’s results are similar in the whole Re number spectrum.

Eventually use of R1234ze gives lower heat transfer coefficients in the turbulent region, in comparison to the other working fluids.

Table 3-1. Evaporation heat transfer coefficient correlations

Correlation	**Working fluid**	**Range**	**Reference**
$Nu = 19.26 Re_{eq} {Re_L}^{-0.5} {Bo_{eq}}^{0.3} {Pr_L}^{1/3}$	R134a	$2{,}000 < Re_{eq} < 10{,}000$	Yan and Lin [13]
$Nu = 18.4096 Re^{0.78} Bo^{0.5} {Pr_L}^{1/3} \cdot \left(\frac{\mu_{bulk}}{\mu_{wall}}\right)^{0.14}$	R410A	$50 < G < 125$ $8.5 < q_{flux} < 30$	Hsieh and Lin [14]
$Nu = Ge_1 \, {Re_{eq}}^{Ge_2} {Bo_{eq}}^{0.3} {Pr_L}^{0.4}$ $Ge_1 = 2.81 \left(\frac{\Lambda}{D_h}\right)^{-0.041} \left(\frac{\pi}{2} - \varphi\right)^{-2.83}$ $Ge_2 = 0.746 \left(\frac{\Lambda}{D_h}\right)^{-0.082} \left(\frac{\pi}{2} - \varphi\right)^{0.61}$	R410A, R22	$13 < G < 34$ $2.5 < q_{flux} < 8.5$	Han et. al [15]
$Nu = 5.323 Re_{eq}^{0.42} Pr^{1/3}$	R410A	$600 < Re < 2{,}300$ $40 \leq G \leq 80$	Kim et. al [16]
$Nu = 2.7 {Re_L}^{0.55} {Pr_L}^{0.5}, (R22, R290, R290/600a)a$ $= \left(\frac{k_l}{D_h}\right) Nu_l^{0.42} Fr^{0.088} \omega^{1.5} Co^{1.5} M^{1.5}, Nu_l$ $= 0.16 Re_L^{0.89} Pr_L^{0.4}, (R32/R152a)$ Where, $Co = \left(\frac{\rho_g}{\rho_l}\right)^{0.5} \left(\frac{1-x_m}{x_m}\right)^{0.8}$, $\omega = -log_{10}\left(\frac{p}{p_{cr}}\right)$, $Fr = \frac{G^2}{\rho^2 g D_h}$	R22,R290, R290/600a, R32/R152a	$13 < Re_{eq} < 230$ $1.6 \leq G \leq 19$ $1.3 \leq q_{flux} \leq 8.3$	Palmer et. al [17]

$\alpha = a_{nucl} + a_{conv}$ $a_{nucl} = 0.58\Phi h_0 \left(\frac{\varepsilon}{\varepsilon_0}\right)^{0.1333} \left(\frac{q_{flux}}{q_{\text{flux},0}}\right)^{0.467}$ With $q_{\text{flux},0} = 20\ kW/m^2$, $\varepsilon_0 = 0.4\ \mu m$, h_0 specific for each refrigerant, $\Phi = \left[1.2p_{red}^{0.27} + \left(2.5 + \frac{1}{1-p_{red}}\right)p_{red}\right]$ $a_{conv} = 0.122\Phi \left(\frac{\lambda}{D_h}\right) Re_{eq}^{0.8} Pr^{1/3}$	R134a, R410A, R507A, R22, R601a, propane, propylene, R236fa, R1234yf	$5.7 < G < 125$ $2.7 < q_{flux} < 36.5$	Longo et. al [18]
$Nu = 532.2{Re_{eq}}^{0.3237}{Bo_{eq}}^{0.3}{Pr_L}^{1/3}Re^{-0.5}$	R134a	$45 \leq G \leq 55$ $4 \leq q_{flux} \leq 8$ T_{sat} $= 10℃, 15℃, 20℃$ $0.1 \leq x_m \leq 0.8$ $\beta = 45^o$	Kim and Park [19]
$Nu = C\left[\frac{{Re_L}^2\gamma}{L_p}\right]^{0.4124} \left(\frac{p}{p_{cr}}\right)^{0.12} \left(\frac{65}{\beta}\right)^{0.35} \left[\frac{Btu}{hr \cdot ft^2 \cdot °\text{F}}\right]$ $\begin{cases} C = 0.1121\ for\ flooded\ and\ thermo-syphon \\ C = 0.0675\ for\ direct\ expansion \end{cases}$	Ammonia,R22	$4000 \leq Re \leq 16000, US\ units$ $30^o < \beta < 65^o$	Ayub [20]

$\mathrm{Nu} = 0.3772\left(\frac{G(1-x)D_h}{\mu_L}\right)^{0.8} {Pr_L}^{0.4}\left(\frac{1}{x_{vv}}\right)^{1.08}$ $X_{vv} = \left(\frac{1-x}{x}\right)^{0.5}\left(\frac{\rho_g}{\rho_l}\right)^{0.5}\left(\frac{\mu_l}{\mu_g}\right)^{0.5}$ (laminar-laminar)	Ammonia	$40 < Re < 3600$ $7.4 \le G \le 15$ $15.4 \le q_{flux} \le 24.5$ $0.1 \le x_m \le 0.9$ $0.7 \le p \le 0.9$	Arima et. al [21]
$\mathrm{Nu} = \left(-\frac{173.52\beta}{60} + 257.12\right)\left(Re_{eq}Bo_{eq}\right)^{-0.09\frac{\beta}{60}+0.0005} {p^*}^{0.624\frac{\beta}{60}-0.822}$ $p^* = \frac{p}{p_c}$	Ammonia	$500 < Re < 2500$ $5.5 < G < 27$ $20 \le q_{flux} \le 70$ $0.1 \le x_m \le 0.9$ $3.5 < Pr < 6$ $30° < \beta < 60°$ $1225 < Re_{eq} < 3000$ $-2℃ \le T_{sat} \le -25℃$	Khan and Chyu and Khan et. al [22, 23]
$a = \begin{cases} a_{nb} = 5Bo^{0.15}a_l, \ for\ u_g < -111.88u_l + 11.848 \\ \max(a_{nb}, a_{cb}), \ for\ u_g > -111.88u_l + 11.848 \end{cases}$ where, $u_g = \frac{Gx}{\rho_g}$, $u_l = \frac{G(1-x)}{\rho_l}$, $a_{cb} = \left(\varphi^2_{Chisholm}\right)^{0.2}a_l$, $\varphi^2_{Chisholm} = 1 + \frac{C}{X_{tt}} + \frac{1}{X^2_{tt}}$, $C = 3$ $0.42 \le Ammonia\ Concetration\ \le 0.62$	Ammonia/water	$70 \le G \le 140$ $20 \le q_{flux} \le 50$ $0.0 \le x_m \le 0.22$ $0.7 \le p \le 1.5$	Taboas et. al [24]

$Nu = 0.00187\left(\frac{qd_0}{T_{sat}k_l}\right)^{0.56}\left(\frac{\gamma d_0}{a_l^2}\right)^{0.31} {Pr_l}^{0.33}, a_{tp} = Nu\left(\frac{k_l}{d_o}\right)$ $d_0 = 0.0146\theta\left(\frac{2\sigma}{g(\rho_l-\rho_g)}\right)^{0.5}, \theta = 35°, a_l = \frac{k_l}{\rho_l c p_l}$	R134a,R507A, R12,Ammonia	$5.6 \le G \le 52.3$ $1.8 \le q_{flux} \le 6.9$ $5.9℃ \le T_{sat} \le 13℃$ $28° < \beta < 60°$	Huang et. al [25]
$\begin{cases} Nu = 98.7\left(\frac{Re_g}{Re_l}\right)^{-0.0848} Bo^{-0.0597} X_{tt}^{0.0973}, \ for \ \frac{Re_g}{Re_l} < 9.0 \\ Nu = 234.9\left(\frac{Re_g}{Re_l}\right)^{-0.576} Bo^{-0.275} X_{tt}^{0.66}, \ for \ \frac{Re_g}{Re_l} > 9.0 \end{cases}$ Where $\frac{Re_g}{Re_l} = \frac{x}{1-x}\frac{\mu_g}{\mu_l}, X_{tt} = \left(\frac{1-x}{x}\right)^{0.875}\left(\frac{\rho_g}{\rho_l}\right)^{0.5}\left(\frac{\mu_l}{\mu_g}\right)^{0.25}$	Water	$\beta = 60°$ $14.5 \le G \le 33.6$ $15 \le q_{flux} \le 30$	Lee et. al [26]
$\begin{cases} Nu = 982\left(\frac{\beta}{\beta_{max}}\right)^{1.101}\left(\frac{G^2 D_h}{\rho_m \sigma}\right)^{0.315}\left(\frac{\rho_l}{\rho_g}\right)^{-0.224} Bo^{0.32}, \ for \ Bd < 4 \\ Nu = 18.495\left(\frac{\beta}{\beta_{max}}\right)^{0.248}\left(\frac{xGD_h}{\mu_g}\right)^{0.135}\left(\frac{GD_h}{\mu_l}\right)^{0.351}\left(\frac{\rho_l}{\rho_g}\right)^{0.223} Bo^{0.198} Bd^{0.235}, \\ for \ Bd \ge 4 \end{cases}$ Where, $Bd = \frac{(\rho_l-\rho_g)gD_h^2}{\sigma}, \beta_{max} = 70°$	R134a, ammonia, R236fa, R600a, R290, R1270, R1234yf, R410A, R507A, ammonia/water, air/water		Almalfi et. al [27]

$Nu_l = 0.023\left(\frac{G(1-x)D_h}{\mu_l}\right)^{0.8} Pr_L^{0.4}$ $\frac{a}{a_l} = 52.2\left(\frac{1}{X_{vv}}\right)^{0.9} \leftarrow \delta = 1\ mm$ $\frac{a}{a_l} = 48.6\left(\frac{1}{X_{vv}}\right)^{0.79} \leftarrow \delta = 2.5\ mm$ $X_{vv} = \left(\frac{1-x}{x}\right)^{0.5}\left(\frac{\rho_g}{\rho_l}\right)^{0.5}\left(\frac{\mu_l}{\mu_g}\right)^{0.5}$	Ammonia	$\delta = 1\ mm$	Koyama et. al [28]
$Nu_{tp} = 13.02Re_v^{0.35}Bd^{0.38}Bo^{0.28}Re_{lo}^{0.15}$ Where, $Bd = \frac{(\rho_l-\rho_g)gD_h^2}{\sigma}$, $Re_v = \frac{GxD_h}{\mu_v}$	R245fa	$\beta = 65^o$ $19 \leq T_{sat} \leq 35$ $10 \leq G \leq 85$ $0.1 \leq q_{flux} \leq 4.2$ $0.01 \leq x_m \leq 0.95$	Vakili- Farahani et. al [29]

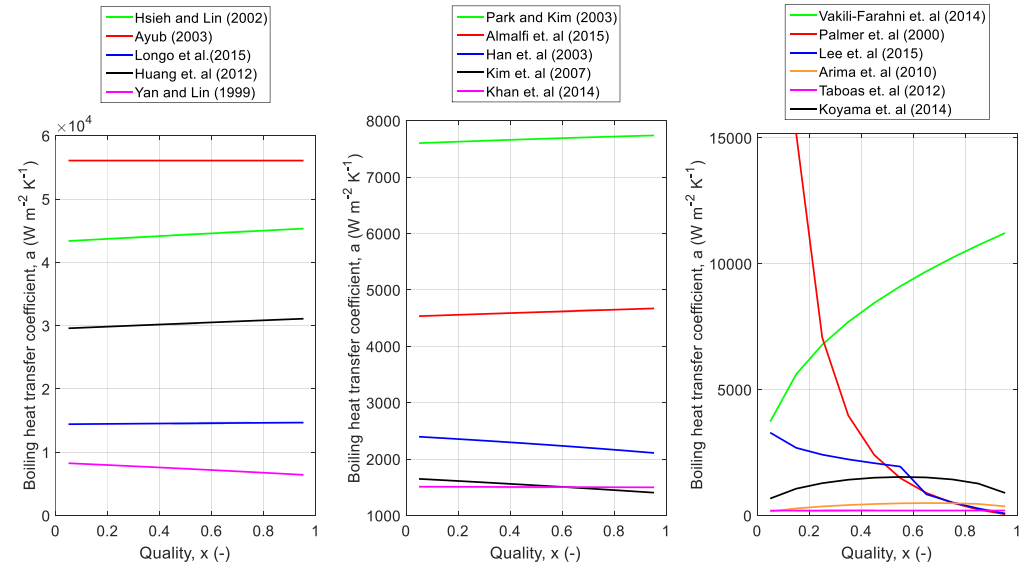
Hsieh and Lin (2002)
Ayub (2003)
Longo et al.(2015)
Huang et. al (2012)
Yan and Lin (1999)
Park and Kim (2003)
Almalfi et. al (2015)
Han et. al (2003)
Kim et. al (2007)
Khan et. al (2014)
Vakili-Farahni et. al (2014)
Palmer et. al (2000)
Lee et. al (2015)
Arima et. al (2010)
Taboas et. al (2012)
Koyama et. al (2014)
Boiling heat transfer coefficient, a (W m-2 K-1)
Quality, x (-)

(a)

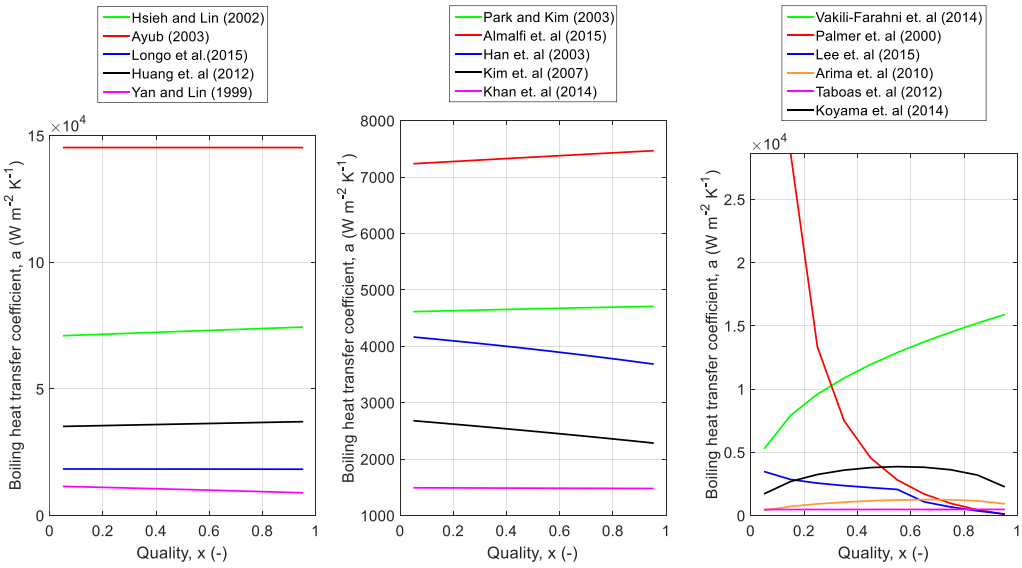
Hsieh and Lin (2002)
Ayub (2003)
Longo et al.(2015)
Huang et. al (2012)
Yan and Lin (1999)
Park and Kim (2003)
Almalfi et. al (2015)
Han et. al (2003)
Kim et. al (2007)
Khan et. al (2014)
Vakili-Farahni et. al (2014)
Palmer et. al (2000)
Lee et. al (2015)
Arima et. al (2010)
Taboas et. al (2012)
Koyama et. al (2014)
Boiling heat transfer coefficient, a (W m-2 K-1)
Quality, x (-)

(b)

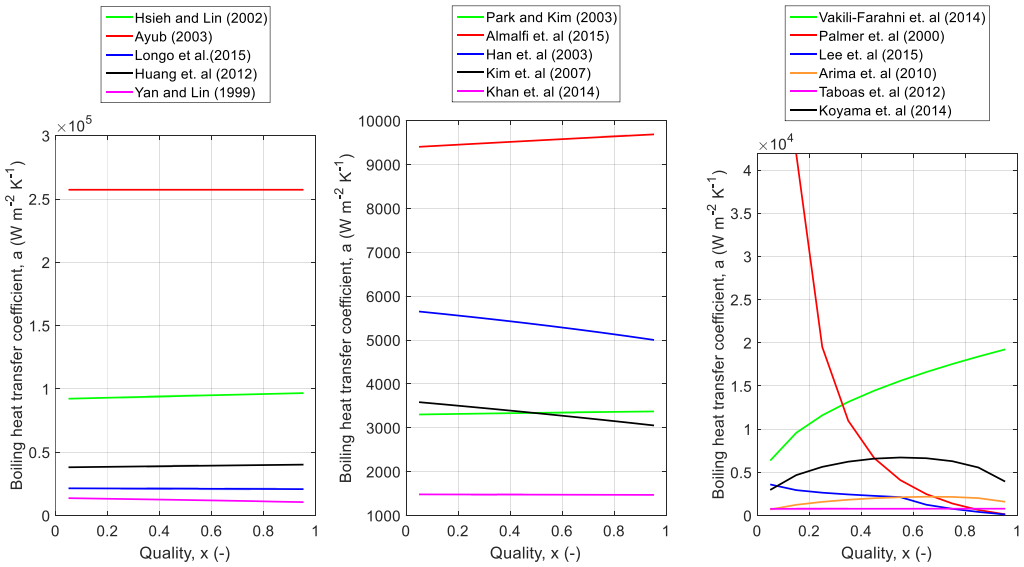

(c)

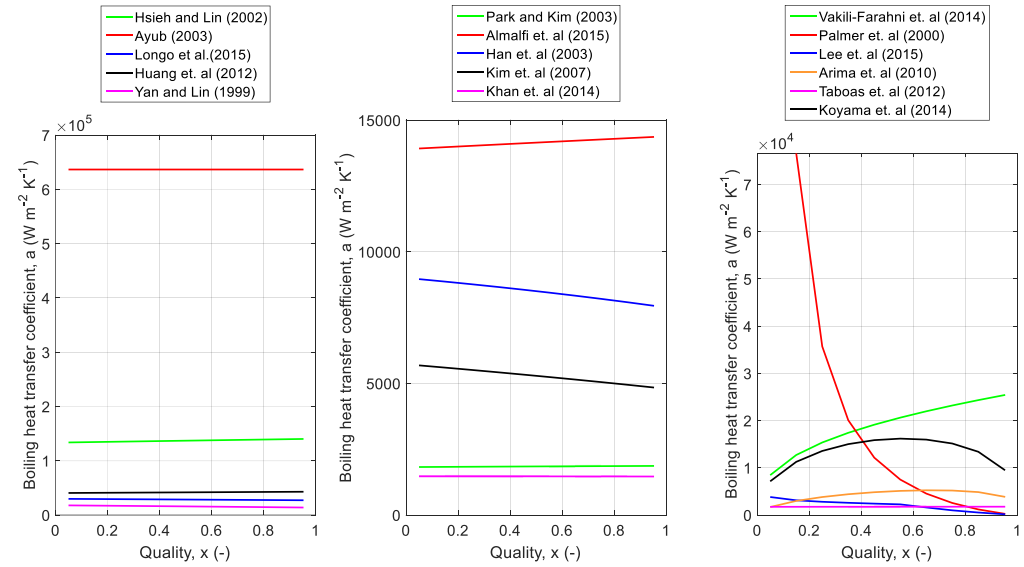

(d)

Fig. 3.1. Overview of boiling heat transfer coefficient predictions for R245ca with (a) Re=157.7, (b) Re=500, (c) Re=1000 and (d) Re=3000.

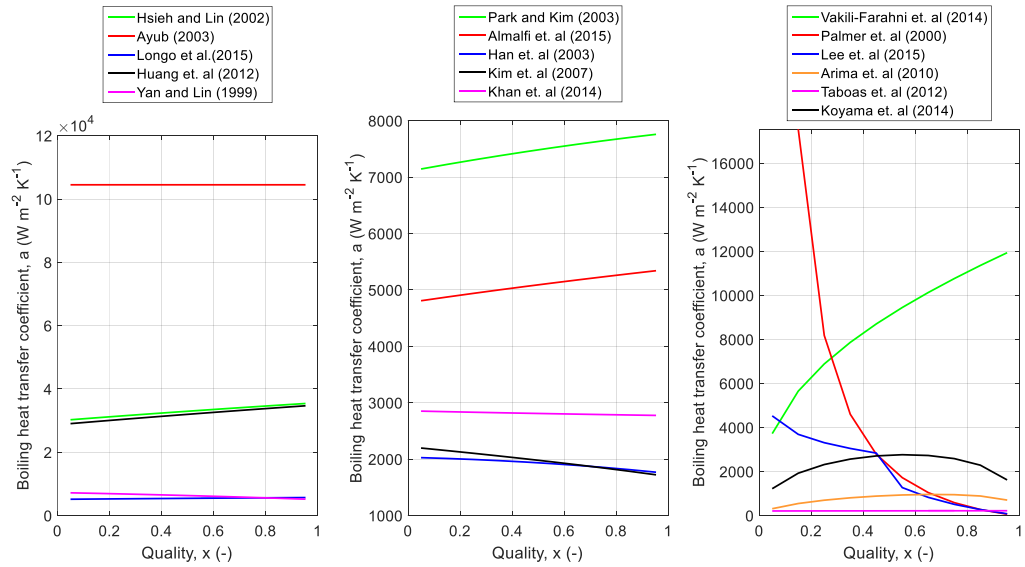
Hsieh and Lin (2002)
Ayub (2003)
Longo et al.(2015)
Huang et. al (2012)
Yan and Lin (1999)
Park and Kim (2003)
Almalfi et. al (2015)
Han et. al (2003)
Kim et. al (2007)
Khan et. al (2014)
Vakili-Farahni et. al (2014)
Palmer et. al (2000)
Lee et. al (2015)
Arima et. al (2010)
Taboas et. al (2012)
Koyama et. al (2014)
Boiling heat transfer coefficient, a (W m-2 K-1)
Quality, x (-)

(a)

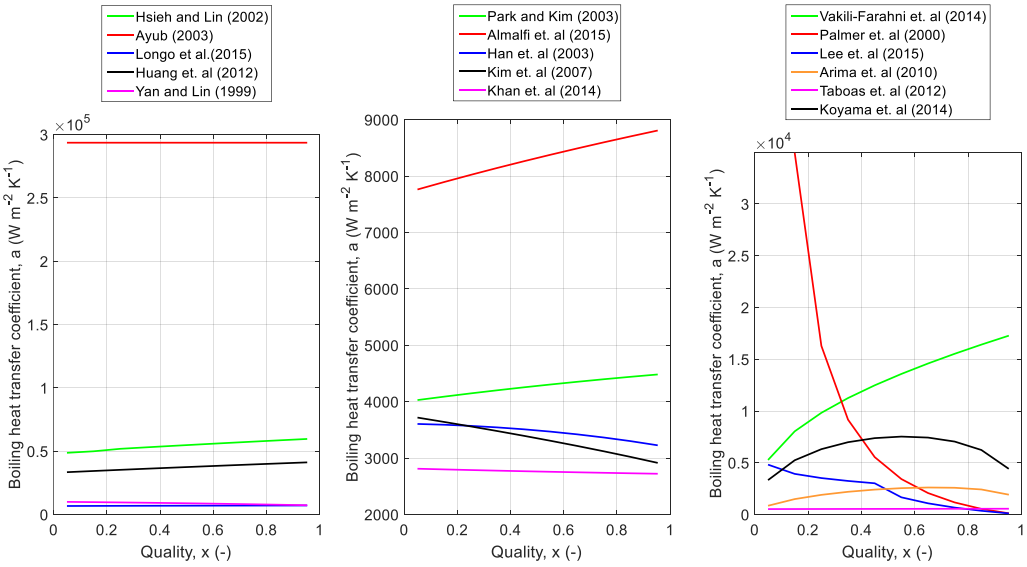
Hsieh and Lin (2002)
Ayub (2003)
Longo et al.(2015)
Huang et. al (2012)
Yan and Lin (1999)
Park and Kim (2003)
Almalfi et. al (2015)
Han et. al (2003)
Kim et. al (2007)
Khan et. al (2014)
Vakili-Farahni et. al (2014)
Palmer et. al (2000)
Lee et. al (2015)
Arima et. al (2010)
Taboas et. al (2012)
Koyama et. al (2014)
Boiling heat transfer coefficient, a (W m-2 K-1)
Quality, x (-)

(b)

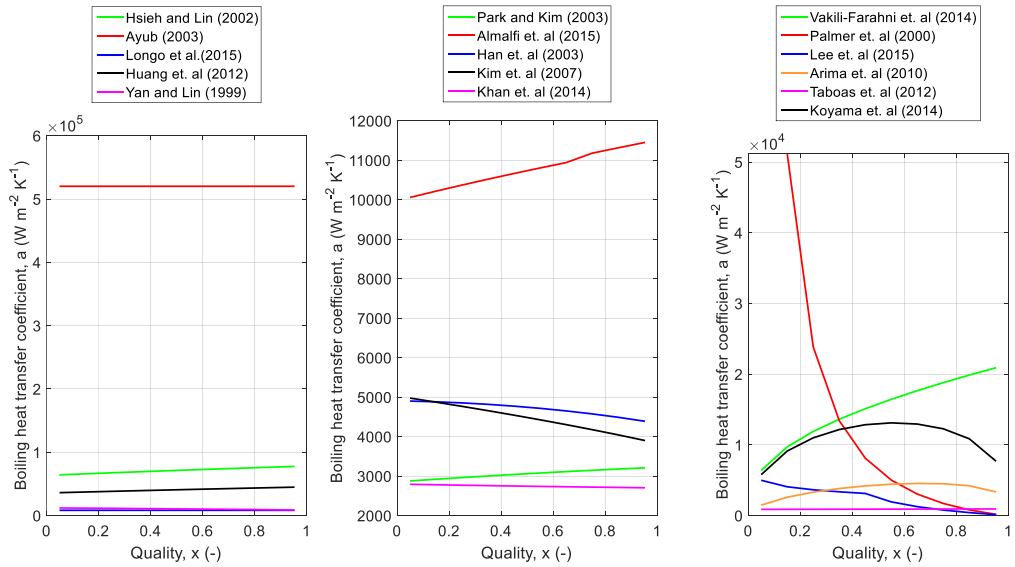

(c)

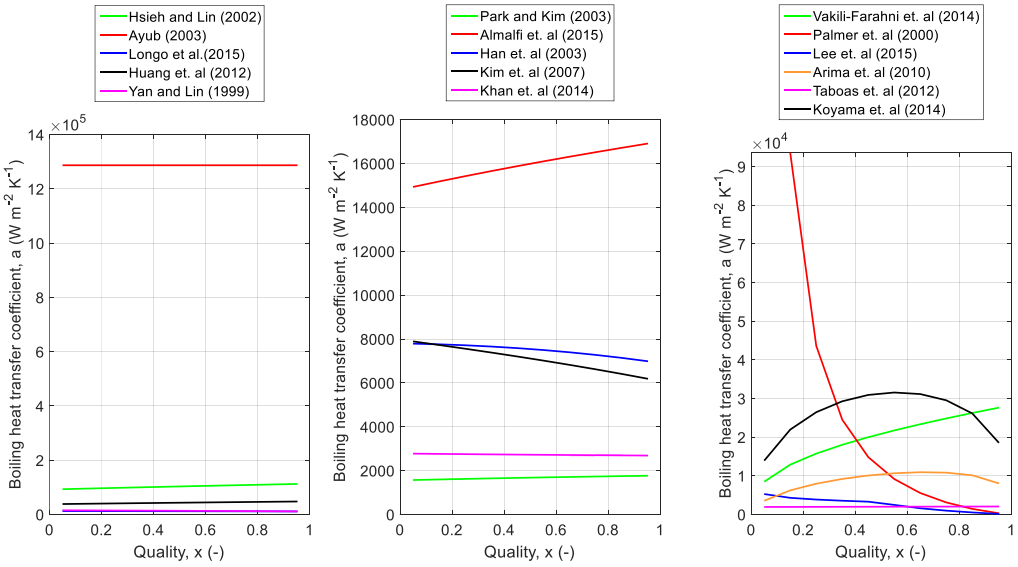

(d)

Fig. 3.2. Overview of boiling heat transfer coefficient predictions for Cyclopentane with (a) Re=143, (b) Re=500, (c) Re=1000 and (d) Re=3000.

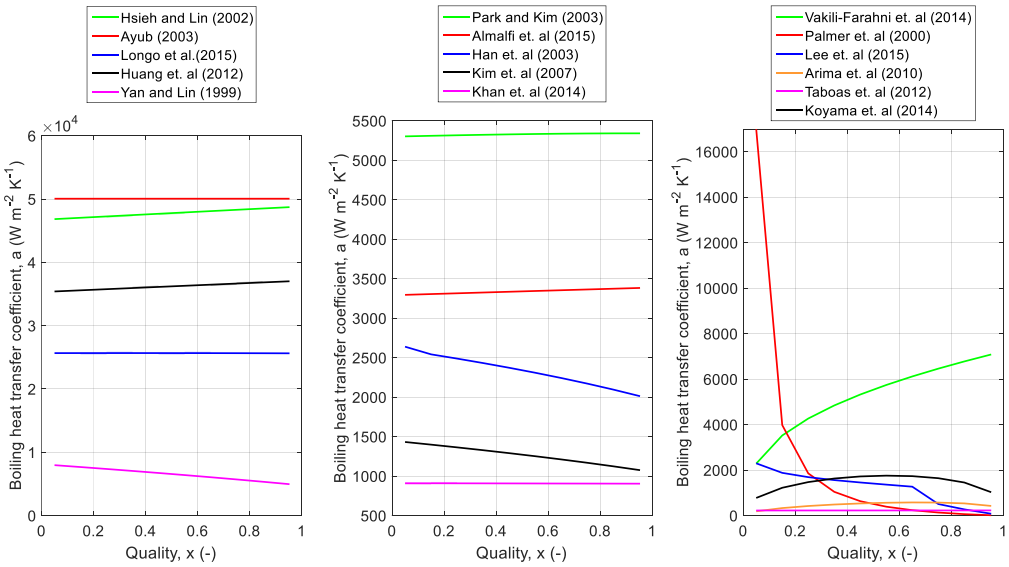
Hsieh and Lin (2002)
Ayub (2003)
Longo et al.(2015)
Huang et. al (2012)
Yan and Lin (1999)
Park and Kim (2003)
Almalfi et. al (2015)
Han et. al (2003)
Kim et. al (2007)
Khan et. al (2014)
Vakili-Farahni et. al (2014)
Palmer et. al (2000)
Lee et. al (2015)
Arima et. al (2010)
Taboas et. al (2012)
Koyama et. al (2014)
Boiling heat transfer coefficient, a (W m-2 K-1)
Quality, x (-)

(a)

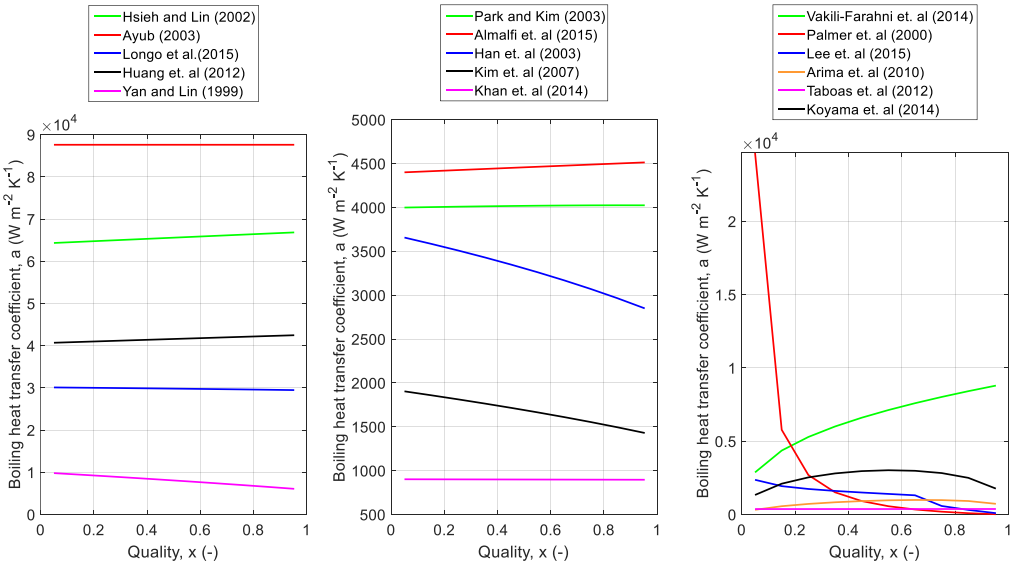
Hsieh and Lin (2002)
Ayub (2003)
Longo et al.(2015)
Huang et. al (2012)
Yan and Lin (1999)
Park and Kim (2003)
Almalfi et. al (2015)
Han et. al (2003)
Kim et. al (2007)
Khan et. al (2014)
Vakili-Farahni et. al (2014)
Palmer et. al (2000)
Lee et. al (2015)
Arima et. al (2010)
Taboas et. al (2012)
Koyama et. al (2014)
Boiling heat transfer coefficient, a (W m-2 K-1)
Quality, x (-)

(b)

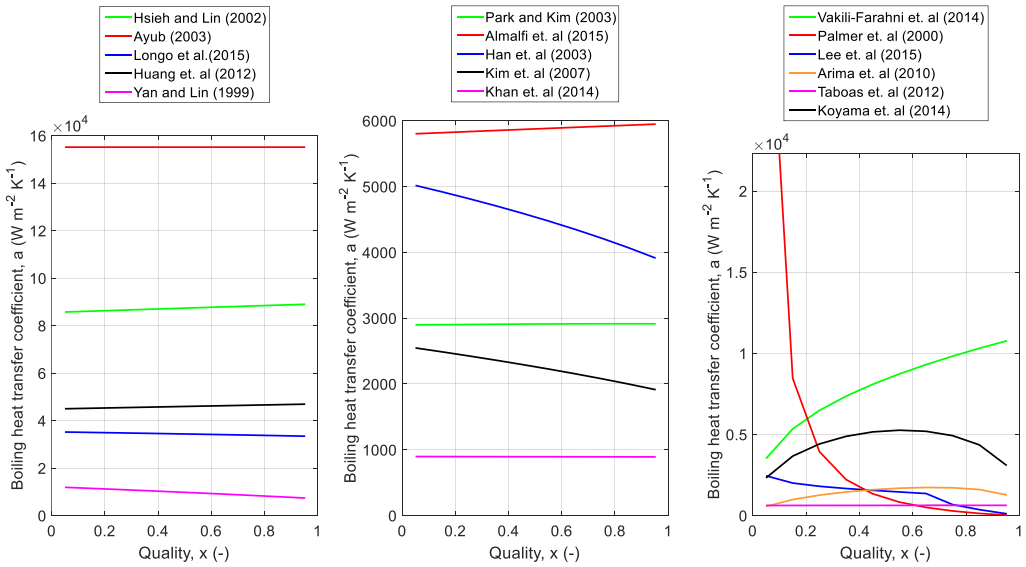

(c)

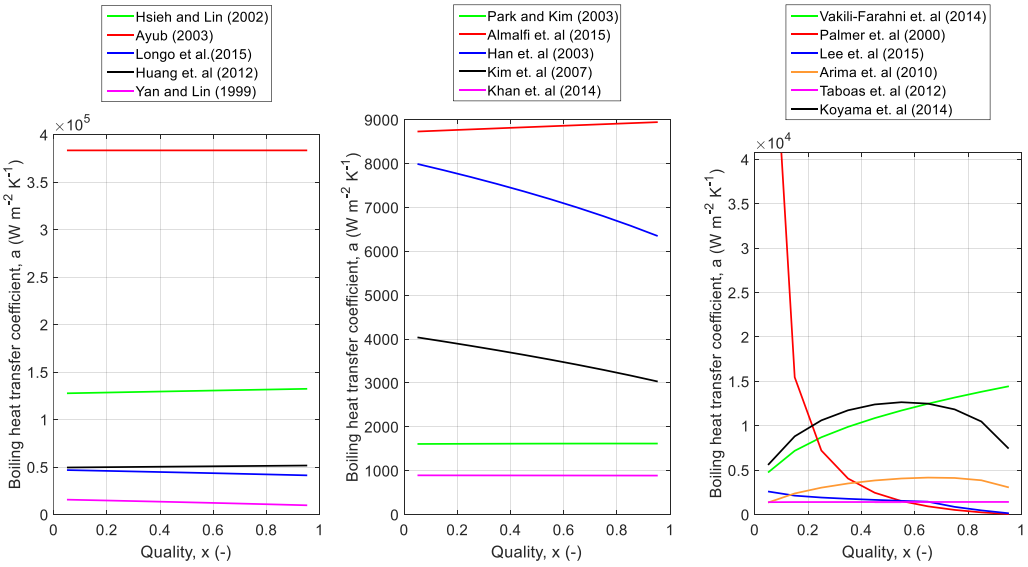

(d)

Fig. 3.3. Overview of boiling heat transfer coefficient predictions for R1234ze with (a) Re=254, (b) Re=500, (c) Re=1000 and (d) Re=3000.

3.2. Condensation

The Nusselt correlation used in the cold side of the plate heat exchanger in equation (2.17) is Donowski's equation shown in Table 3-3 in single phase correlations.

For the hot side the Nusselt number used in equation (2.30) is calculated using various correlations shown in Table 3-2.

The correlations listed in Table 3-2 are introduced to the condenser's modeling, which was presented at Chapter 2.2 and the heat transfer coefficient for the hot side is calculated.

The analysis is carried out using three different, condensing fluids: R245ca, R1234ze and Cyclopentane. For each fluid the heat transfer coefficient is calculated for various Reynolds numbers, to take in to account the flow's turbulence. For the first set of calculations, of each fluid, the parameters are set as default, with the mass flow of the cold side $m_c = 0.2\ kg/sec$ and the hot side mass flow $m_h = 0.07\ kg/sec$. The inlet temperatures are set at 15 °C for the cold side and at 100 °C for the hot side. Three more calculations are carried out, changing the mass flows to increase the Reynolds number to 500, 1000 and 3000. Below the calculations results are shown in heat transfer coefficient ($a\left[\frac{W}{m^2K}\right]$)- Quality ($x$) diagrams. In the case of R245ca the hot side inlet temperature was set at 85°C and the cold side inlet temperature at 12°C, while for R1234ze the hot side inlet temperature was set at 80°C and the cold side inlet temperature at 12°C, to reach a similar pinch point.

The key conclusions by the analysis are summarized below:

- Thonon and Bontemps' is the only correlation producing results in decreasing slope.

With the use of R245ca as working fluid:

- Winkelmann's, Sho's, Shi's and Kuo's correlations produce similar results for all the Re numbers.
- Joakr's and Wang and Zhao's calculations are proportionate to the Re number in each case.
- Shah's results in a curve's slope increase with the increase of the Reynolds number.
- Mancin's correlation produces complex number results, hence they are excluded from the figures. The same occurs with the use of R123ze.
- Palmer's results in a curve with zero slope in each scenario.
- Longo's result displays a discontinuity due to the use of two equations for its calculation.

With the use of Cyclopen:

- Heat transfer coefficents increase, in comparison to the use of other working fluids, for all the correlations, except Jokar's.

On the other hand with the use of R245ca Soontarapiromsook's correlation seems to overpredict, as does Zhang's correlation with the use of R1234ze and Cyclopen.

Table 3-2 Condensation heat transfer coefficient correlations

Correlation	**Working fluid**	**Range**	**Reference**
$Nu = 0.023 Re_L^{0.8} Pr_L^{0.4} \left[(1-x)^{0.8} + \frac{3.8 x^{0.76} (1-x)^{0.04}}{p_{red}^{0.38}} \right]$	Various refrigerants		Shah (modified) [30]
$Nu = 4.118 {Re_{eq}}^{0.4} {Pr_L}^{1/3}$	R134a	$500 < Re_{eq} < 1{,}000$ $60 \leq G \leq 120$	Yan et. al [31]
$a = 1.564 a_{lo} {Re_{eq}}^{-0.76}$ $a_{lo} = 0.347 \left(\frac{\lambda}{D_h}\right) Re^{0.653} Pr^{1/3}$	Hydrocarbons	$100 < Re_{eq} < 2{,}000$ $(\varphi = 45°)$	Thonon and Bontemps [32]
$Nu = Ge_1 {Re_{eq}}^{Ge_2} {Pr_L}^{1/3}$ $Ge_1 = 11.22 \left(\frac{\Lambda}{D_h}\right)^{-2.83} \left(\frac{\pi}{2} - \varphi\right)^{-4.5}$ $Ge_2 = 0.35 \left(\frac{\Lambda}{D_h}\right)^{0.23} \left(\frac{\pi}{2} - \varphi\right)^{1.48}$	R410A, R22	$10 < G < 35$ $4.7 < q < 5.3$	Han et. al [33]
$a = 0.943 \Phi \left[\frac{\lambda_L^3 \rho_L^3 g h_{fg}}{\mu_L L_p (T_{sat} - T_{wall})} \right]^{1/4}, Re_{eq} < 1{,}600$ $a = a_{sat} + F \left(a_L + \frac{c_p q_{flux}}{h_{fg}} \right), Re_{eq} \geq 1{,}600$ $a_{sat} = 1.875 \Phi \, (\lambda_L / D_h) Re_{eq}^{0.445} Pr_L^{1/3}$ $a_L = 0.2267 \, (\lambda_v / D_h) Re_v^{0.631} Pr_v^{1/3}$, $F = \frac{T - T_{sat}}{T_{sat} - T_{wall}}$	R134a		Longo et. al [34, 35]
$a = \left(\frac{k_l}{D_h}\right) Nu_l^{0.387} \varphi_l^{0.0824} Ga^{0.346} P_{red}^{1.5} \omega^{1.5}$, $(R22, R290, R290/600a)$ $a = \left(\frac{k_l}{D_h}\right) Nu_l^{0.298} Ga^{0.346} P_{red}^{1.5} \omega^{1.5}, (R32/R152a)$	R22, R290, R290/600a, R32/R152a	$13 < Re_{eq} < 230$ $1.6 \leq G \leq 19$ $1.3 \leq q'' \leq 8.3$	Palmer et. al [17]

Where, $\begin{cases} Nu_l = 0.16Re_l^{0.89}Pr_l^{0.4}, Ga = \frac{\rho_l(\rho_l-\rho_g)gD_h^3}{\mu_l^2} \\ \omega = -log_{10}\left(\frac{p}{p_{cr}}\right) \end{cases}$			
$Nu = 0.2092Re_l^{0.78}Pr_l^{\frac{1}{3}}\left(\frac{\mu_m}{\mu_w}\right)^{0.14}(0.25Co^{-0.45}Fr_l^{0.25} + 75Bo^{0.75})$ Where, $Co = \left(\frac{\rho_g}{\rho_l}\right)^{0.5}\left(\frac{1-x_m}{x_m}\right)^{0.8}, Fr_l = \frac{G^2}{\rho_l^2 gD_h}$	R410A	$50 \le G \le 150$ $10 \le q'' \le 20$ $0.1 \le x_m \le 0.9$ $1.44 \le P_m \le 1.95$	Kuo et. al [36]
$a = \left(a_{Nu}^2 + a_{shear}^2\right)^{0.5}[1.074(T_{sat} - T_w)^{-0.386}]$ Where, $\begin{cases} a_{Nu} = 0.943\left[\frac{\rho_l(\rho_l-\rho_g)g\gamma k_l^3}{\mu_l L_p(T_{sat}-T_w)}\right]^{0.25} \\ a_{shear} = a_l\left[1 + 1.128x^{0.817}\left(\frac{\rho_l}{\rho_g}\right)^{0.3685}\left(\frac{\mu_l}{\mu_g}\right)^{0.2363}\left(1-\frac{\mu_g}{\mu_l}\right)^{2.144}Pr^{-0.1}\right] \end{cases}$	R410A, R407C	$15 \le G \le 40$ $0.01 < x < 0.58$	Mancin et. al [37]
$Nu = 4.3375Re_{eq}^{0.5383}Pr_L^{0.333}Bo^{-0.3872}$	R134a, R1234ze(E), R245fa, R1233zd(E)	$16 \le G \le 90$ $4 \le q'' \le 57.4$ $29.7 \le T_{sat} \le 71$	Zhang et. al [38]
$Nu = 0.00115\left(\frac{Re_L}{Ja}\right)^{0.983}Pr_L^{0.333}\left(\frac{\rho_L}{\rho_G}\right)^{0.248}$ Where, $Ja = \frac{Cp_L(T_{sat}-T_{wall})}{\Delta h_{LG}+0.68Cp_L(T_{sat}-T_{wall})}$	n/a		Wang and Zhao [39]
$Nu = 94Co^{-0.46}Pr_L^{0.333}$ Where, $Co = \left(\frac{\rho_g}{\rho_l}\right)^{0.5}\left(\frac{1-x_m}{x_m}\right)^{0.8}$	R134a	$0.07 < Co < 0.28$ $6.9 \le q'' \le 51$ $28.2 \le T_{sat} \le 39.9$	Winkelmann [40]
$Nu = 2.337Re_{eq}^{1.024}Re_{lo}^{-0.294}Pr_L^{0.333}Bo_{eq}^{0.361}$	R1233zd(E)	$13 \le G \le 23.8$ $2.5 \le q'' \le 4.5$ $38.6 \le T_{sat} \le 51.5$	Shon et. al [41]

$Nu = 3.371 Re_L^{0.55} Pr_L^{0.3} Ja^{-1.05} \left(\frac{G^2}{\rho_L^2 Cp_L (T_{sat} - T_{wall})}\right)^{0.25} \left(\frac{\rho_L \sigma}{\mu_L G}\right)^{0.05} \left(\frac{\rho_L}{\rho_L - \rho_G}\right)^2$ Where, $Ja = \frac{Cp_L (T_{sat} - T_{wall})}{\Delta h_{LG} + 0.68 Cp_L (T_{sat} - T_{wall})}$	n/a		Jokar et. al [42]
$a = a_{lo}\left((1-x)^{0.8} + \frac{3.00388 x^{1.296}}{(1-x)^{0.496}\left(\frac{P_{sat}}{P_{cr}}\right)^{0.648}}\right)$ Where, $a_{lo} = 0.347\left(\frac{k_l}{D_h}\right) \mathrm{Re}_{\mathrm{LO}}^{0.653} Pr_L{}^{1/3}$	R134a	$22 \le G \le 65$ $11.5 \le q'' \le 35$ $16.2 \le T_{sat} \le 29$	Shi et. al [43]
$Nu = 5.095 \cdot 10^{-6} Re_{eq}^{0.566} Pr_L^{9.753} \left(\frac{\delta}{D_h}\right)^{0.121}$	R134a	$61 \le G \le 89$ $5 \le q'' \le 15$ $40 \le T_{sat} \le 50$	Soontarapiromsook et al. [44]

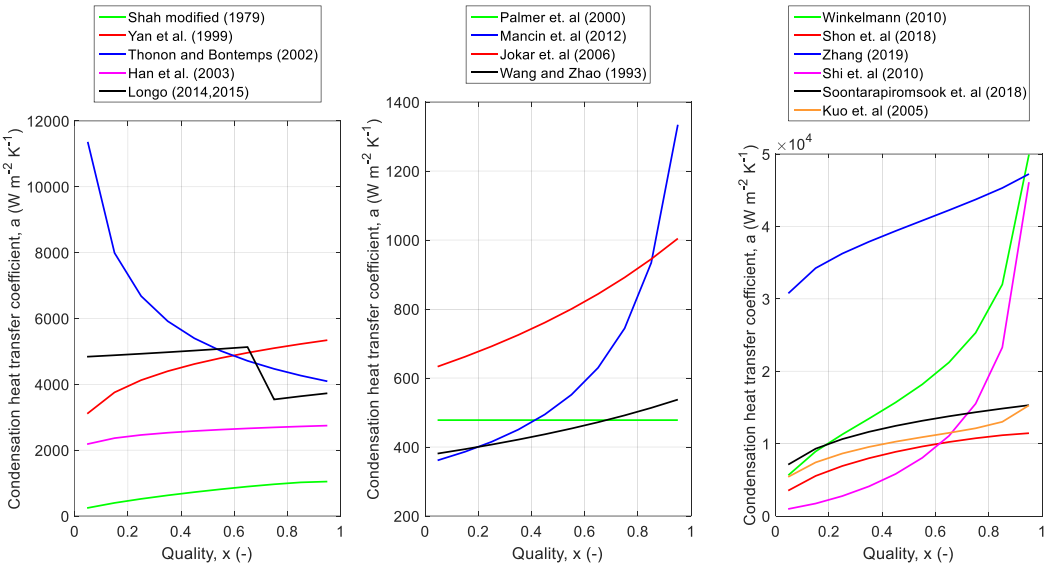
Shah modified (1979)
Yan et al. (1999)
Thonon and Bontemps (2002)
Han et al. (2003)
Longo (2014,2015)
Palmer et. al (2000)
Mancin et. al (2012)
Jokar et. al (2006)
Wang and Zhao (1993)
Winkelmann (2010)
Shon et. al (2018)
Zhang (2019)
Shi et. al (2010)
Soontarapiromsook et. al (2018)
Kuo et. al (2005)
Condensation heat transfer coefficient, a (W m-2 K-1)
Quality, x (-)
×10^4

(a)

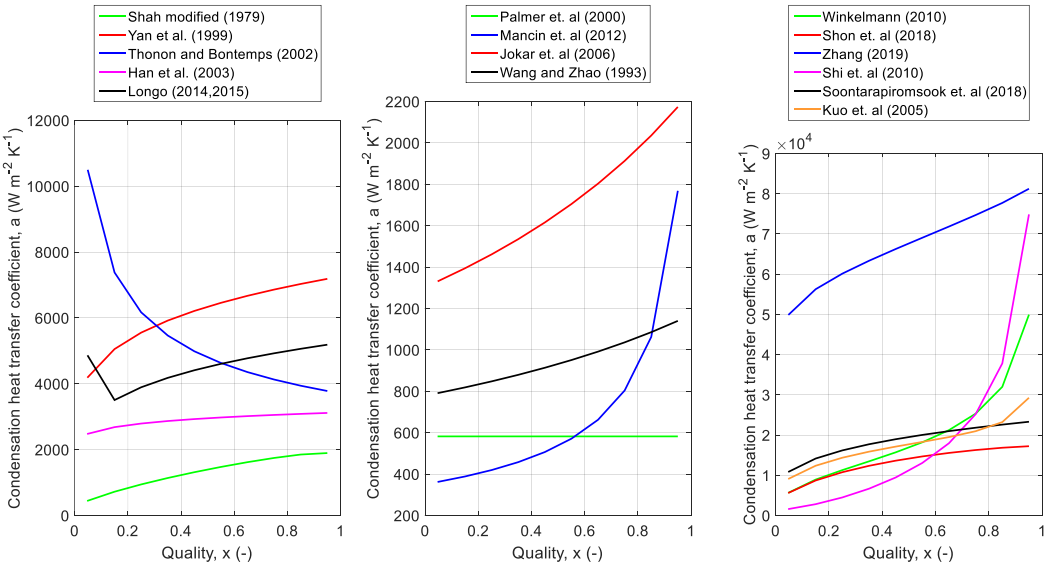
Shah modified (1979)
Yan et al. (1999)
Thonon and Bontemps (2002)
Han et al. (2003)
Longo (2014,2015)
Palmer et. al (2000)
Mancin et. al (2012)
Jokar et. al (2006)
Wang and Zhao (1993)
Winkelmann (2010)
Shon et. al (2018)
Zhang (2019)
Shi et. al (2010)
Soontarapiromsook et. al (2018)
Kuo et. al (2005)
Condensation heat transfer coefficient, a (W m-2 K-1)
Quality, x (-)
×10^4

(b)

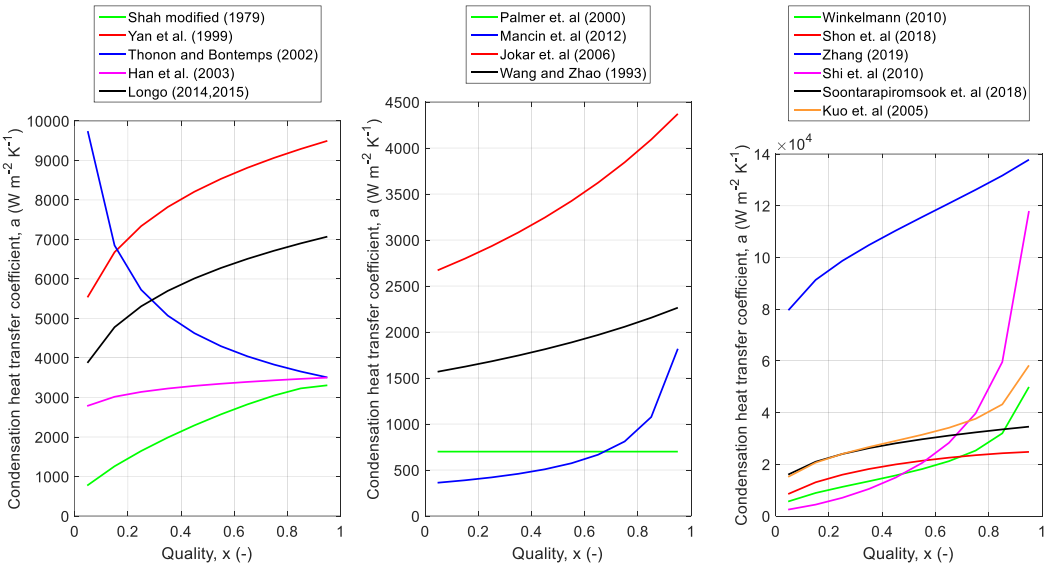

(c)

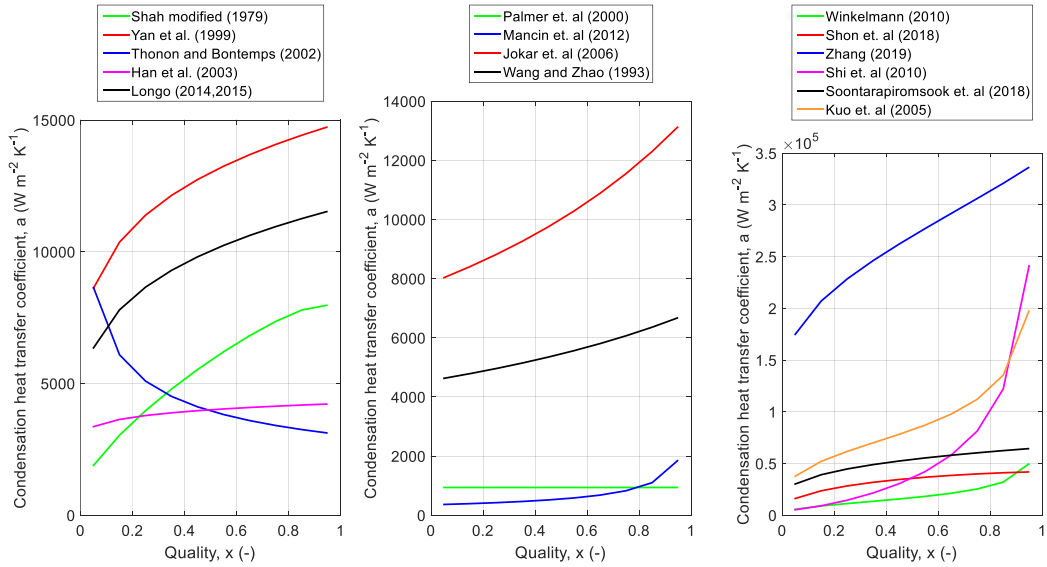

(d)

Fig. 3.4. Overview of condensation heat transfer coefficient predictions for Cyclopentane with (a) Re=237.7, (b) Re=500, (c) Re=1000 and (d) Re=3000.

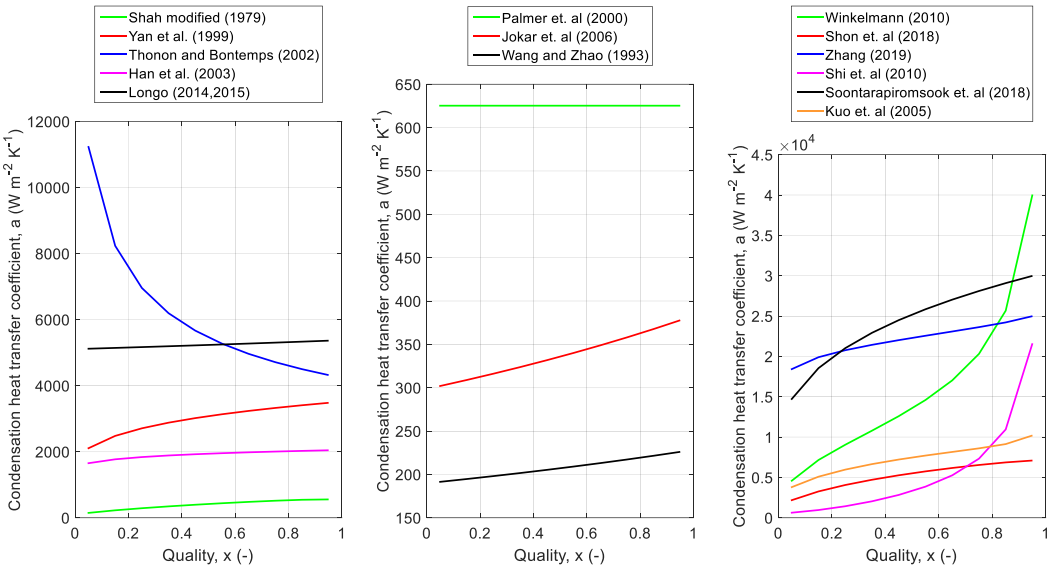
Shah modified (1979)
Yan et al. (1999)
Thonon and Bontemps (2002)
Han et al. (2003)
Longo (2014,2015)
Palmer et. al (2000)
Jokar et. al (2006)
Wang and Zhao (1993)
Winkelmann (2010)
Shon et. al (2018)
Zhang (2019)
Shi et. al (2010)
Soontarapiromsook et. al (2018)
Kuo et. al (2005)
Condensation heat transfer coefficient, a (W m-2 K-1)
Quality, x (-)
×10^4

(a)

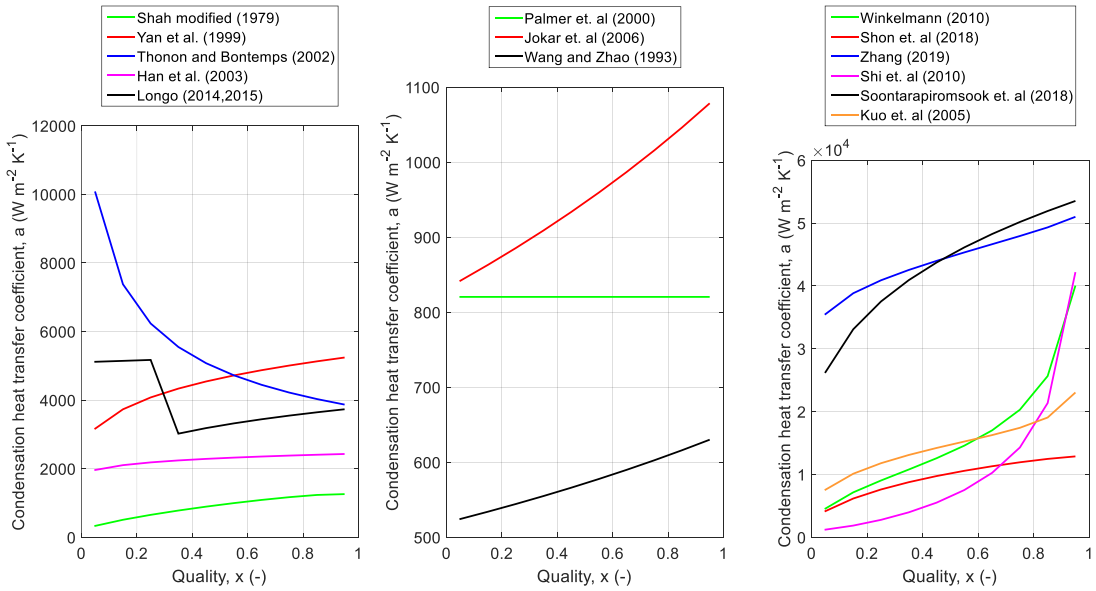
Shah modified (1979)
Yan et al. (1999)
Thonon and Bontemps (2002)
Han et al. (2003)
Longo (2014,2015)
Palmer et. al (2000)
Jokar et. al (2006)
Wang and Zhao (1993)
Winkelmann (2010)
Shon et. al (2018)
Zhang (2019)
Shi et. al (2010)
Soontarapiromsook et. al (2018)
Kuo et. al (2005)
Condensation heat transfer coefficient, a (W m-2 K-1)
Quality, x (-)
×10^4

(b)

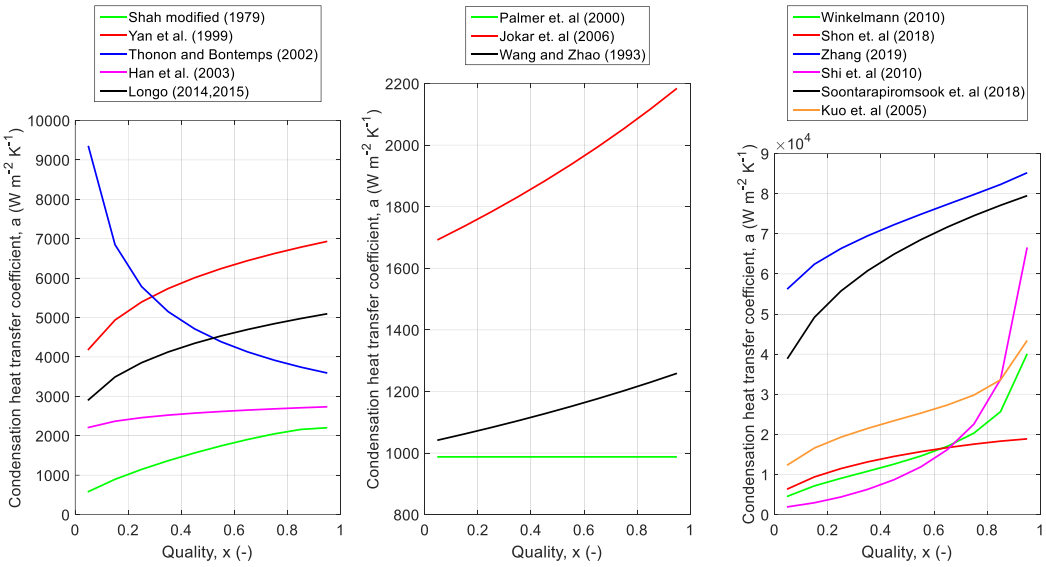

(c)

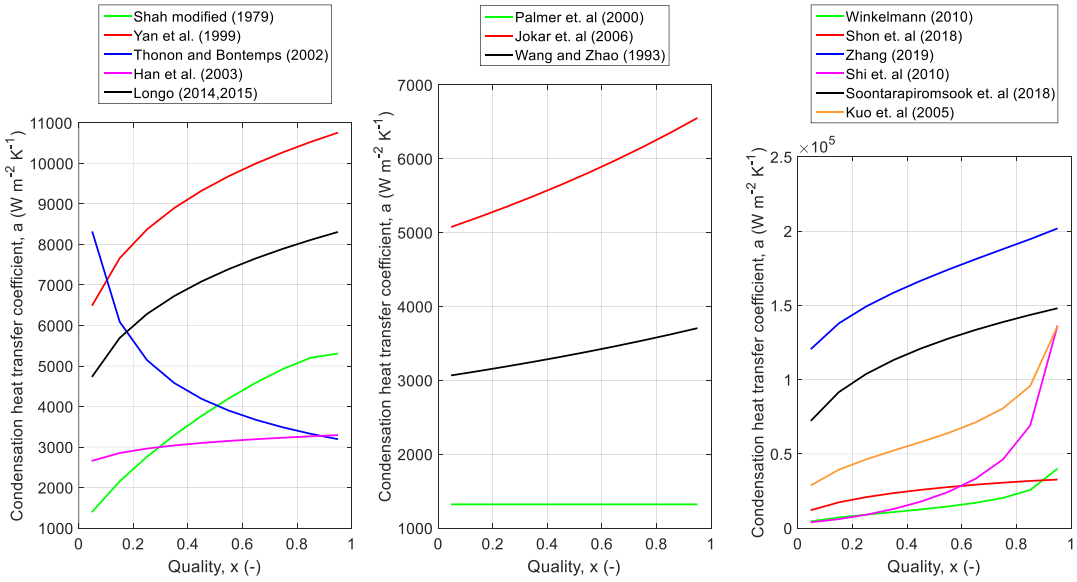

(d)

Fig. 3.5. Overview of condensation heat transfer coefficient predictions for R245ca with (a) Re=179, (b) Re=500, (c) Re=1000 and (d) Re=3000.

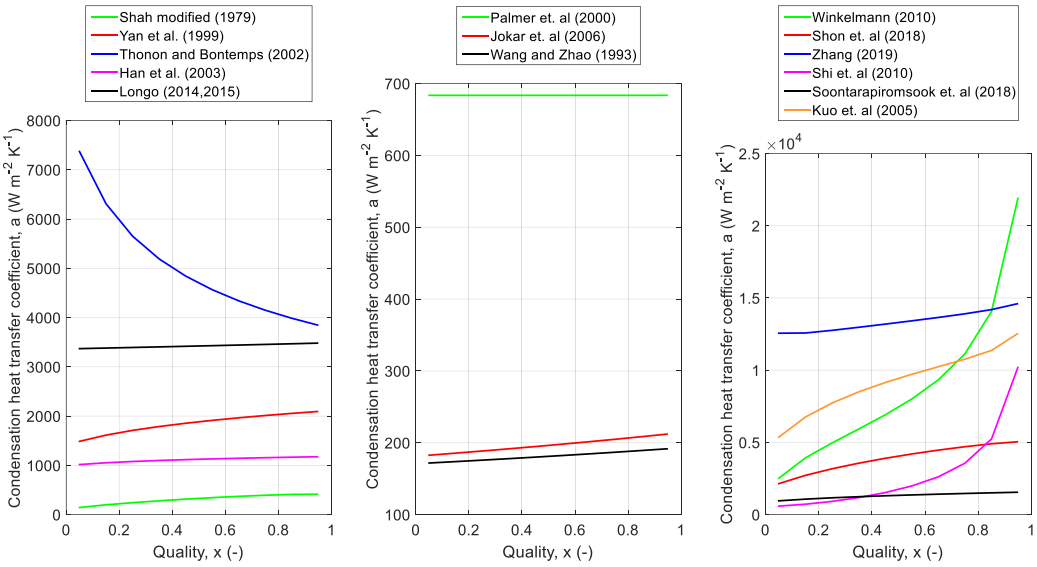
Shah modified (1979)
Yan et al. (1999)
Thonon and Bontemps (2002)
Han et al. (2003)
Longo (2014,2015)
Palmer et. al (2000)
Jokar et. al (2006)
Wang and Zhao (1993)
Winkelmann (2010)
Shon et. al (2018)
Zhang (2019)
Shi et. al (2010)
Soontarapiromsook et. al (2018)
Kuo et. al (2005)
Condensation heat transfer coefficient, a (W m-2 K-1)
Quality, x (-)
×10^4

(a)

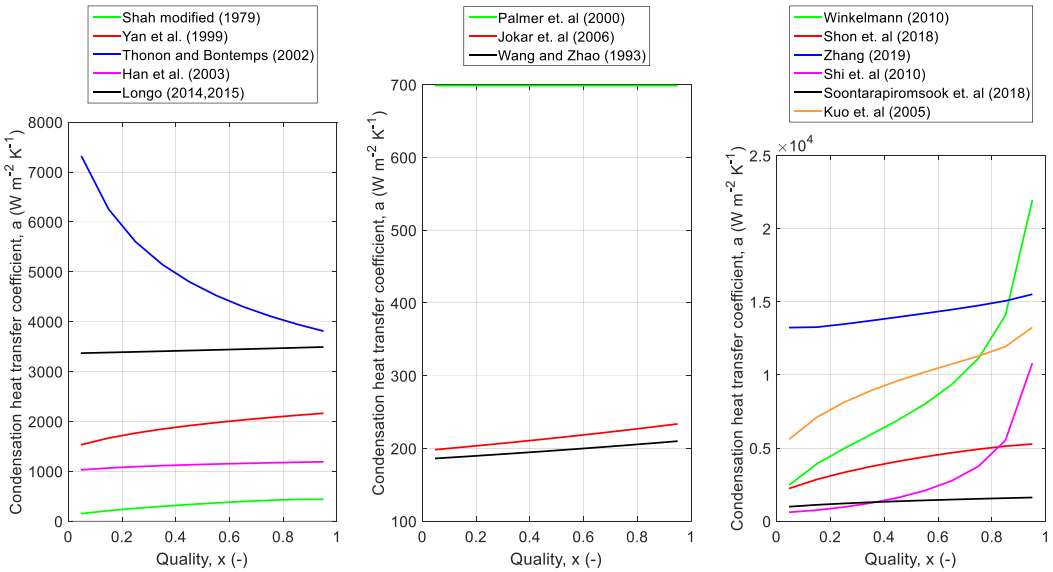
Shah modified (1979)
Yan et al. (1999)
Thonon and Bontemps (2002)
Han et al. (2003)
Longo (2014,2015)
Palmer et. al (2000)
Jokar et. al (2006)
Wang and Zhao (1993)
Winkelmann (2010)
Shon et. al (2018)
Zhang (2019)
Shi et. al (2010)
Soontarapiromsook et. al (2018)
Kuo et. al (2005)
Condensation heat transfer coefficient, a (W m-2 K-1)
Quality, x (-)
×10^4

(b)

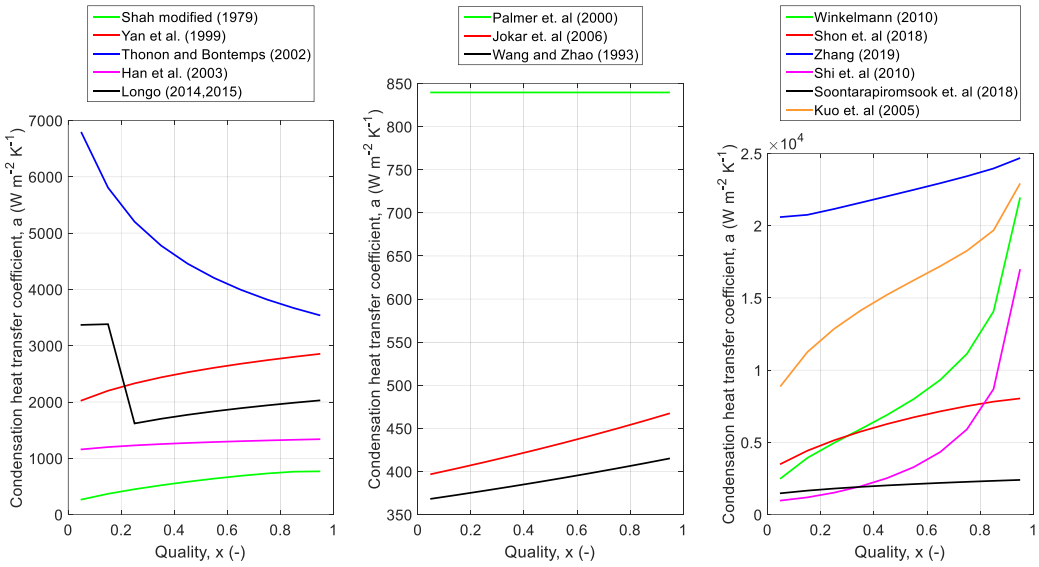

(c)

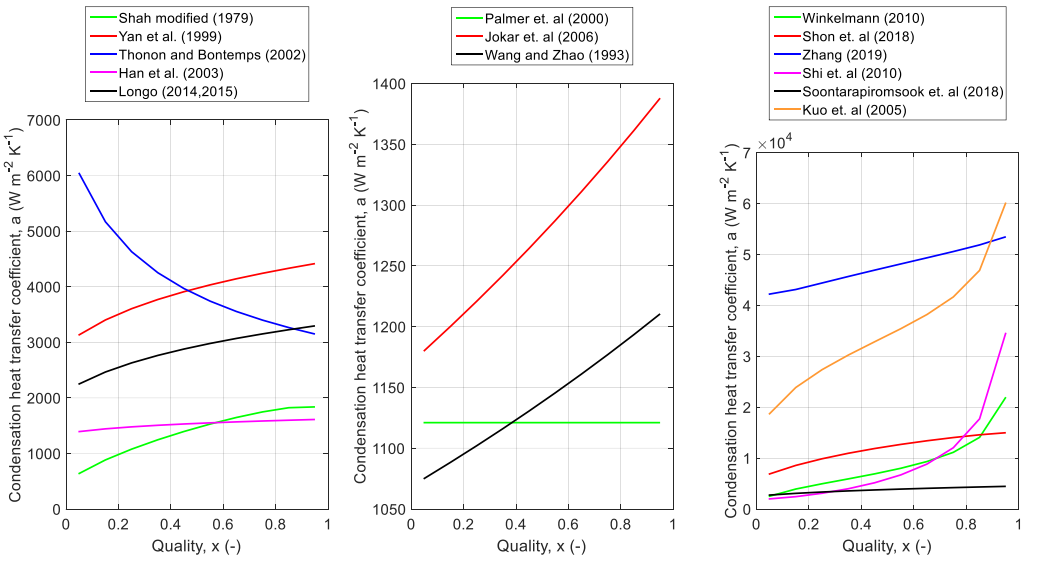

(d)

Fig. 3.6. Overview of condensation heat transfer coefficient predictions for R1234ze with (a) Re=462, (b) Re=500, (c) Re=1000 and (d) Re=3000.

3.3. Single Phase heat transfer

The correlations used in equations (2.16) and (2.17) for the calculation of the Nusselt number, will be shown in the following table. Considering that single phase heat transfer is taking place, these correlations will be used for both the hot and cold side.

The correlations shown in Table 3-3 are introduced to the condenser's modeling, which was presented at Chapter 2.3 and the heat transfer coefficient for both sides is calculated.

The analysis is conducted using three different fluids for the cold side: R245ca, R1234ze and Cyclopentane. For each fluid the heat transfer coefficient is calculated for various Reynolds numbers, to take in to account the flow's turbulence. For the first set of calculations, of each fluid, the parameters are set as default, with the mass flow of the cold side $m_c = 0.075\ kg/sec$ and the hot side mass flow $m_h = 0.5\ kg/sec$. The inlet temperatures are set at 90 ^oC for the cold side and at 200 ^oC for the hot side. Three more calculations are carried out, changing the mass flows to increase the Reynolds number to 500, 1000 and 3000. Below the calculations results are shown in heat transfer coefficient ($a\left[\frac{W}{m^2K}\right]$)- Re diagrams. In the case of R1234ze the hot side inlet temperature was set at 120^{o}C and the cold side inlet temperature at 50^{o}C. Also the cold side outlet temperature range was adjusted in orded to fit each case's inlet temperatures. The key conclusions of the analysis are summarized below:

- The discontinuity shown in some results is caused by the use of the $\left(\frac{\mu}{\mu_w}\right)$ ratio.
- All the results are proportional to the Re number and increase with it, except with the use of R1234ze, where Maslov and Kovalenko's correlation results seem to be relatively unaffected with the increase of the Re number.
- Use of Cyclopen seems to produce higher heat transfer coefficients
- Use of R1234ze seems to produces results with lower slopes (closer to zero).
- Hayes' correlation overpredicts the heat transfer phenomena on all cases.
- In general, the form and shape of the diagrams tends to be constant for all the scenarios.

Table 3-3 Single phase heat transfer coefficient correlations

Correlation	**Working fluid**	**Range**	**Reference**
$Nu = 1.67Re^{0.44}Pr^{0.5}, \quad 45 < Re < 300$ $Nu = 0.405Re^{0.7}Pr^{0.5}, \quad 300 < Re < 2{,}000$ $Nu = 0.84Re^{0.6}Pr^{0.5}, \quad 2{,}000 < Re < 20{,}000$	Electrolyte solutions	$\beta = 60°$	Focke [45]
$Nu = 0.768Re^{0.59}Pr^{0.4}$	n/a	$1{,}000 < Re < 40{,}000$ $30° < \beta < 80°$	Chisholm [46]
$Nu = 0.26437Re^{0.7152}Pr^{c}\left(\frac{\mu_{bulk}}{\mu_{wall}}\right)^{n}$, $n = \frac{0.3}{(Re+6)^{0.125}}$, $c = 0.333e^{6.4/(Pr+30)}$	Mineral Oil (NUTO H5)	$80 < Re$	Bogaert and Boles [47]
$Nu = 0.122(Pr)^{1/3}\left(\frac{\mu_{bulk}}{\mu_{wall}}\right)^{1/6}[\xi Re^2 \sin(2\varphi)]^{0.374}$, $\frac{1}{\sqrt{\xi}} = \frac{cos\varphi}{\sqrt{0.18tan\varphi + 0.36sin\varphi + \frac{\xi_0}{cos\varphi}}} + \frac{1-cos\varphi}{\sqrt{3.8\xi_1}}$ $\xi_1 = \frac{597}{Re} + 3.85$, $\xi_0 = \frac{64}{Re}$, $Re < 2{,}000$ $\xi_1 = \frac{39}{Re^{0.229}}, \xi_0 = (1.8 \cdot logRe - 1{,}5)^{-2}$, $Re \geq 2{,}000$	n/a	$25° < \beta < 65°$	Walraven [48]
$Nu = 0.2121Pr^{1/3}Re^{0.78}\left(\frac{\mu_{bulk}}{\mu_{wall}}\right)^{0.14}$	Water		Yan and Lin [13]
$Nu = 0.2875Pr^{1/3}Re^{0.78}$	R134a	$Re \geq 200$	Donowski [49]
$Nu = 0.724\left(\frac{6\beta}{\pi}\right)^{0.646} Re^{0.583}Pr^{1/3}$	n/a	$Re > 1000$ $\frac{\pi}{6} \leq \beta \leq \frac{4\pi}{6}$	Chisholm and Wanniarachchi [50]
$Nu = 0.295Re^{0.64}Pr^{0.32}\left(\frac{\pi}{2} - \beta\right)^{0.09}$	Water		Kim [51]

$Nu = j_{Nu} Pr^{\frac{1}{3}} \left(\frac{\mu}{\mu_w}\right)^{0.17}$ *Where,* $j_{Nu} = \sqrt[3]{j_{Nu,l}^3 + j_{Nu,t}^3}$, $j_{Nu,l} = \frac{3.65}{\left(90 - \frac{180\beta}{\pi}\right)^{0.445}} Re^{0.339}$, $j_{Nu,t} = \frac{12.6}{\left(90 - \frac{180\beta}{\pi}\right)^{1.142}} Re^{0.646 + 0.00111\left(90 - \frac{180\beta}{\pi}\right)}$	n/a		Wanniarachchi [52]
$Nu = 0.248 Re^{0.7} Pr^{0.4}$	n/a	$1{,}450 \leq Re \leq 11{,}460$ $2.5 \leq Pr \leq 5.0$	Talik et. al [54]
$Nu = 0.295 \beta^{0.09} Re^{0.64} Pr^{0.32}$	n/a	$2{,}000 \leq Re$ $2 \leq Pr \leq 6$	Han et. al [15]
$Nu = \left(\frac{0.0161\beta}{\beta_{max}} + 0.1298\right) Re^{\frac{0.198\beta}{\beta_{max}} + 0.6398} Pr^{0.35} \left(\frac{\mu}{\mu_w}\right)^{0.14}$	n/a	$500 \leq Re \leq 2{,}500$ $3.5 \leq Pr \leq 6.5$	Khan et. al [23]
$Nu = 0.561 Re^{0.726} Pr^{0.333} \left(\frac{\mu}{\mu_w}\right)^{0.14}$, $400 \leq Re \leq 700$ $Nu = 0.240 Re^{0.724} Pr^{0.333} \left(\frac{\mu}{\mu_w}\right)^{0.14}$, $2{,}000 \leq Re \leq 4{,}500$	n/a	$\beta = 63^o$	Hayes et. al [55]
$Nu = 0.78 Re^{0.5} Pr^{1/3}$	n/a	$50 < Re < 20{,}000$	Maslov and Kovalenko [56]
$Nu = 0.277 Re^{0.766} Pr^{0.333}$	n/a	$350 < Re < 1{,}100$ $5 < Pr < 10$	Longo and Gasparella [57]
$Nu = 0.3174 Re^{0.65} Pr^{0.4}$	n/a	$\beta = 60^o$ $400 < Re < 15{,}000$	Okada et. al [58]

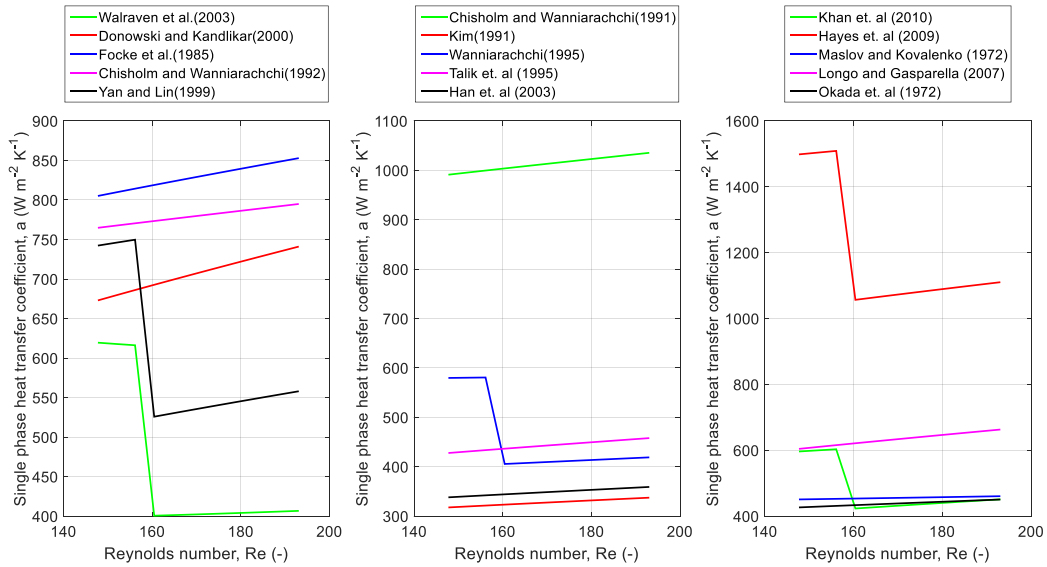
Walraven et al.(2003)
Donowski and Kandlikar(2000)
Focke et al.(1985)
Chisholm and Wanniarachchi(1992)
Yan and Lin(1999)
Chisholm and Wanniarachchi(1991)
Kim(1991)
Wanniarachchi(1995)
Talik et. al (1995)
Han et. al (2003)
Khan et. al (2010)
Hayes et. al (2009)
Maslov and Kovalenko (1972)
Longo and Gasparella (2007)
Okada et. al (1972)
Single phase heat transfer coefficient, a (W m-2 K-1)
Reynolds number, Re (-)

(a)

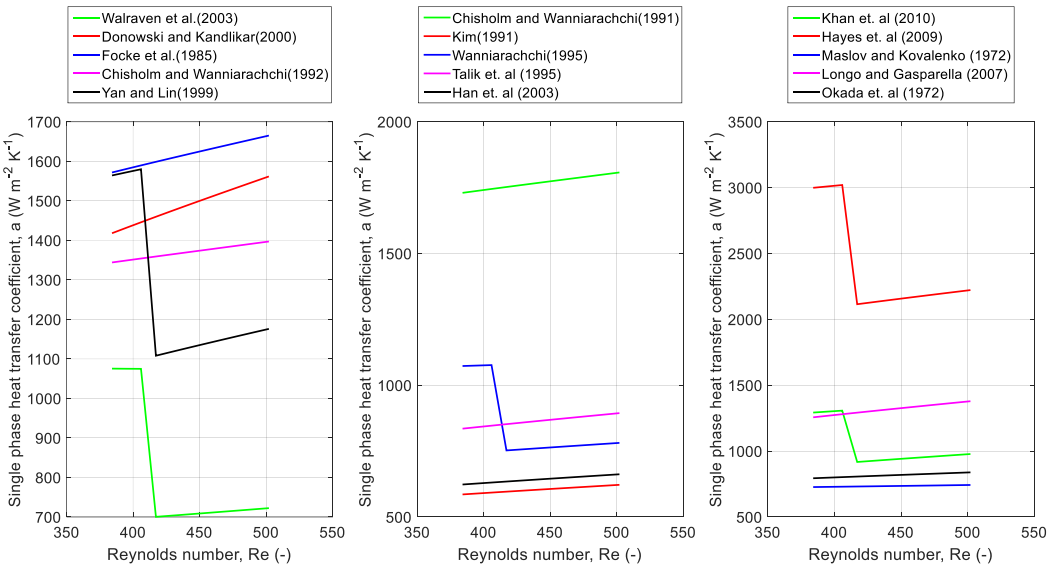
Walraven et al.(2003)
Donowski and Kandlikar(2000)
Focke et al.(1985)
Chisholm and Wanniarachchi(1992)
Yan and Lin(1999)
Chisholm and Wanniarachchi(1991)
Kim(1991)
Wanniarachchi(1995)
Talik et. al (1995)
Han et. al (2003)
Khan et. al (2010)
Hayes et. al (2009)
Maslov and Kovalenko (1972)
Longo and Gasparella (2007)
Okada et. al (1972)
Single phase heat transfer coefficient, a (W m-2 K-1)
Reynolds number, Re (-)

(b)

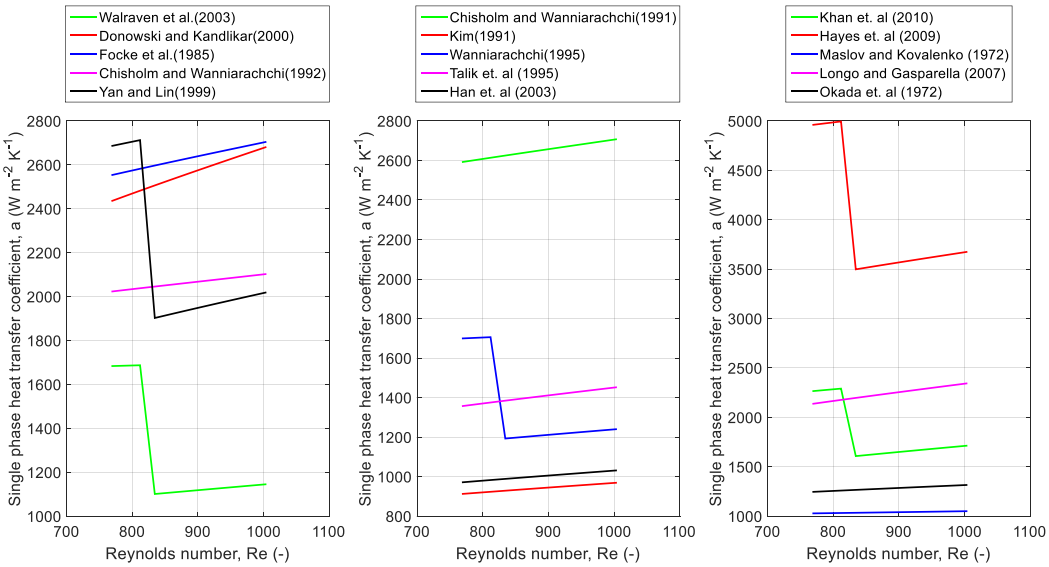

(c)

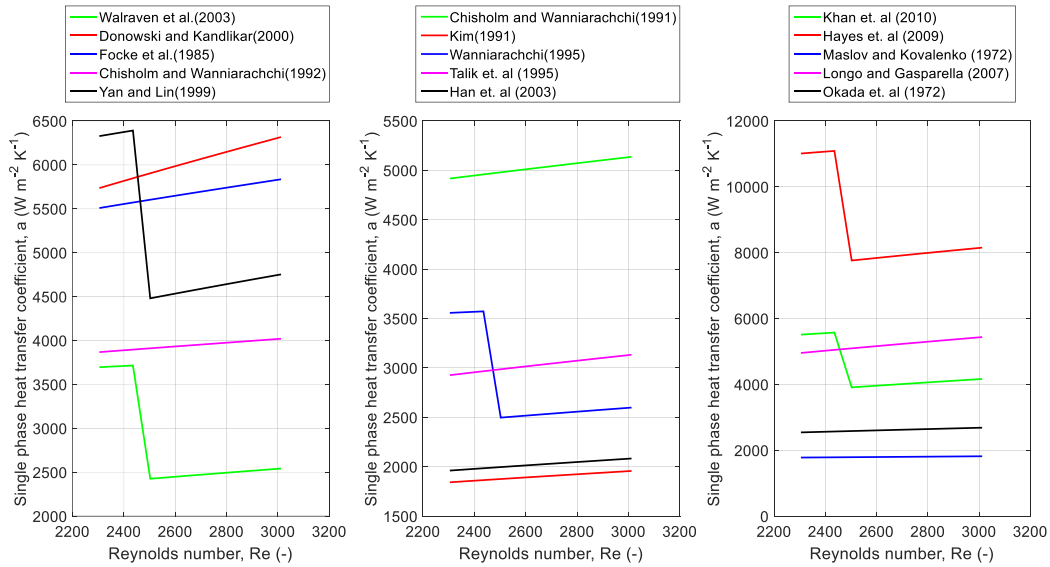

(d)

Fig. 3.7. Overview of single phase heat transfer coefficient predictions for Cyclopentane with (a) Re=192, (b) Re=500, (c) Re=1000 and (d) Re=3000.

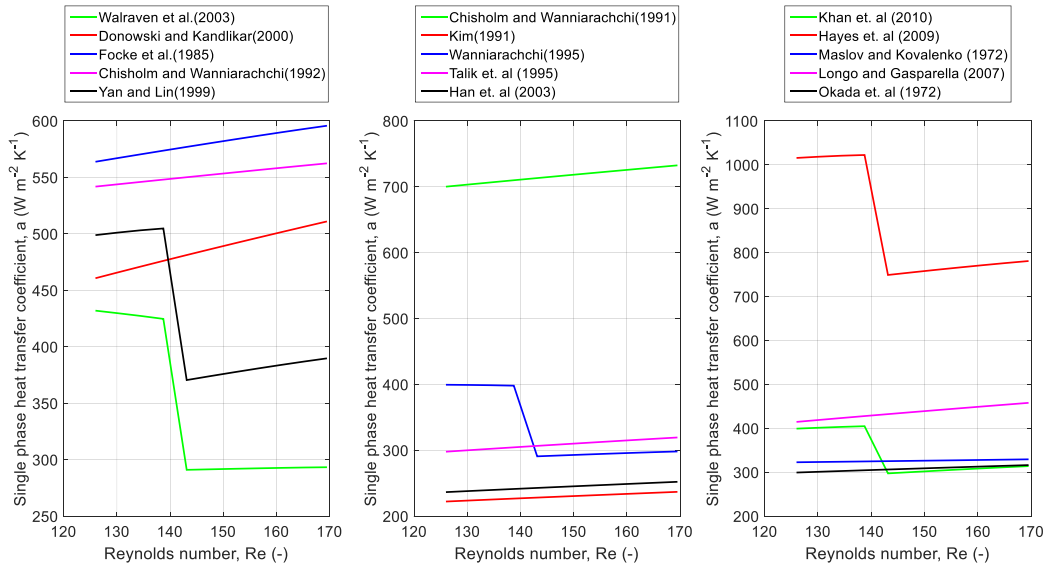
Walraven et al.(2003)
Donowski and Kandlikar(2000)
Focke et al.(1985)
Chisholm and Wanniarachchi(1992)
Yan and Lin(1999)
Chisholm and Wanniarachchi(1991)
Kim(1991)
Wanniarachchi(1995)
Talik et. al (1995)
Han et. al (2003)
Khan et. al (2010)
Hayes et. al (2009)
Maslov and Kovalenko (1972)
Longo and Gasparella (2007)
Okada et. al (1972)
Single phase heat transfer coefficient, a (W m-2 K-1)
Reynolds number, Re (-)

(a)

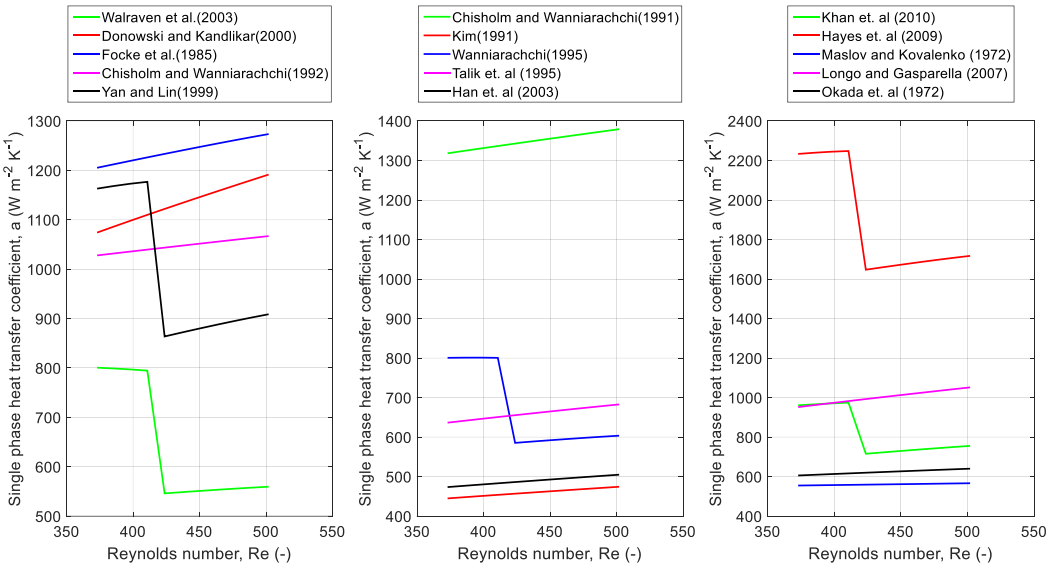
Walraven et al.(2003)
Donowski and Kandlikar(2000)
Focke et al.(1985)
Chisholm and Wanniarachchi(1992)
Yan and Lin(1999)
Chisholm and Wanniarachchi(1991)
Kim(1991)
Wanniarachchi(1995)
Talik et. al (1995)
Han et. al (2003)
Khan et. al (2010)
Hayes et. al (2009)
Maslov and Kovalenko (1972)
Longo and Gasparella (2007)
Okada et. al (1972)
Single phase heat transfer coefficient, a (W m-2 K-1)
Reynolds number, Re (-)

(b)

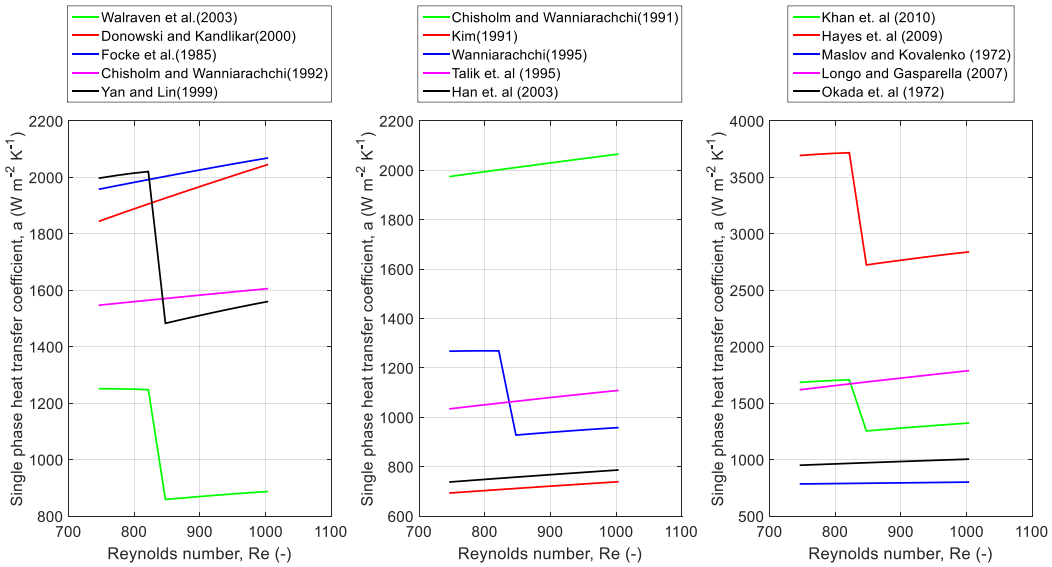

(c)

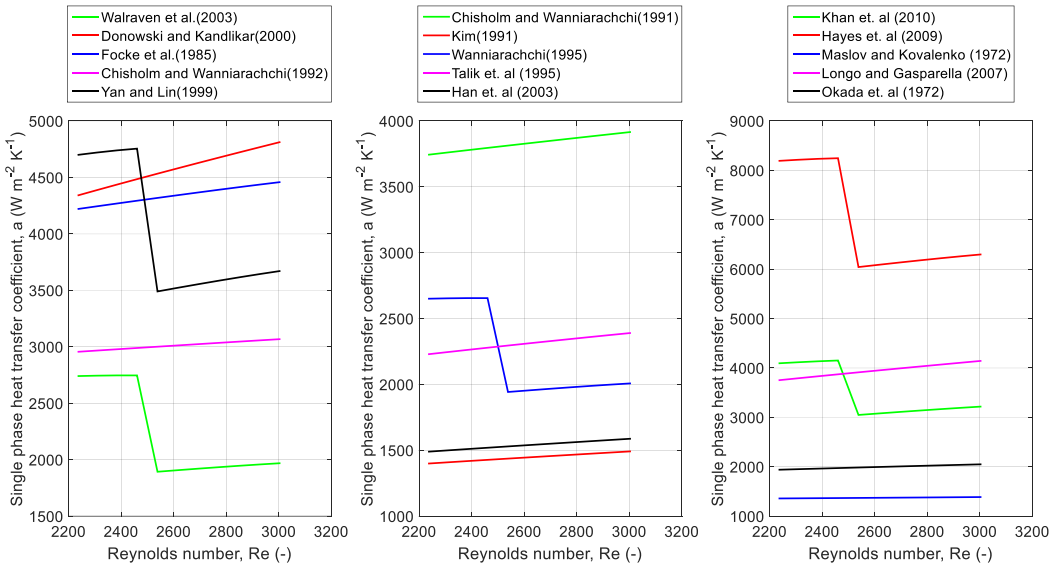

(d)

Fig. 3.8. Overview of single phase heat transfer coefficient predictions for R245ca with (a) Re=169, (b) Re=500, (c) Re=1000 and (d) Re=3000.

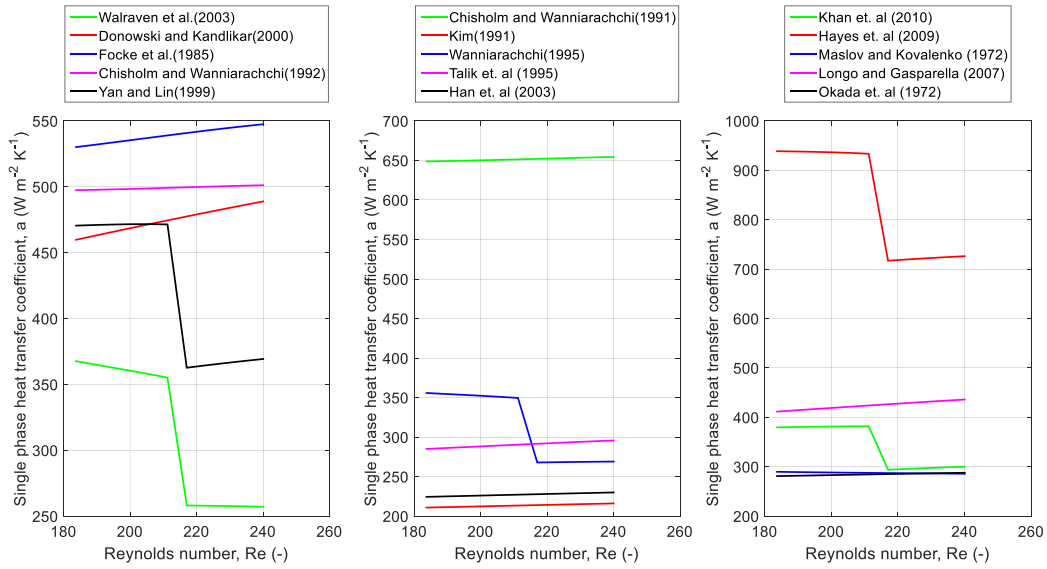
Walraven et al.(2003)
Donowski and Kandlikar(2000)
Focke et al.(1985)
Chisholm and Wanniarachchi(1992)
Yan and Lin(1999)
Chisholm and Wanniarachchi(1991)
Kim(1991)
Wanniarachchi(1995)
Talik et. al (1995)
Han et. al (2003)
Khan et. al (2010)
Hayes et. al (2009)
Maslov and Kovalenko (1972)
Longo and Gasparella (2007)
Okada et. al (1972)
Single phase heat transfer coefficient, a (W m-2 K-1)
Reynolds number, Re (-)

(a)

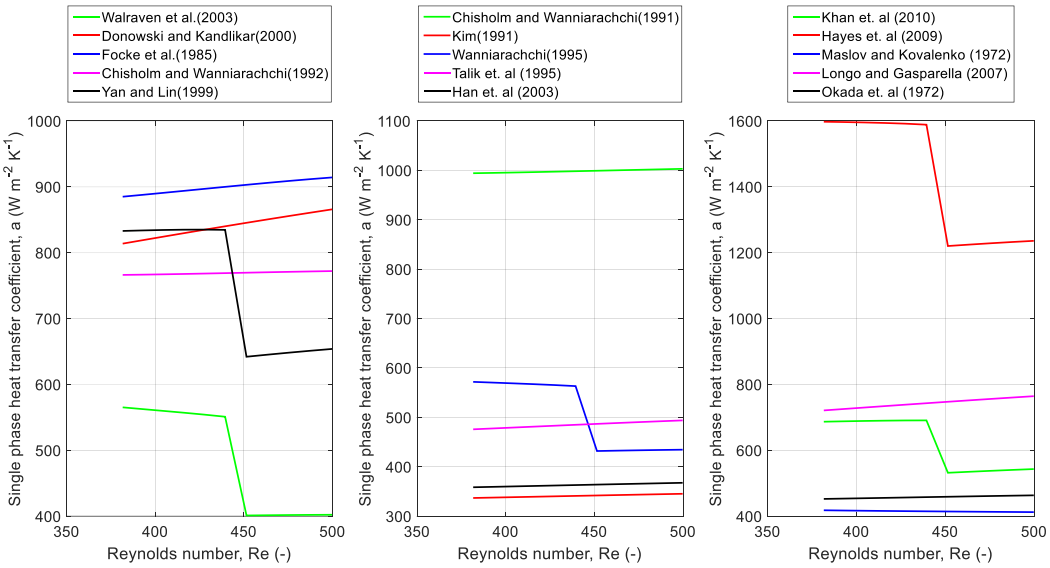
Walraven et al.(2003)
Donowski and Kandlikar(2000)
Focke et al.(1985)
Chisholm and Wanniarachchi(1992)
Yan and Lin(1999)
Chisholm and Wanniarachchi(1991)
Kim(1991)
Wanniarachchi(1995)
Talik et. al (1995)
Han et. al (2003)
Khan et. al (2010)
Hayes et. al (2009)
Maslov and Kovalenko (1972)
Longo and Gasparella (2007)
Okada et. al (1972)
Single phase heat transfer coefficient, a (W m-2 K-1)
Reynolds number, Re (-)

(b)

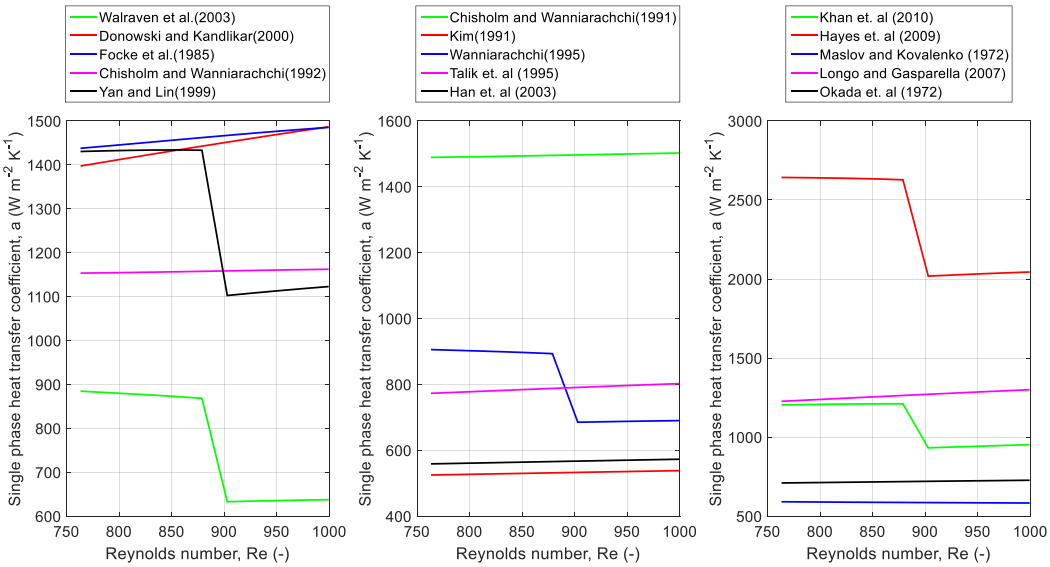

(c)

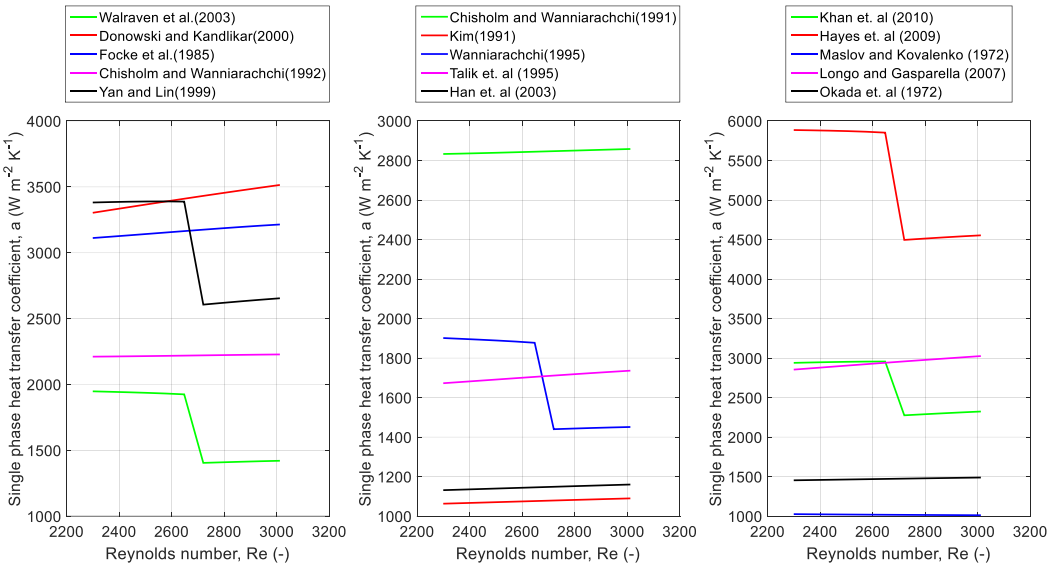

(d)

Fig. 3.9. Overview of single phase heat transfer coefficient predictions for R1234ze with (a) Re=240, (b) Re=500, (c) Re=1000 and (d) Re=3000.

Chapter 4. Pressure drop correlations

In this chapter the correlations to determine the pressure drop will be presented similarly to the heat transfer correlations also in correspondence to the 2nd chapter's heat transfer analysis for the single phase, heat transfer, evaporation and condensation, respectively, using a number of working fluids and flow regimes.

In the following sections the pressure drop inside the plate heat exchanger will be calculated using the equation:

$$\Delta p = f \frac{L_p G_{eq}}{D_h \rho} \qquad (4.1)$$

Hence, by assessing the friction number, f, the pressure drop can then be determined. These correlations calculate the pressure drop taking place within the plates not considering the port pressure drop which is calculated by equation (2.29).

4.1. Evaporation

The pressure drop will be calculated and used in the heat transfer analysis in place of equations (2.27) and (2.28).

The correlations shown in Table 4-1 are introduced to the evaporator's modeling, which was presented at Chapter 2.1 and the pressure drop for the cold side is calculated.

The analysis is carried out using three different vaporizing fluids: R245ca, R1234ze and Cyclopentane. The working conditions are identical to the ones used in Chapter 3.1. The key conclusions are summarized below:

- In general results tend to be higher with the use of R245ca.
- All results' curves have a negative slope.
- Pressure drop results are proportional to the Reynolds number.
- Lee's correlation is the least effected by the increase of the Reynolds number.
- Almalfi's correlation is the most dependable on the increase of the Reynolds number.
- Hsieh and Lin's and Yan and Lin's correlations tend to produce similar results with the increase of the Reynolds number. Furthermore, the results are increased with the use of Cyclopentane.
- Han, Lee and Ayub correlations' result are similar for low Reynolds numbers, but are differentiated in the turbulent region.
- Almalfi's correlation results are the highest for Re>500 for all three fluids.
- With the use of Cyclopentane Huang's correlation produces lower results in comparison to the use of the other two working fluids.

Table 4-1 Evaporation friction factor correlations

Correlation	**Working fluid**	**Range**	**Reference**
$f = 6.947 \cdot 10^5 {Re_L}^{-0.5} {Re_{eq}}^{-1.109}, \quad Re_{eq} < 6{,}000$ $f = 31.21 {Re_L}^{-0.5} {Re_{eq}}^{0.04557}, \quad Re_{eq} \geq 6{,}000$	R134a		Yan and Lin [13]
$f = 6.1 \cdot 10^4 \cdot {Re_{eq}}^{-1.25}$	R410A		Hsieh and Lin [14]
$f = 64{,}710 \left(\frac{\Lambda}{D_h}\right)^{-5.27} \left(\frac{\pi}{2} - \varphi\right)^{-3.03} {Re_{eq}}^{Ge_4}$ $Ge_4 = -1.314 \left(\frac{\Lambda}{D_h}\right)^{-0.62} \left(\frac{\pi}{2} - \varphi\right)^{-0.47}$	R410A, R22	$13 < G < 34$ $2.5 < q < 8.5$	Han et. al [15]
$f = \left(\left(\frac{2.99}{Re^{0.137}}\right)(-1.89 + 6.56R - 3.69R^2)\right)$ $R = \beta/30$	Ammonia,R22	$4000 \leq Re \leq 16000, US\ units$ $30^o < \beta < 65^o$	Ayub [20]
$f = 4 \cdot 305{,}590 Re_{eq}^{-1.26} p^{*0.9}$	Ammonia	$500 < Re < 2500$ $5.5 < G < 27$ $20 \leq q_{flux} \leq 70$ $0.1 \leq x_m \leq 0.9$ $3.5 < Pr < 6$ $30° < \beta < 60°$ $1225 < Re_{eq} < 3000$ $-2℃ \leq T_{sat} \leq -25℃$	Khan and Chyu and Khan et. al [22, 23]
$f = \frac{3.81 \cdot 10^4 F_{R_f}}{Re_{tp}^{0.9} \left(\frac{\rho_l}{\rho_g}\right)^{0.16}}$ $F_{R_f} = 0.183R^2 - 0.275R + 1.10, R = \frac{\beta}{30}$	R134a,R507A, R12,Ammonia	$5.6 \leq G \leq 52.3$ $1.8 \leq q_{flux} \leq 6.9$ $5.9℃ \leq T_{sat} \leq 13℃$ $28° < \beta < 60°$	Huang et. al [25]

$f = 4 \cdot 49.13 Re_{eq}^{-0.4386} Re^{-0.4074}$	Water	$\beta = 60°$ $14.5 \leq G \leq 33.6$ $15 \leq q_{flux} \leq 30$	Lee et. al [26]
$f = 4 \cdot 15.698 C \left(\frac{G^2 D_h}{\rho_m \sigma}\right)^{-0.475} \left(\frac{(\rho_l - \rho_g) g D_h^2}{\sigma}\right)^{0.255} \left(\frac{\rho_l}{\rho_g}\right)^{-0.571}$ $C = 2.125 \left(\frac{\beta}{\beta_{max}}\right)^{9.993} + 0.955$	R134a, ammonia, R236fa, R600a, R290, R1270, R1234yf, R410A, R507A, ammonia/water, air/water		Almalfi et. al [27]

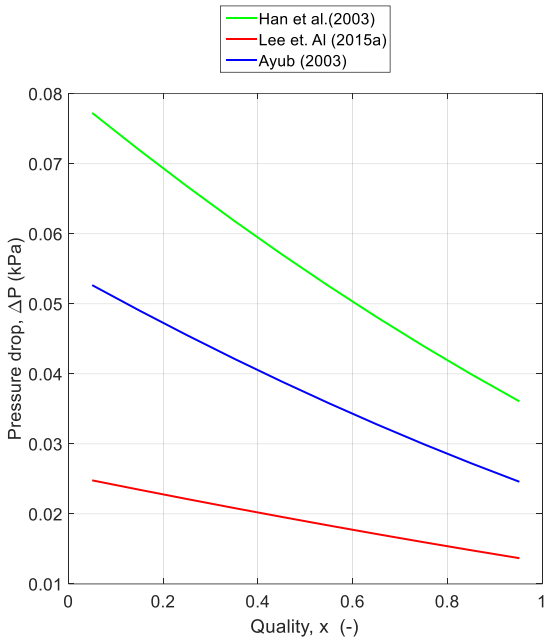
Han et al.(2003)
Lee et. Al (2015a)
Ayub (2003)
Pressure drop, ΔP (kPa)
Quality, x (-)

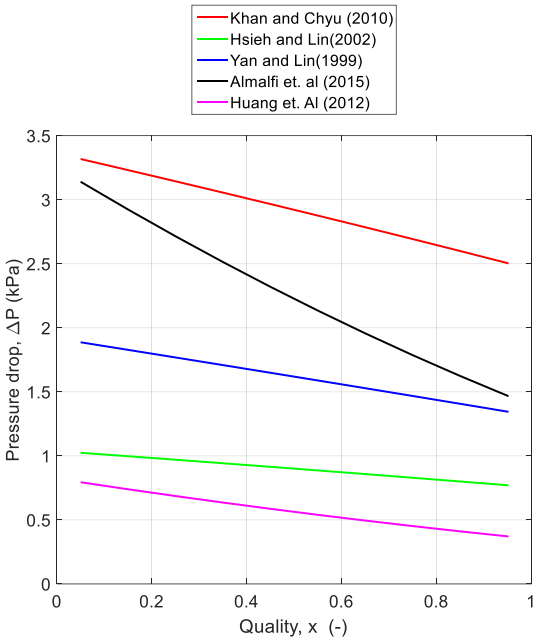
Khan and Chyu (2010)
Hsieh and Lin(2002)
Yan and Lin(1999)
Almalfi et. al (2015)
Huang et. Al (2012)
Pressure drop, ΔP (kPa)
Quality, x (-)

(a)

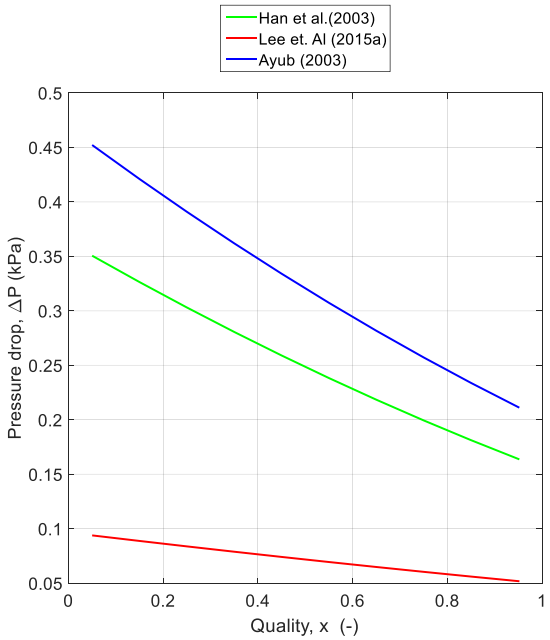
Han et al.(2003)
Lee et. Al (2015a)
Ayub (2003)
Pressure drop, ΔP (kPa)
Quality, x (-)

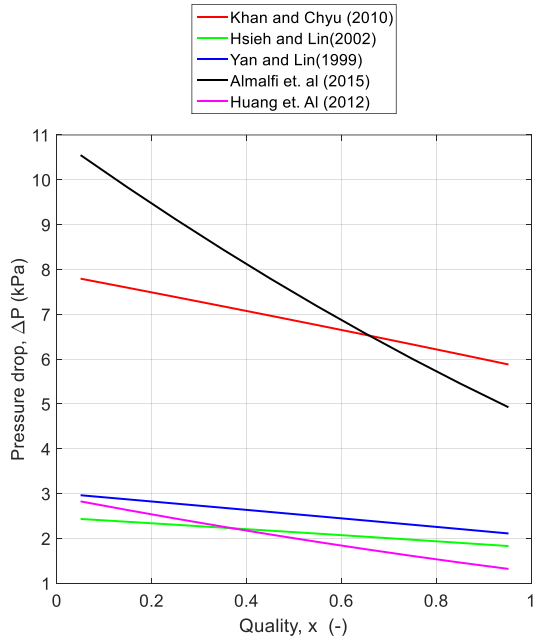
Khan and Chyu (2010)
Hsieh and Lin(2002)
Yan and Lin(1999)
Almalfi et. al (2015)
Huang et. Al (2012)
Pressure drop, ΔP (kPa)
Quality, x (-)

(b)

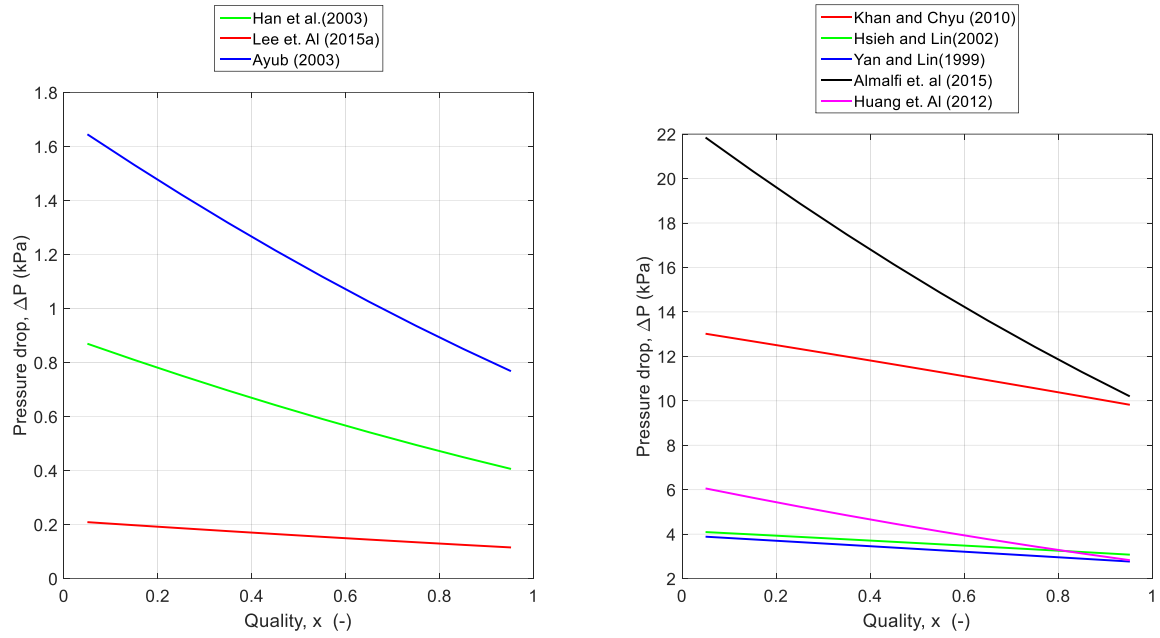

(c)

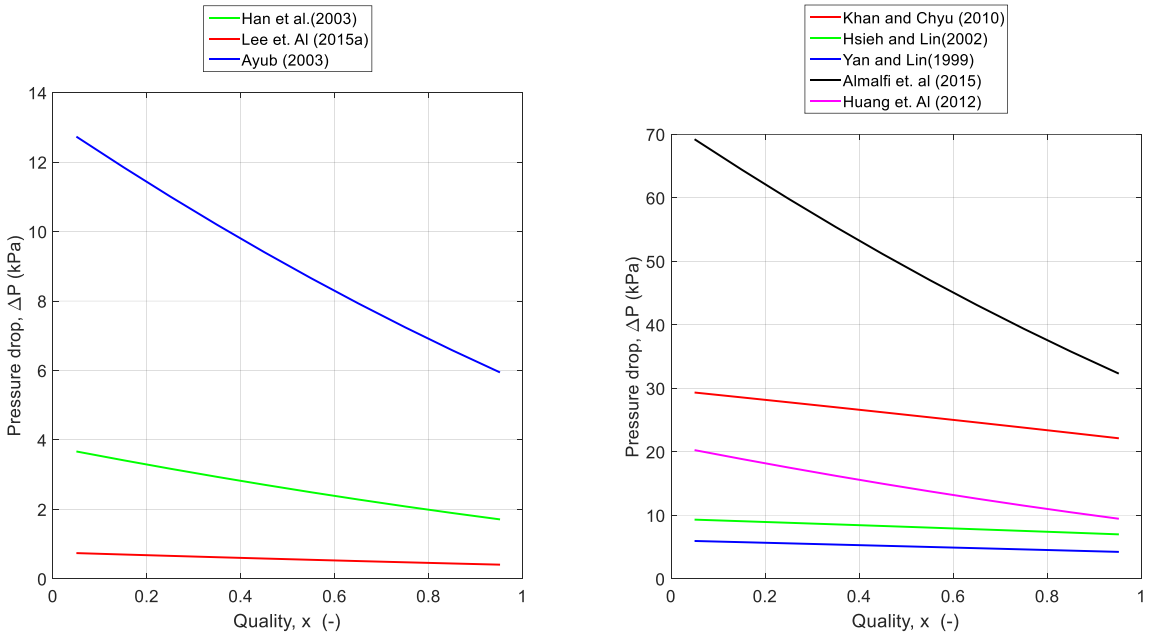

(d)

Fig. 4.1. Overview of boiling pressure drop predictions for R245ca with (a) Re=157.7, (b) Re=500, (c) Re=1000 and (d) Re=3000.

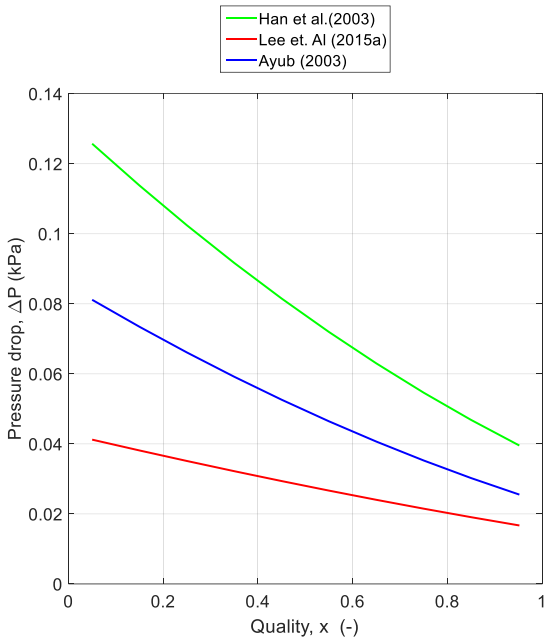
Han et al.(2003)
Lee et. Al (2015a)
Ayub (2003)
Pressure drop, ΔP (kPa)
Quality, x (-)

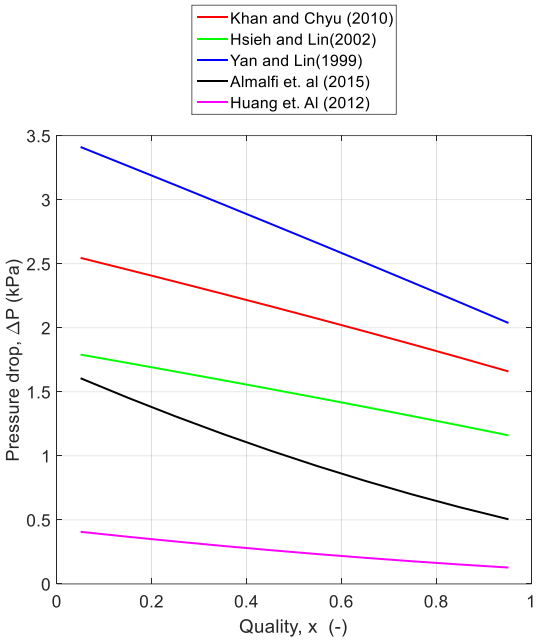
Khan and Chyu (2010)
Hsieh and Lin(2002)
Yan and Lin(1999)
Almalfi et. al (2015)
Huang et. Al (2012)
Pressure drop, ΔP (kPa)
Quality, x (-)

(a)

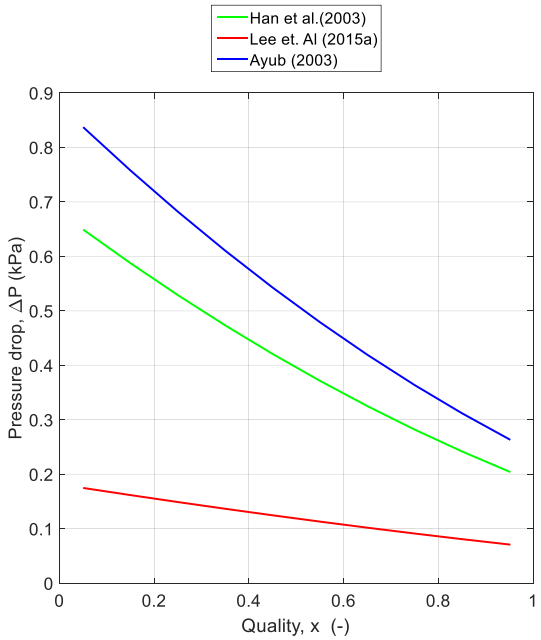
Han et al.(2003)
Lee et. Al (2015a)
Ayub (2003)
Pressure drop, ΔP (kPa)
Quality, x (-)

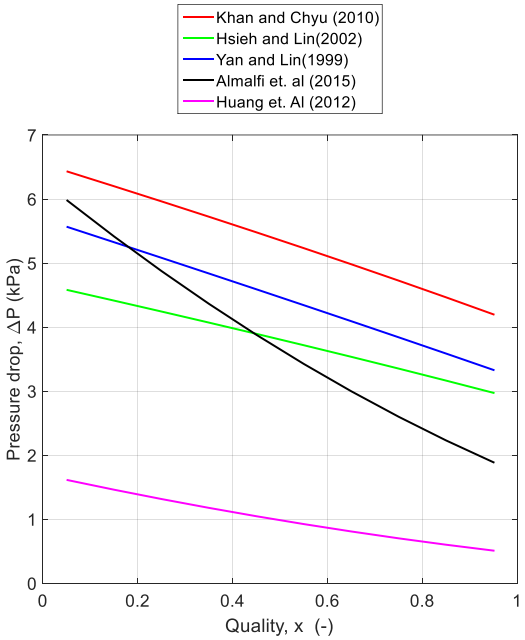
Khan and Chyu (2010)
Hsieh and Lin(2002)
Yan and Lin(1999)
Almalfi et. al (2015)
Huang et. Al (2012)
Pressure drop, ΔP (kPa)
Quality, x (-)

(b)

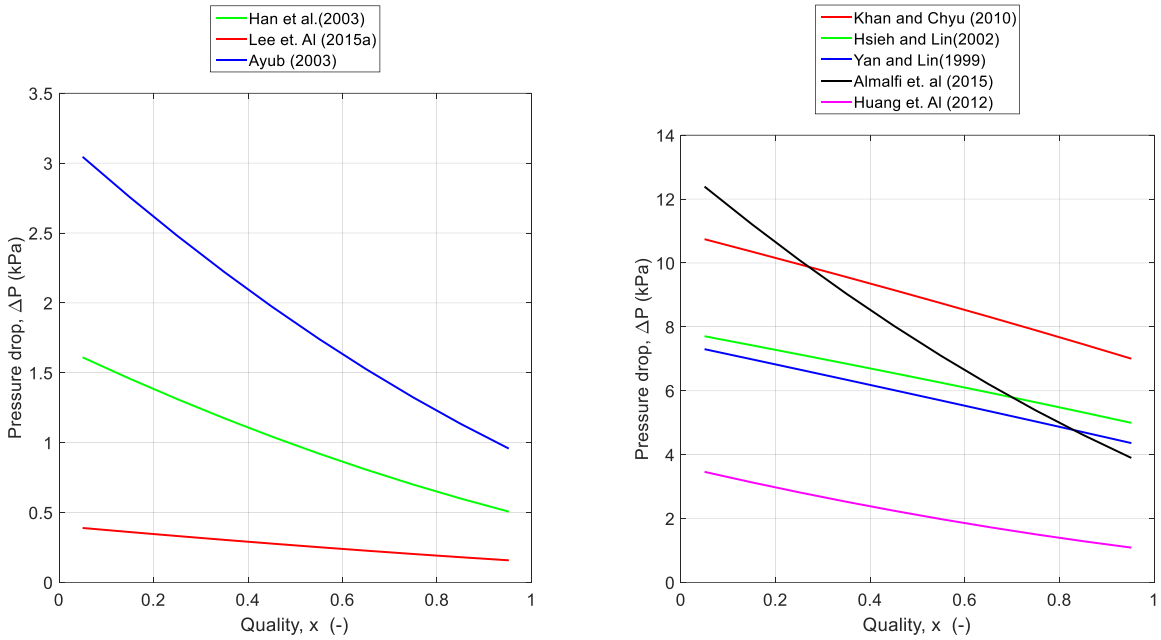

(c)

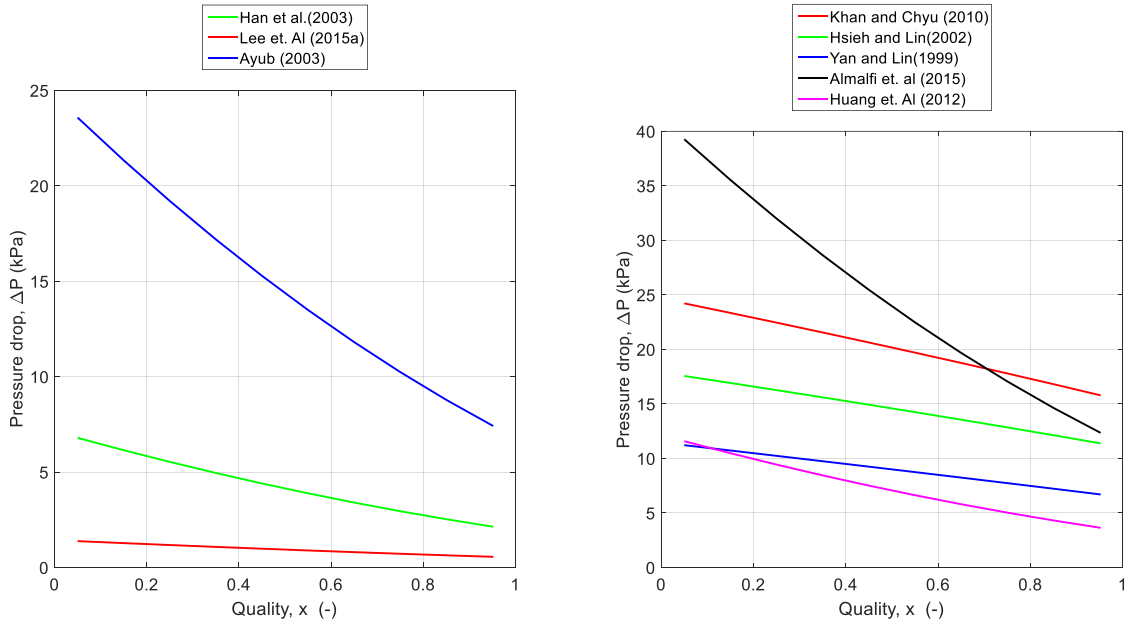

(d)

Fig. 4.2. Overview of boiling pressure drop predictions for Cyclopentane with (a) Re=143, (b) Re=500, (c) Re=1000 and (d) Re=3000.

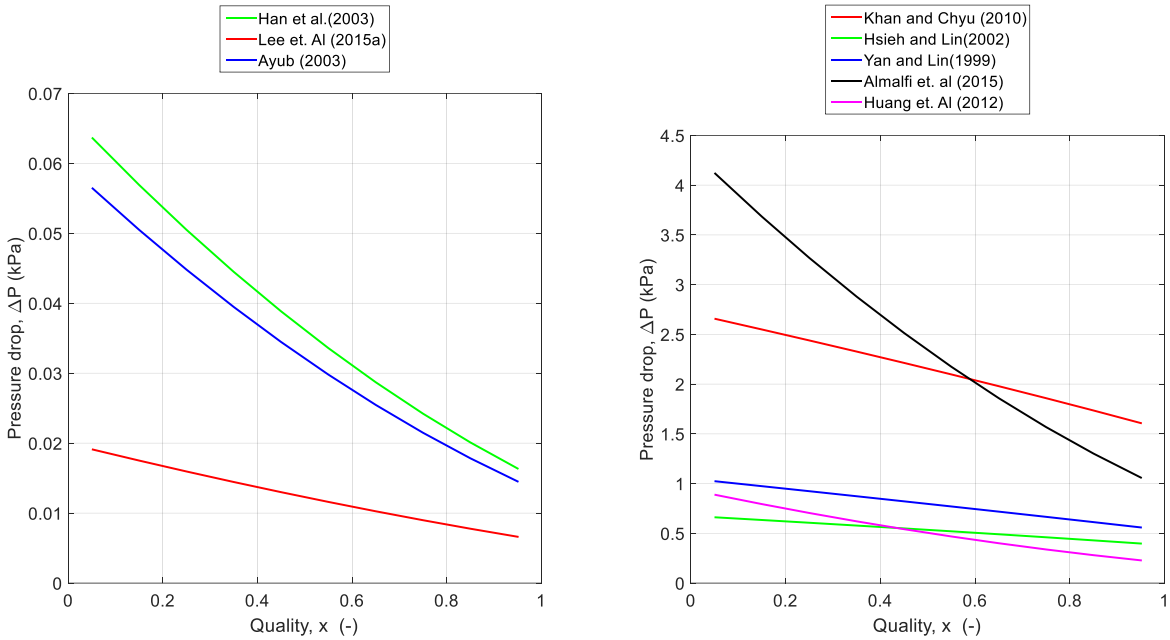
Han et al.(2003)
Lee et. Al (2015a)
Ayub (2003)
Pressure drop, ΔP (kPa)
Quality, x (-)
Khan and Chyu (2010)
Hsieh and Lin(2002)
Yan and Lin(1999)
Almalfi et. al (2015)
Huang et. Al (2012)
Pressure drop, ΔP (kPa)
Quality, x (-)

(a)

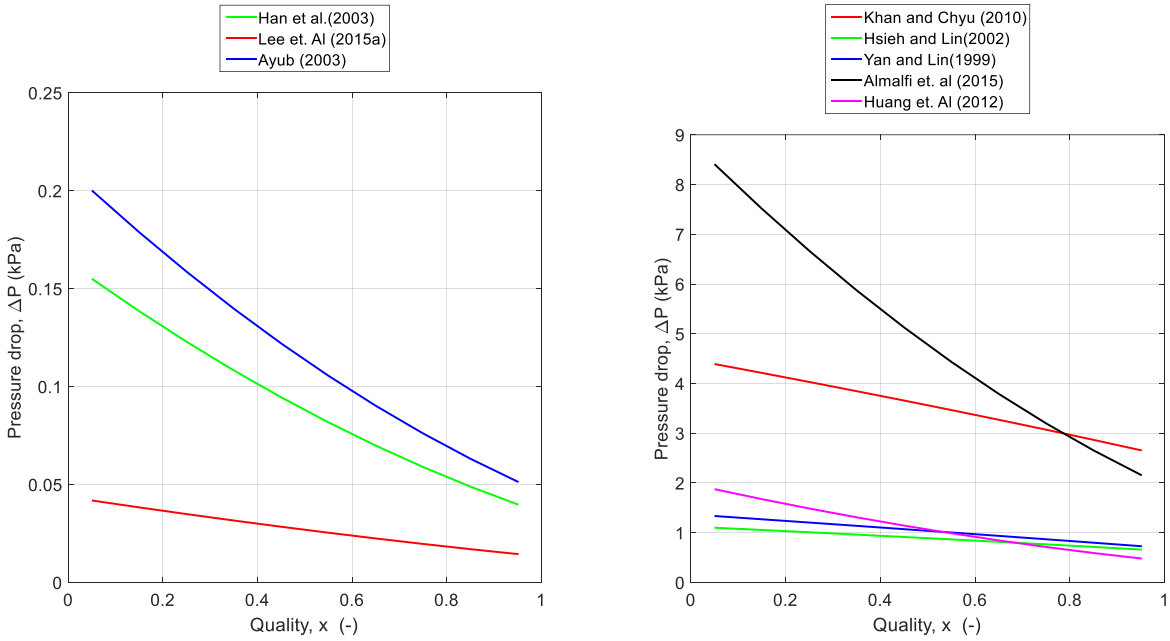
Han et al.(2003)
Lee et. Al (2015a)
Ayub (2003)
Pressure drop, ΔP (kPa)
Quality, x (-)
Khan and Chyu (2010)
Hsieh and Lin(2002)
Yan and Lin(1999)
Almalfi et. al (2015)
Huang et. Al (2012)
Pressure drop, ΔP (kPa)
Quality, x (-)

(b)

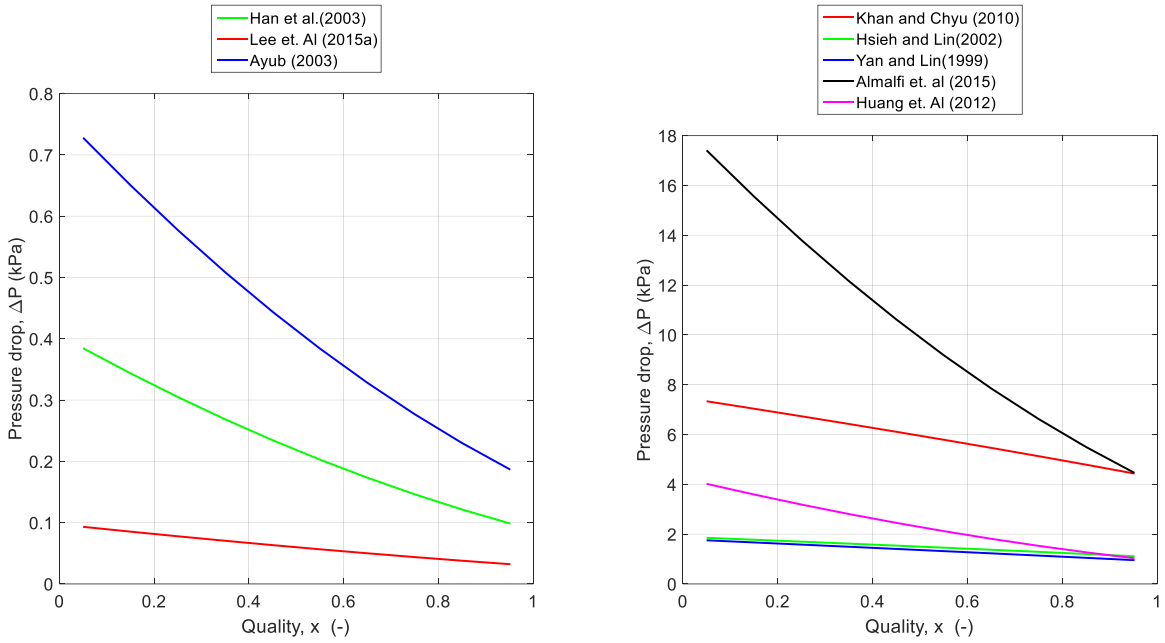

(c)

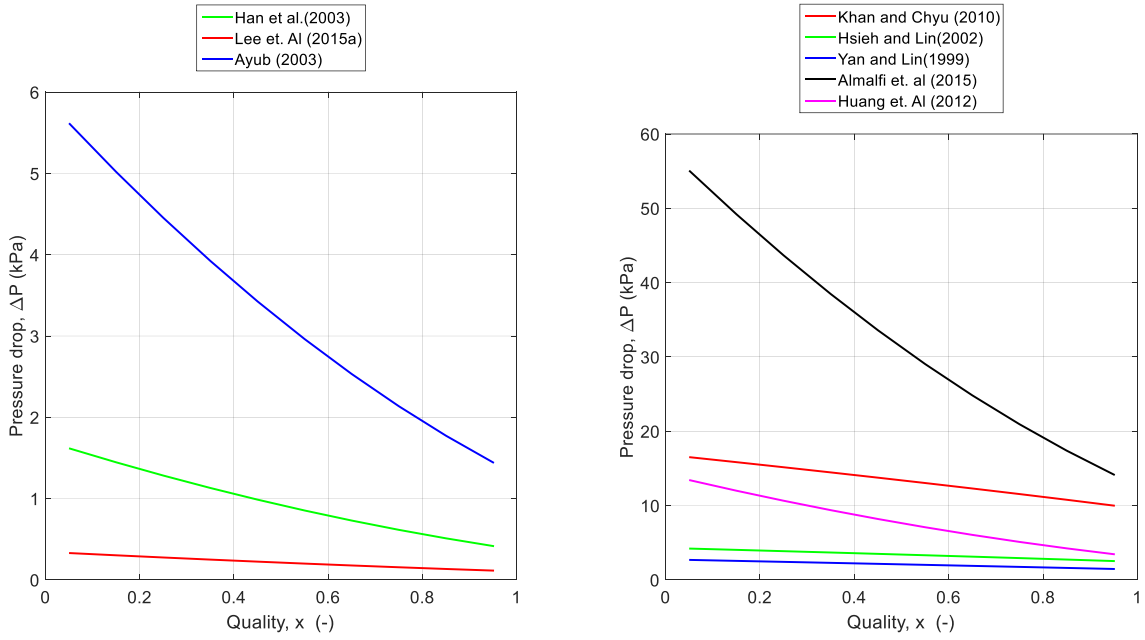

(d)

Fig. 4.3. Overview of boiling pressure drop predictions for R1234ze with (a) Re=254, (b) Re=500, (c) Re=1000 and (d) Re=3000.

4.2. Condensation

The pressure drop will be calculated and used in the heat transfer analysis in place of equation (2.34).

The correlations shown in Table 4-2 are introduced to the condenser's modeling, which was presented at Chapter 2.2 and the pressure drop for the hot side is calculated.

The analysis is carried out using three different vaporizing fluids: R245ca, R1234ze and Cyclopentane. The working conditions are identical to the ones used in Chapter 3.2. The key conclusions are summarized below:

- In general results tend to be higher with the use of Cyclopentane.
- All results' curves have a positive slope, except for Jokar's correlation results which have a negative slope.
- Pressure drop results are proportional to the Reynolds number.
- Han and Shi correlations' results are the least effected by the increase of the Reynolds number.
- Use of R1234ze produces significantly lower results.
- Kuo and Soontarapiromsook correlations' results are similar for low Reynolds number ($Re \leq 1000$).
- Hayes correlation's results are strongly affected by the increase of the Reynolds number. With the use of R245ca and Cyclopentane for $Re > 1000$ this correlation's results are the highest.

Table 4-2 Condensation friction factor correlations

Correlation	Working fluid	Range	Reference
$f = 94.75 Re_{eq}^{-0.0467} Re^{-0.4} Bo^{0.5} p_{red}^{0.8}$	R134a	$500 < Re < 1{,}000$ $60 \leq G \leq 120$	Yan [31]
$f = 3521.1 \left(\frac{\Lambda}{D_h}\right)^{4.17} \left(\frac{\pi}{2} - \varphi\right)^{-7.75} \left[Re_{eq}\right]^{Ge_4}$ $Ge_4 = -1.024 \left(\frac{\Lambda}{D_h}\right)^{0.0925} \left(\frac{\pi}{2} - \varphi\right)^{-1.3}$	R410A, R22	$10 < G < 35$ $4.7 < q < 5.3$	Han et. al [33]
$f = 21{,}500 Re_{eq}^{-1.14} Bo^{-0.085}$	R410A	$50 \leq G \leq 150$ $10 \leq q'' \leq 20$ $0.1 \leq x_m \leq 0.9$ $1.44 \leq P_m \leq 1.95$	Kuo et. al [36]
$f = 350{,}188 Re_{eq}^{-2.19} Bo_{eq}^{-0.23}$	R134a	$22 \leq G \leq 65$ $11.5 \leq q'' \leq 35$ $16.2 \leq T_{sat} \leq 29$	Shi et. al [43]
$f = 0.0146 Re_{eq}^{-0.9814} We^{-1.0064}$ $We = \frac{G^2 D_h}{\rho_m \sigma}$	R134a, R1234ze(E), R245fa, R1233zd(E)	$16 \leq G \leq 90$ $4 \leq q'' \leq 57.4$ $29.7 \leq T_{sat} \leq 71$	Zhang et. al [38]
$f = 1261.067 Re_{eq}^{-0.411} Re_{LO}^{-0.57}$	R1233zd(E)	$13 \leq G \leq 23.8$ $2.5 \leq q'' \leq 4.5$ $38.6 \leq T_{sat} \leq 51.5$	Shon et. al [41]
$f = 2671.743 Re_{eq}^{-0.818} \left(\frac{\delta}{D_h}\right)^{0.065}$	R134a	$61 \leq G \leq 89$ $5 \leq q'' \leq 15$ $40 \leq T_{sat} \leq 50$	Soontarapiromsook et al. [44]
$f = 2.139 \cdot 10^7 Re_{mod}^{-1.6}$	n/a		Jokar et. al [42]

$Re_{mod} = GD_h\left(\frac{1-x}{\mu_l}+\frac{x}{\mu_g}\right)$			
$f = 1221.3Re^{-0.815}$	CO_2	$2 \leq G \leq 45$ $2.5 \leq q'' \leq 15.7$ $-34.4 \leq T_{sat} \leq -17.8$	Hayes et. al [59]

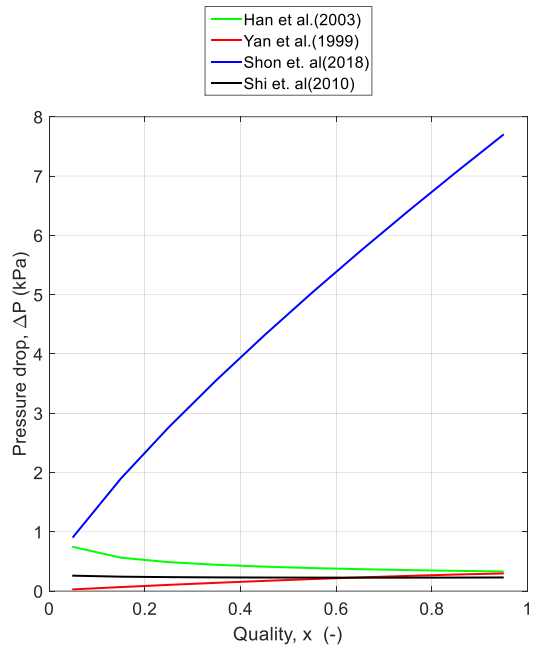
Han et al.(2003)
Yan et al.(1999)
Shon et. al(2018)
Shi et. al(2010)
Pressure drop, ΔP (kPa)
Quality, x (-)

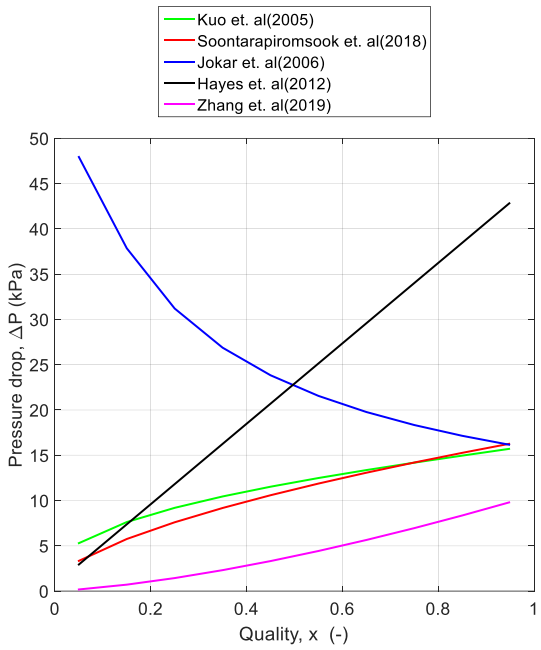
Kuo et. al(2005)
Soontarapiromsook et. al(2018)
Jokar et. al(2006)
Hayes et. al(2012)
Zhang et. al(2019)
Pressure drop, ΔP (kPa)
Quality, x (-)

(a)

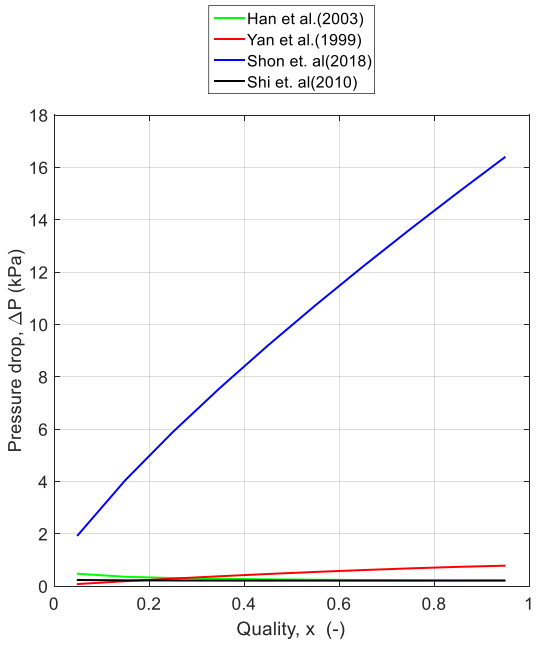
Han et al.(2003)
Yan et al.(1999)
Shon et. al(2018)
Shi et. al(2010)
Pressure drop, ΔP (kPa)
Quality, x (-)

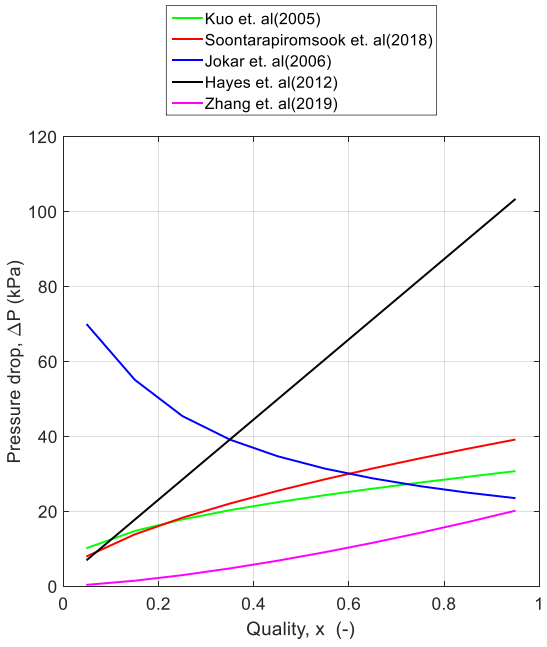
Kuo et. al(2005)
Soontarapiromsook et. al(2018)
Jokar et. al(2006)
Hayes et. al(2012)
Zhang et. al(2019)
Pressure drop, ΔP (kPa)
Quality, x (-)

(b)

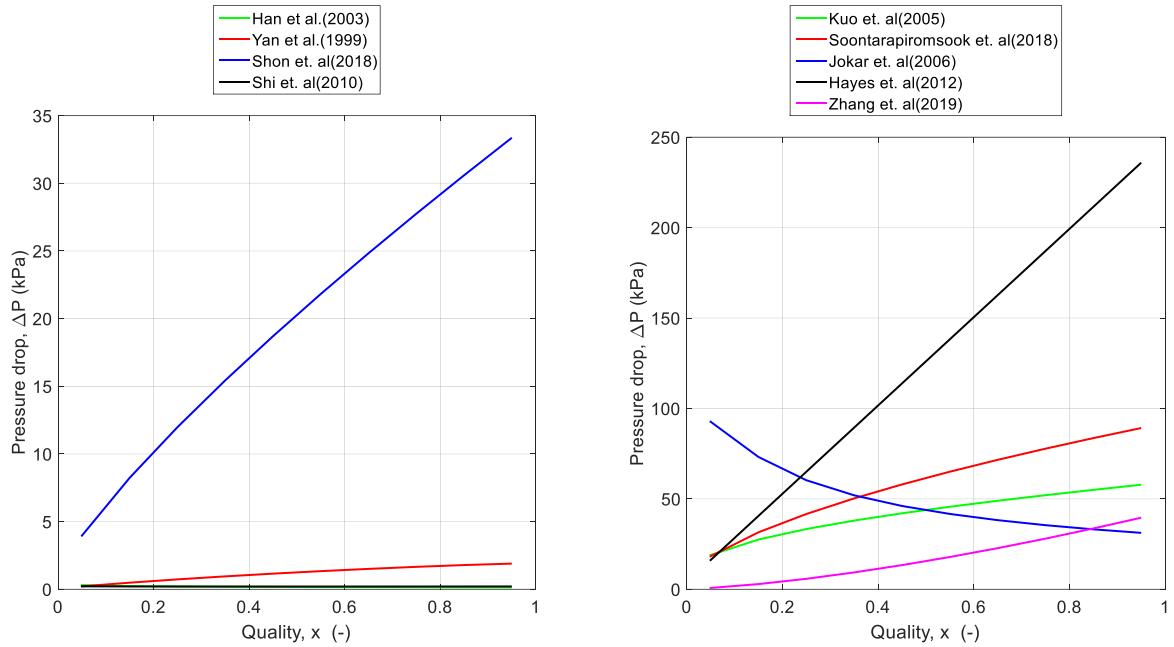

(c)

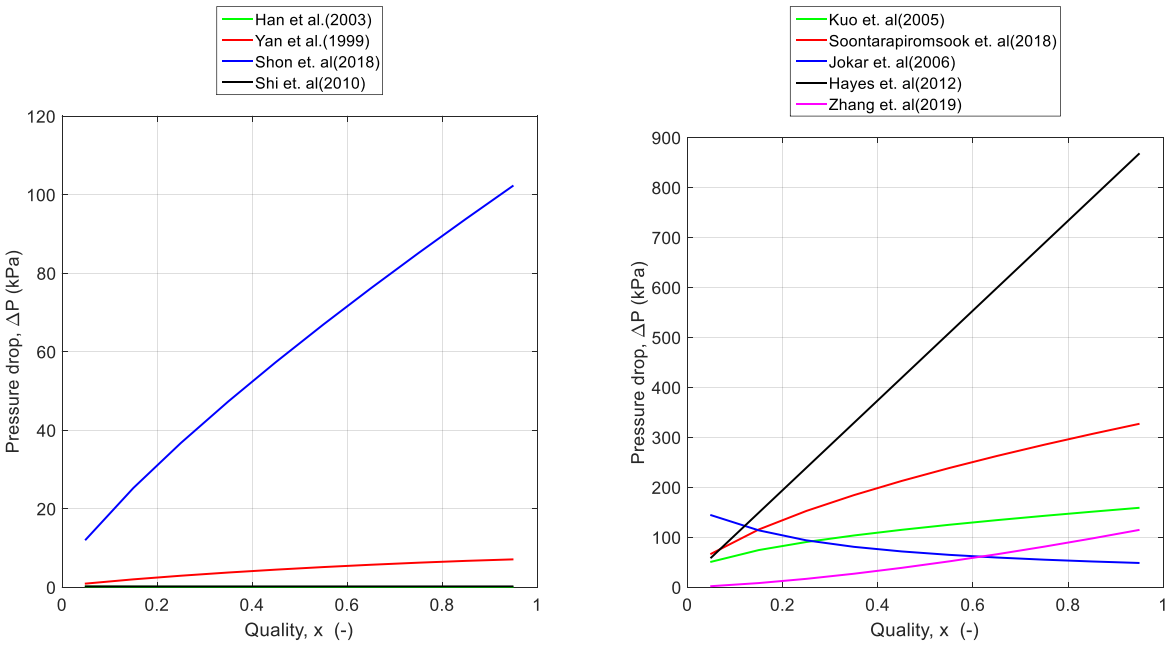

(d)

Fig. 4.4. Overview of condensation pressure drop predictions for Cyclopentane with (a) Re=237.7, (b) Re=500, (c) Re=1000 and (d) Re=3000.

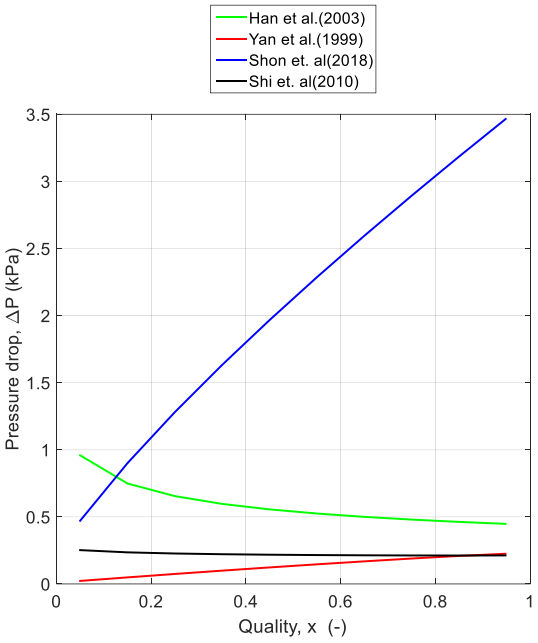
Han et al.(2003)
Yan et al.(1999)
Shon et al.(2018)
Shi et al.(2010)
Pressure drop, ΔP (kPa)
Quality, x (-)

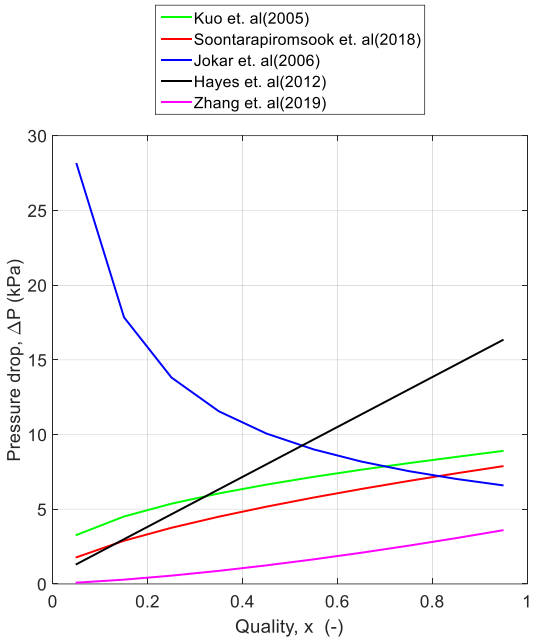
Kuo et. al(2005)
Soontarapiromsook et. al(2018)
Jokar et. al(2006)
Hayes et. al(2012)
Zhang et. al(2019)
Pressure drop, ΔP (kPa)
Quality, x (-)

(a)

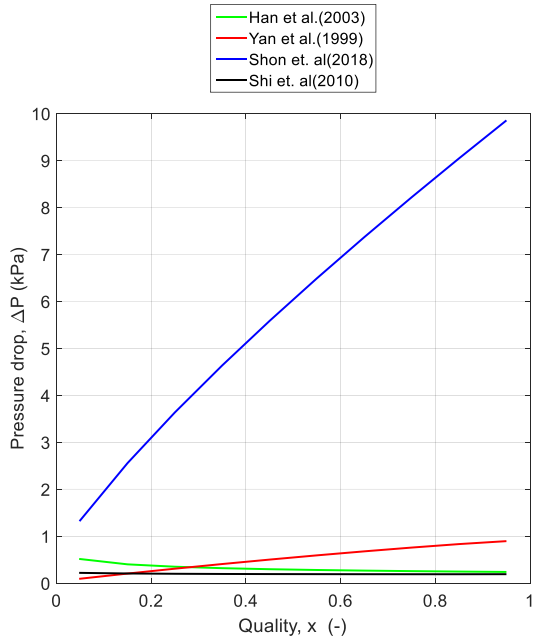
Han et al.(2003)
Yan et al.(1999)
Shon et al.(2018)
Shi et al.(2010)
Pressure drop, ΔP (kPa)
Quality, x (-)

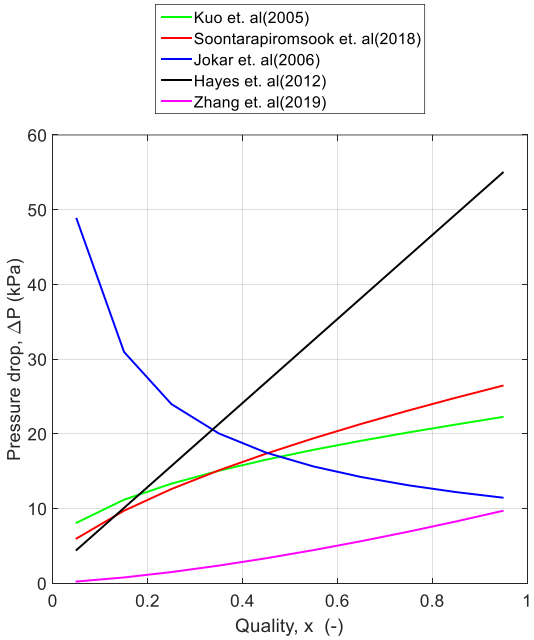
Kuo et. al(2005)
Soontarapiromsook et. al(2018)
Jokar et. al(2006)
Hayes et. al(2012)
Zhang et. al(2019)
Pressure drop, ΔP (kPa)
Quality, x (-)

(b)

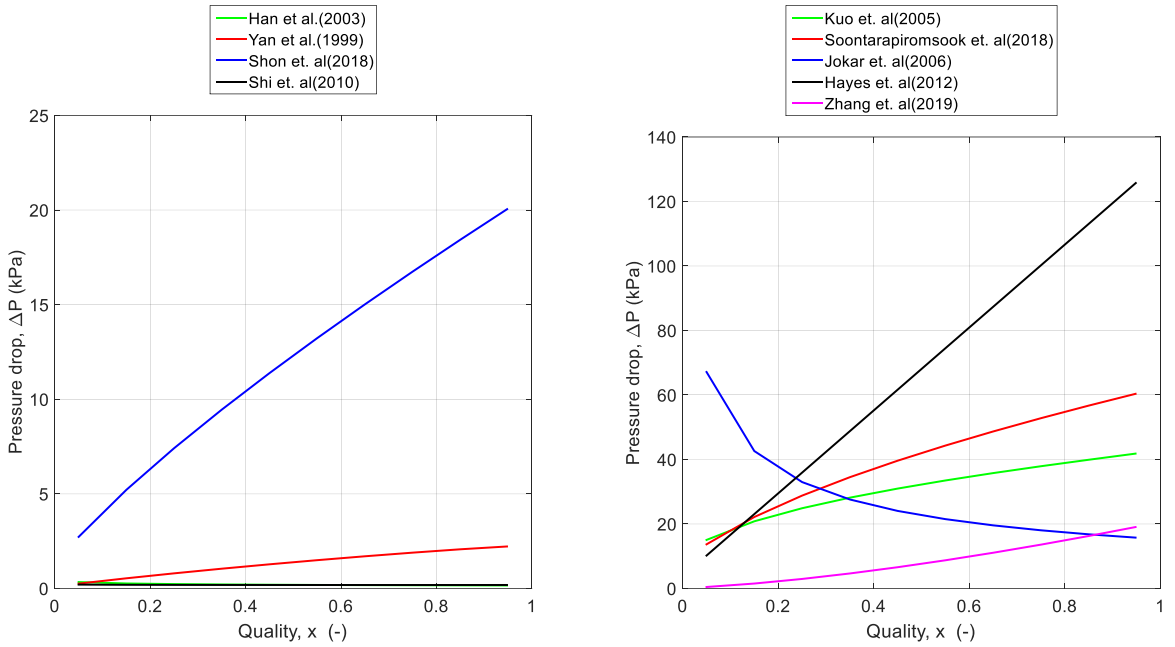

(c)

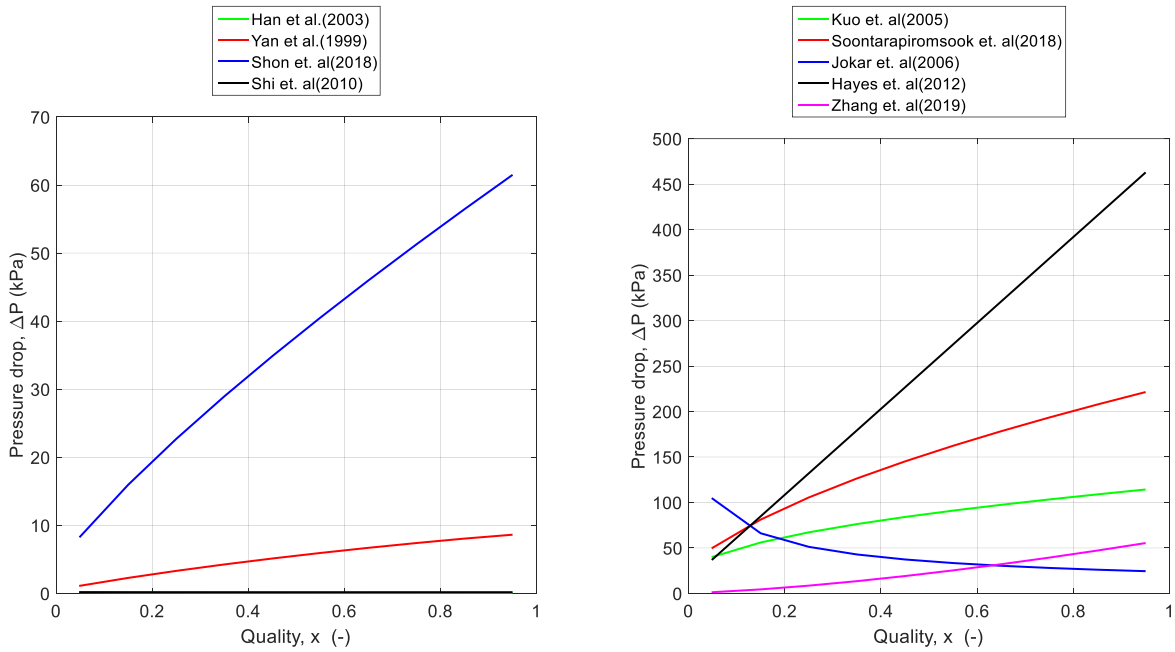

(d)

Fig. 4.5. Overview of condensation pressure drop predictions for R245ca with (a) Re=179, (b) Re=500, (c) Re=1000 and (d) Re=3000.

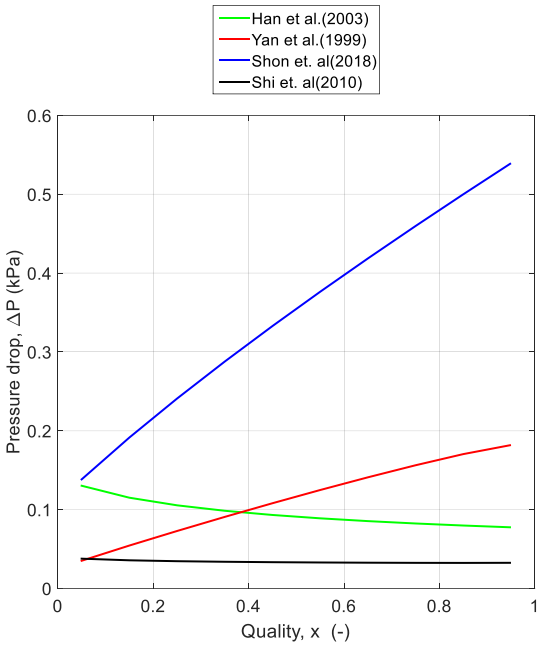
Han et al.(2003)
Yan et al.(1999)
Shon et. al(2018)
Shi et. al(2010)
Pressure drop, ΔP (kPa)
Quality, x (-)

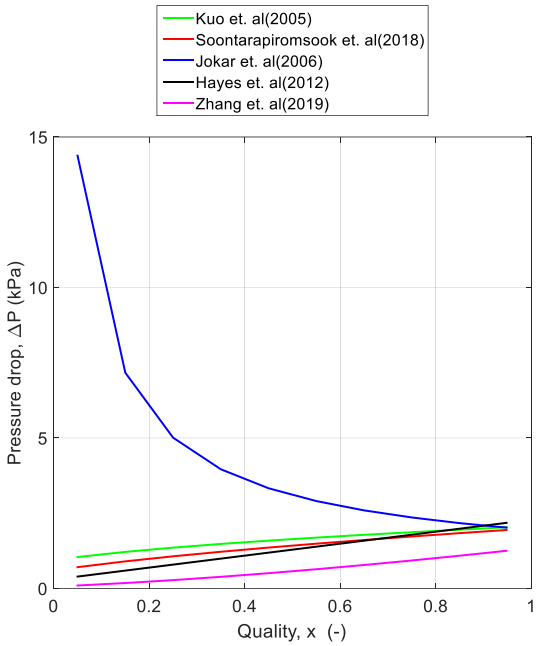
Kuo et. al(2005)
Soontarapiromsook et. al(2018)
Jokar et. al(2006)
Hayes et. al(2012)
Zhang et. al(2019)
Pressure drop, ΔP (kPa)
Quality, x (-)

(a)

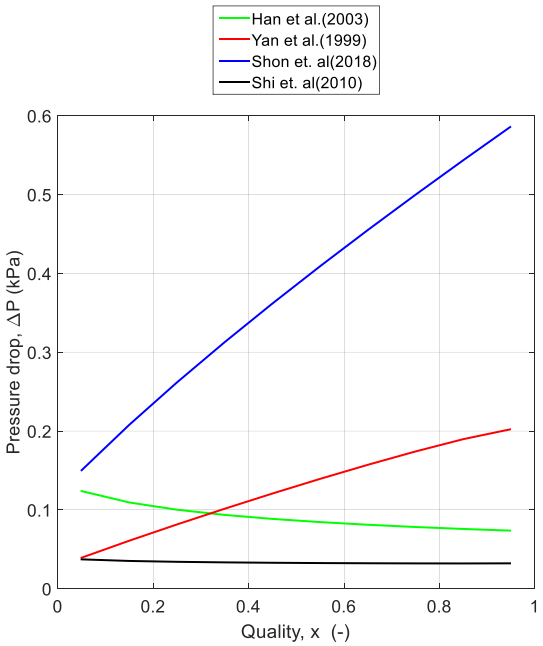
Han et al.(2003)
Yan et al.(1999)
Shon et. al(2018)
Shi et. al(2010)
Pressure drop, ΔP (kPa)
Quality, x (-)

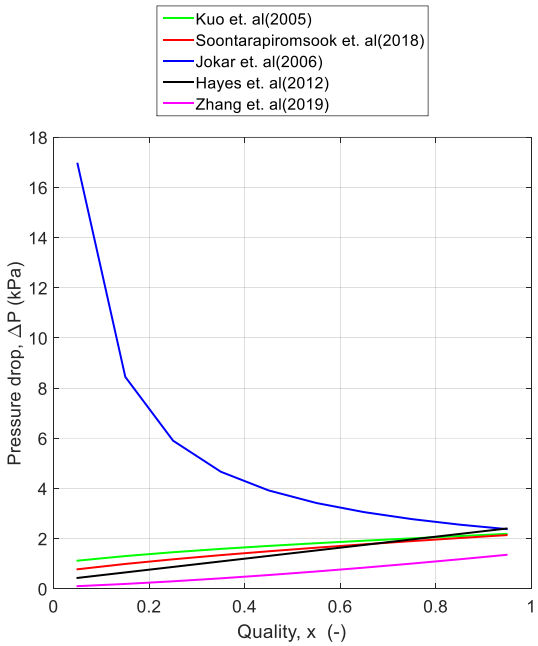
Kuo et. al(2005)
Soontarapiromsook et. al(2018)
Jokar et. al(2006)
Hayes et. al(2012)
Zhang et. al(2019)
Pressure drop, ΔP (kPa)
Quality, x (-)

(b)

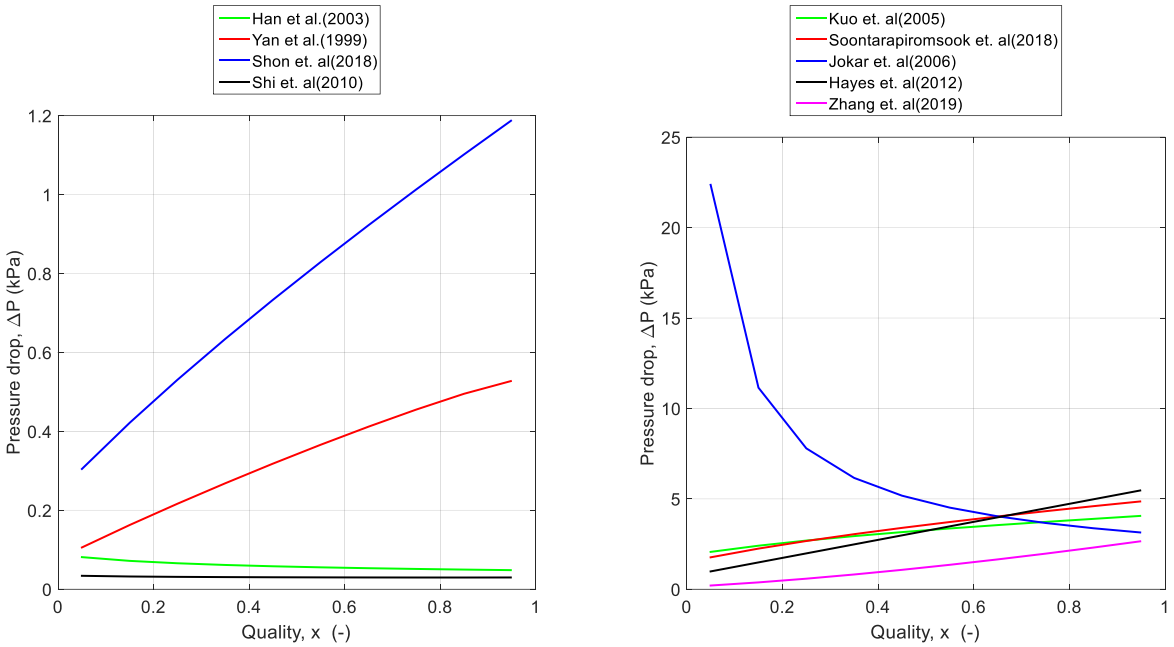

(c)

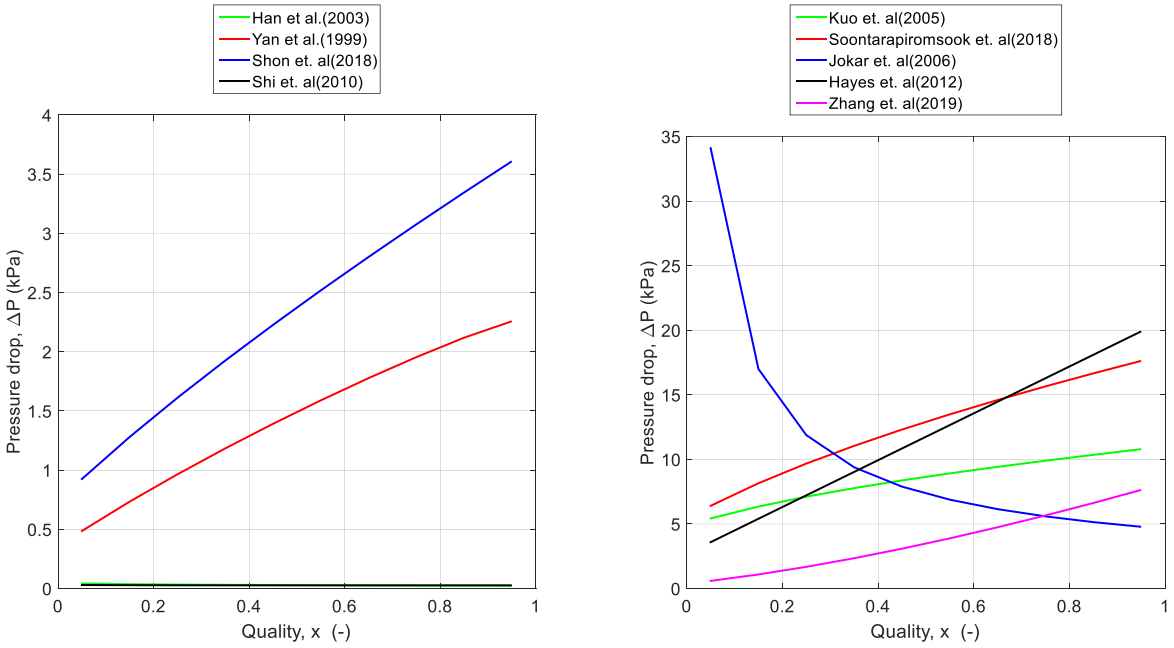

(d)

Fig. 4.6. Overview of condensation pressure drop predictions for R1234ze with (a) Re=462, (b) Re=500, (c) Re=1000 and (d) Re=3000.

4.3. Single phase heat transfer

The pressure drop will be calculated and used in the heat transfer analysis as mentioned in Chapter 2.3.

The correlations shown in Table 4-3 are introduced to the single phase heat exchanger's modeling, which was presented at Chapter 2.3 and the pressure drop for both sides is calculated.

The analysis is carried out using three different vaporizing fluids: R245ca, R1234ze and Cyclopentane. The working conditions are identical to the ones used in Chapter 3.3. The key conclusions are summarized below:

- In general results tend to be higher with the use of Cyclopentane and lower with the use of R1234ze.
- All results' curves have approximately zero slope.
- Pressure drop results are proportional to the Reynolds number.
- Muley and Manglik's correlation is piecewise, something appearing when Reynolds number reaches 1000.
- Focke correlation's results are the highest.
- Chisholm and Wanniarachchi and Thonon correlation's results are similar.
- Sinnott, Muley and Manglik and Tovazhnyanski correlation's results tend to be similar in the turbulent region.

Table 4-3 Single phase heat transfer friction factor correlations

Correlation	**Working fluid**	**Range**	**Reference**
$f = 5.03 + 755/Re, \quad 90 < Re < 400$ $f = 26.8Re^{-0.209}, \quad 400 < Re < 16{,}000$	Electrolyte solutions		Focke et al. [45]
$f = 0.973Re^{-0.25}$	n/a	$1{,}000 < Re < 40{,}000$ $30° < \varphi < 80°$	Chisholm and Wanniarachchi [46]
$f = 45.57Re^{-0.67}, \quad Re < 160$ $f = 0.37Re^{-0.172}, \quad 160 < Re$	n/a		Thonon et al. [60]
$\Delta p = \frac{\xi L_p}{D_h} \cdot \frac{\rho v^2}{2}$, the friction factor ξ derived from respective equations presented in Chapter 3	n/a		Martin [61]
$f = 0.085e^{1.52tan\beta}Re^{-(0.25-0.06ln\beta)}$	n/a	$2{,}000 < Re < 25{,}000$	Tovazhnyanski et. al [62]
$f = \begin{cases} \left(\left(\frac{40.32}{Re}\right)^5 + (8.12Re^{-0.5})^5\right)^{0.2}, 2 \le Re \le 200 \\ 1.274Re^{-0.15}, Re \ge 1{,}000 \end{cases}$	n/a		Muley and Manglik [63]
$f = 8 * 0.6Re^{-0.3}$	n/a	Turbulent region	Sinnott [64]
$f = 915Re^{-0.25}\left(\frac{D_h}{L}\right)$	n/a	$50 < Re < 20{,}000$	Maslov and Kovalenko [56]
$f = \left(f_l^3 + f_t^3\right)^{\frac{1}{3}}$ $f_t = 46.6\beta^{-1.08}\varphi^{1-p}Re^{-p}$ $f_l = 1774\beta^{-1.026}\varphi^2 Re^{-1}$ $p = 0.00423\beta + 0.0000223\beta^2$ *(β in deg)*	n/a	$1 < Re < 10{,}000$	Wanniarachchi et al. [52]

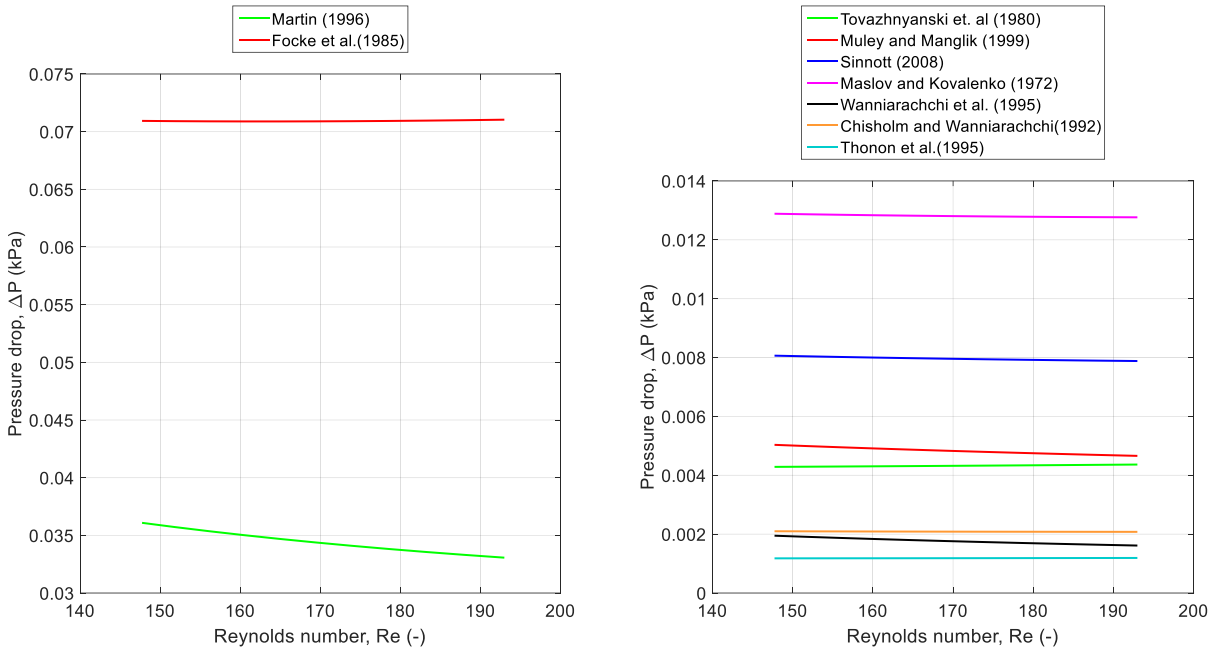
Martin (1996)
Focke et al.(1985)
Pressure drop, ΔP (kPa)
Reynolds number, Re (-)
Tovazhnyanski et. al (1980)
Muley and Manglik (1999)
Sinnott (2008)
Maslov and Kovalenko (1972)
Wanniarachchi et al. (1995)
Chisholm and Wanniarachchi(1992)
Thonon et al.(1995)
Pressure drop, ΔP (kPa)
Reynolds number, Re (-)

(a)

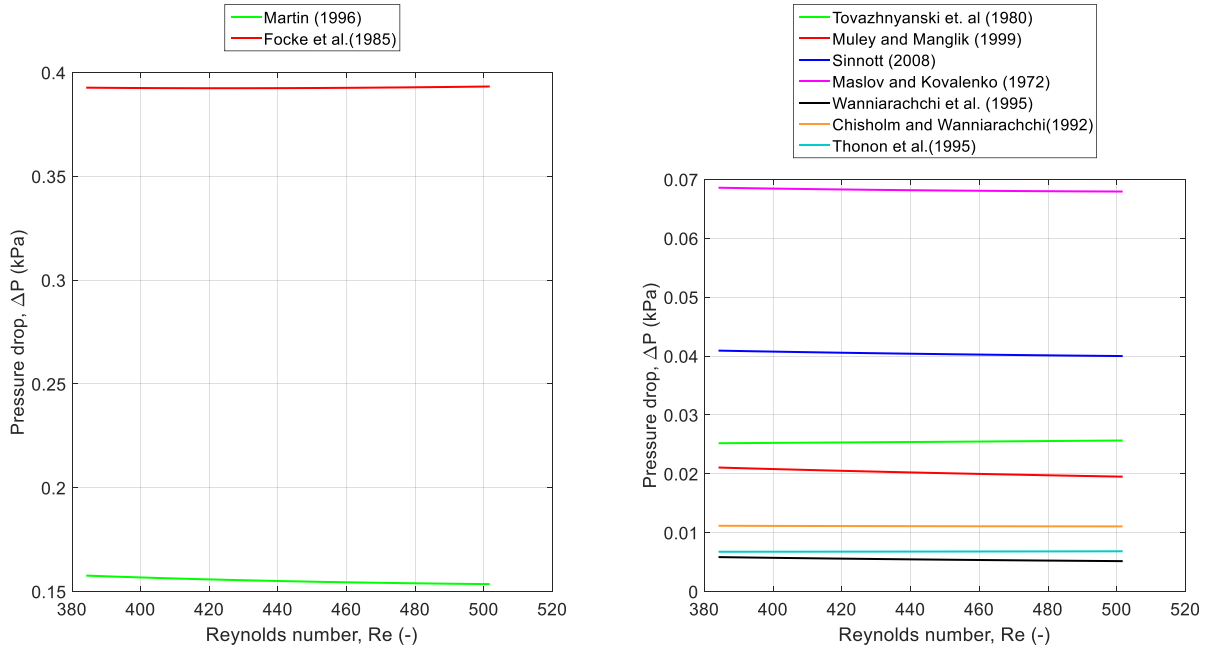
Martin (1996)
Focke et al.(1985)
Pressure drop, ΔP (kPa)
Reynolds number, Re (-)
Tovazhnyanski et. al (1980)
Muley and Manglik (1999)
Sinnott (2008)
Maslov and Kovalenko (1972)
Wanniarachchi et al. (1995)
Chisholm and Wanniarachchi(1992)
Thonon et al.(1995)
Pressure drop, ΔP (kPa)
Reynolds number, Re (-)

(b)

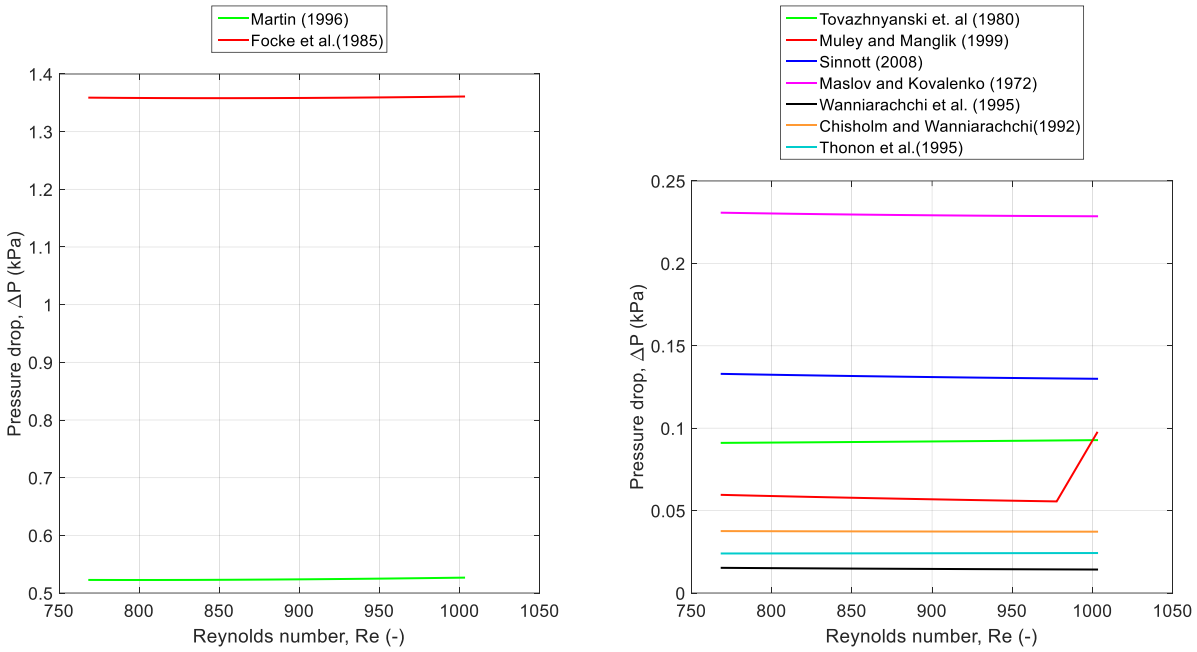

(c)

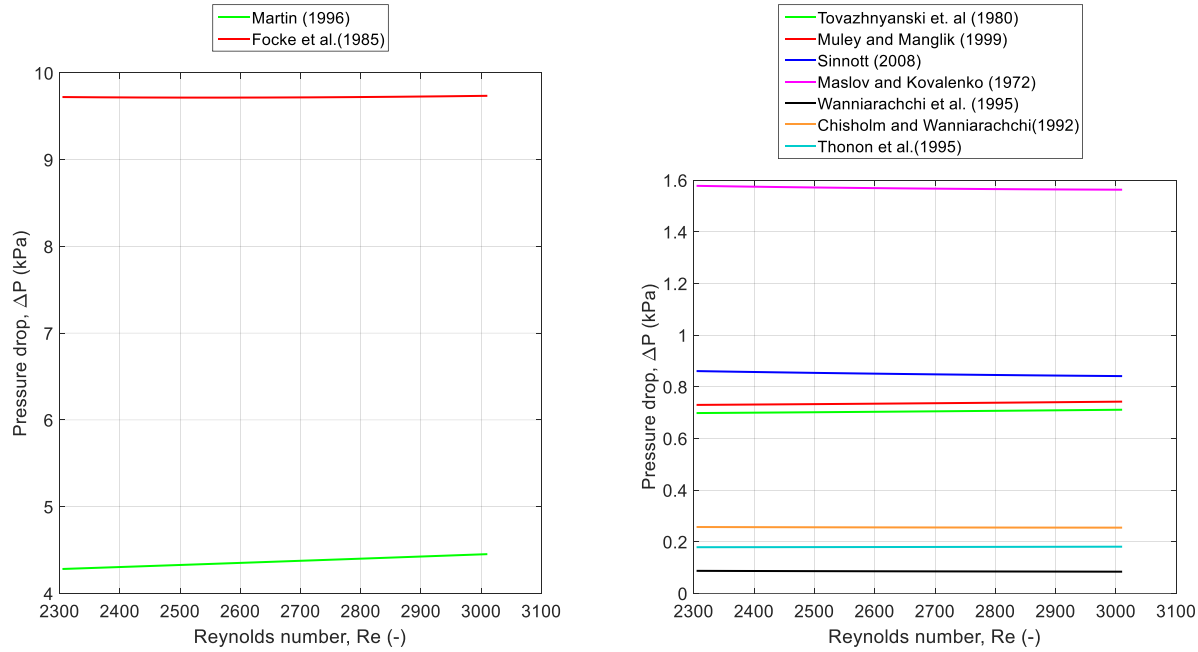

(d)

Fig. 4.7. Overview of single phase pressure drop predictions for Cyclopentane with (a) Re=192, (b) Re=500, (c) Re=1000 and (d) Re=3000.

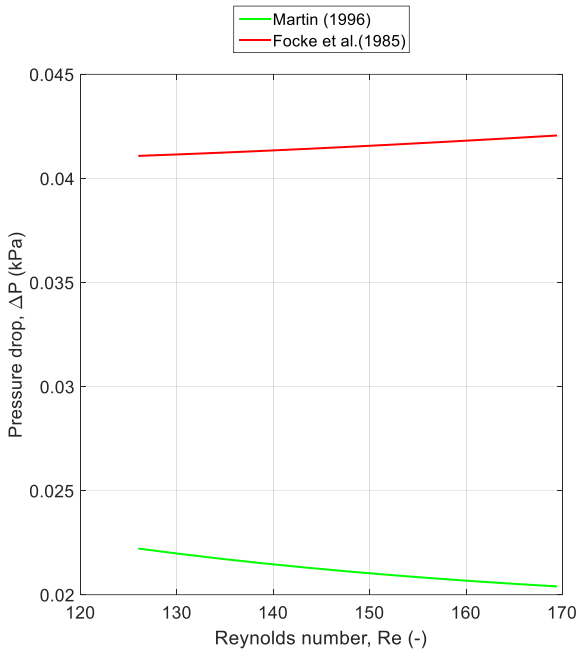
Martin (1996)
Focke et al.(1985)
Pressure drop, ΔP (kPa)
Reynolds number, Re (-)

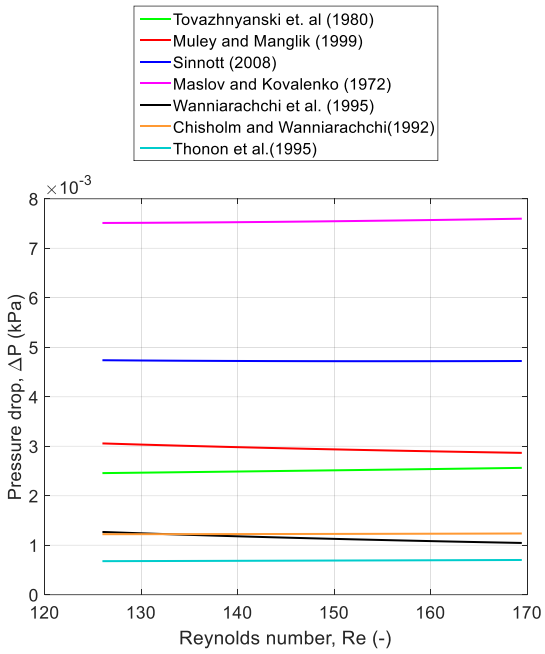
Tovazhnyanski et. al (1980)
Muley and Manglik (1999)
Sinnott (2008)
Maslov and Kovalenko (1972)
Wanniarachchi et al. (1995)
Chisholm and Wanniarachchi(1992)
Thonon et al.(1995)
×10^-3
Pressure drop, ΔP (kPa)
Reynolds number, Re (-)

(a)

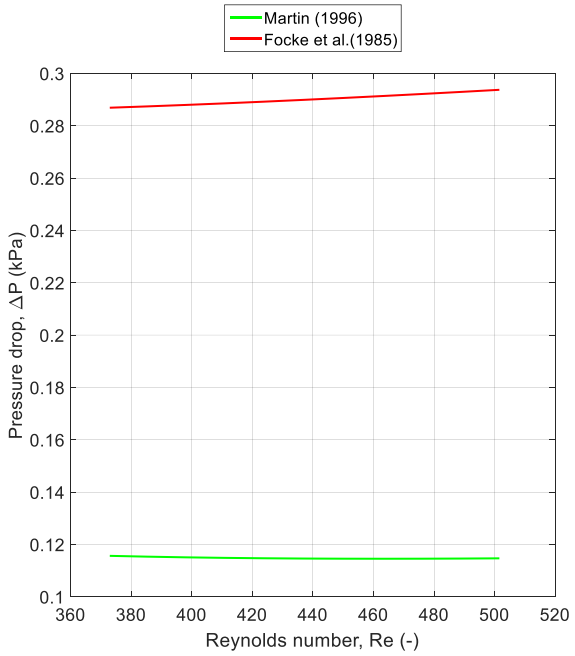
Martin (1996)
Focke et al.(1985)
Pressure drop, ΔP (kPa)
Reynolds number, Re (-)

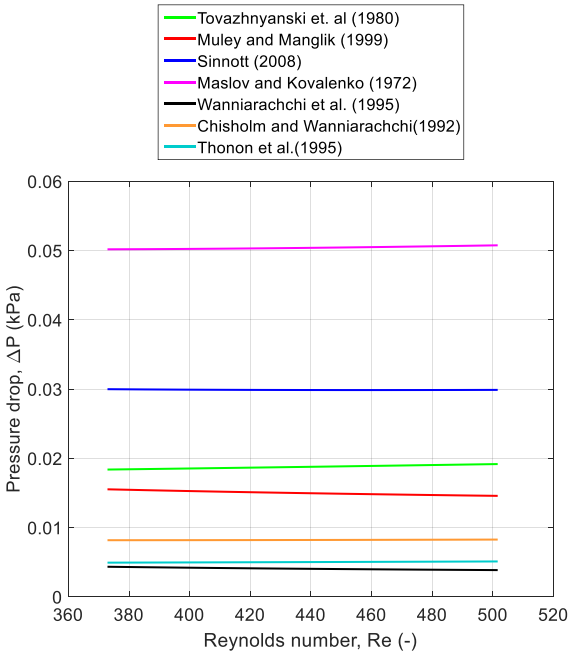
Tovazhnyanski et. al (1980)
Muley and Manglik (1999)
Sinnott (2008)
Maslov and Kovalenko (1972)
Wanniarachchi et al. (1995)
Chisholm and Wanniarachchi(1992)
Thonon et al.(1995)
Pressure drop, ΔP (kPa)
Reynolds number, Re (-)

(b)

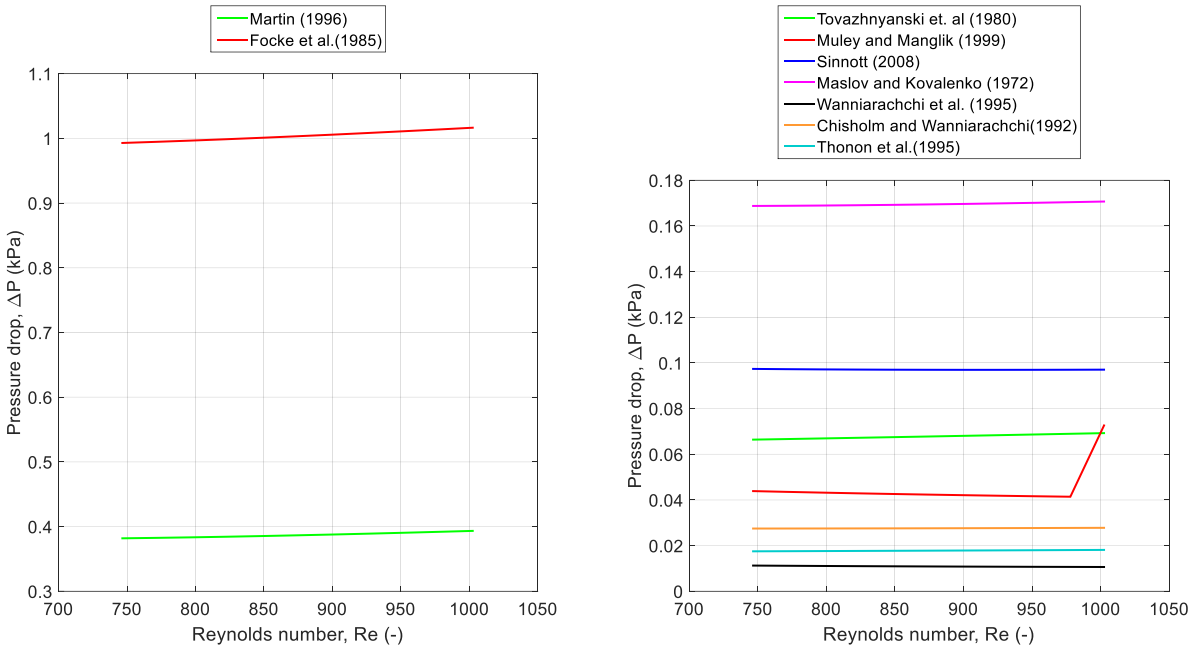

(c)

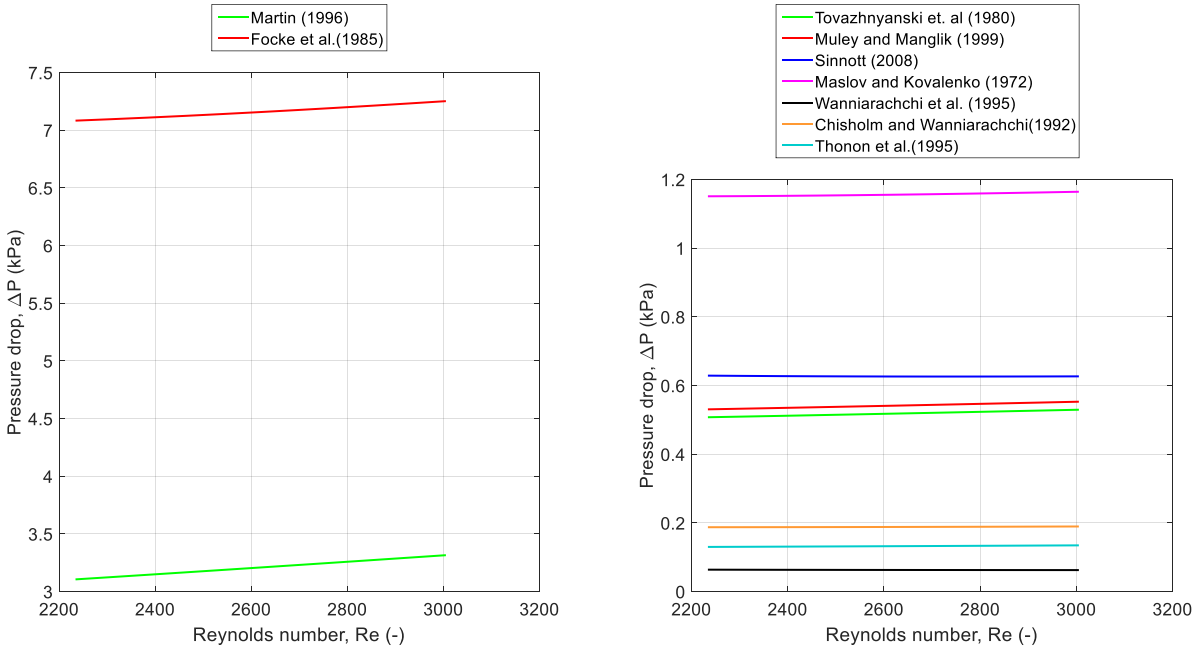

(d)

Fig. 4.8. Overview of single phase pressure drop predictions for R245ca with (a) Re=169, (b) Re=500, (c) Re=1000 and (d) Re=3000.

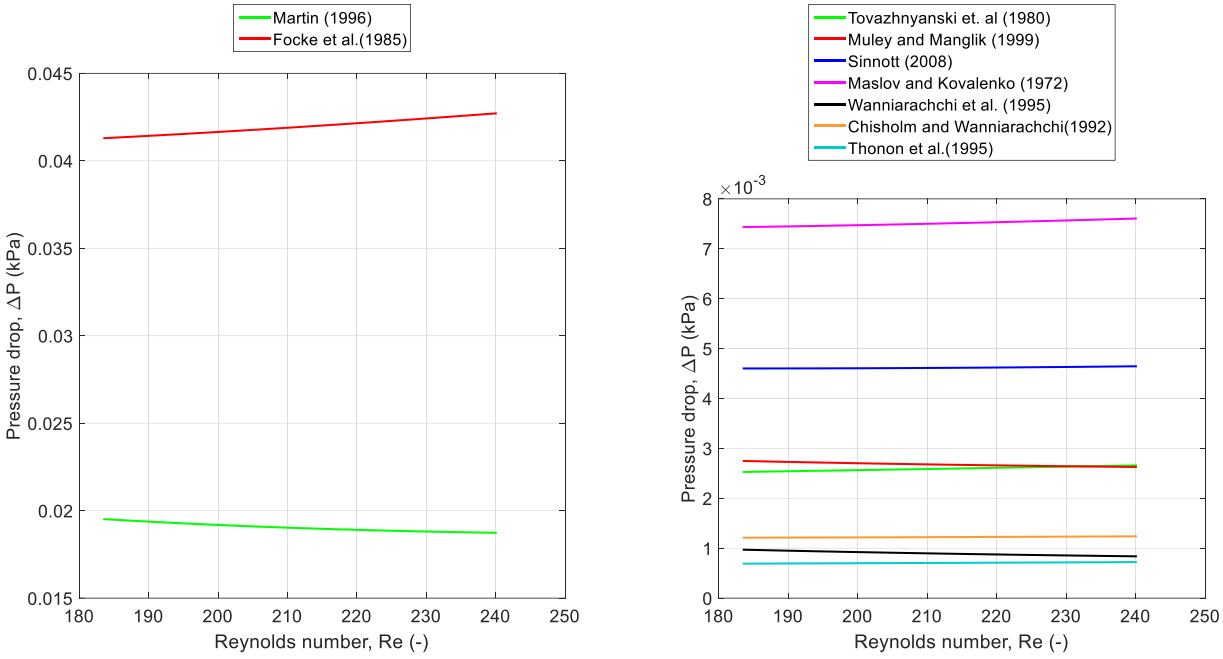
Martin (1996)
Focke et al.(1985)
Pressure drop, ΔP (kPa)
Reynolds number, Re (-)
Tovazhnyanski et. al (1980)
Muley and Manglik (1999)
Sinnott (2008)
Maslov and Kovalenko (1972)
Wanniarachchi et al. (1995)
Chisholm and Wanniarachchi(1992)
Thonon et al.(1995)
×10-3
Pressure drop, ΔP (kPa)
Reynolds number, Re (-)

(a)

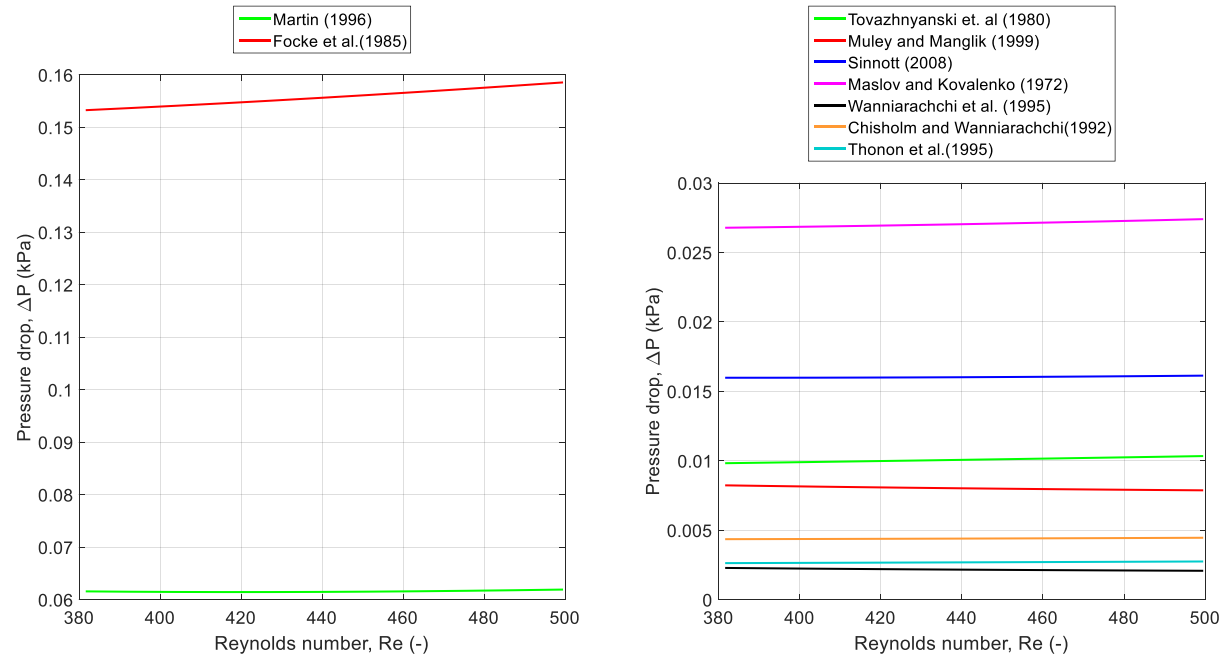
Martin (1996)
Focke et al.(1985)
Pressure drop, ΔP (kPa)
Reynolds number, Re (-)
Tovazhnyanski et. al (1980)
Muley and Manglik (1999)
Sinnott (2008)
Maslov and Kovalenko (1972)
Wanniarachchi et al. (1995)
Chisholm and Wanniarachchi(1992)
Thonon et al.(1995)
Pressure drop, ΔP (kPa)
Reynolds number, Re (-)

(b)

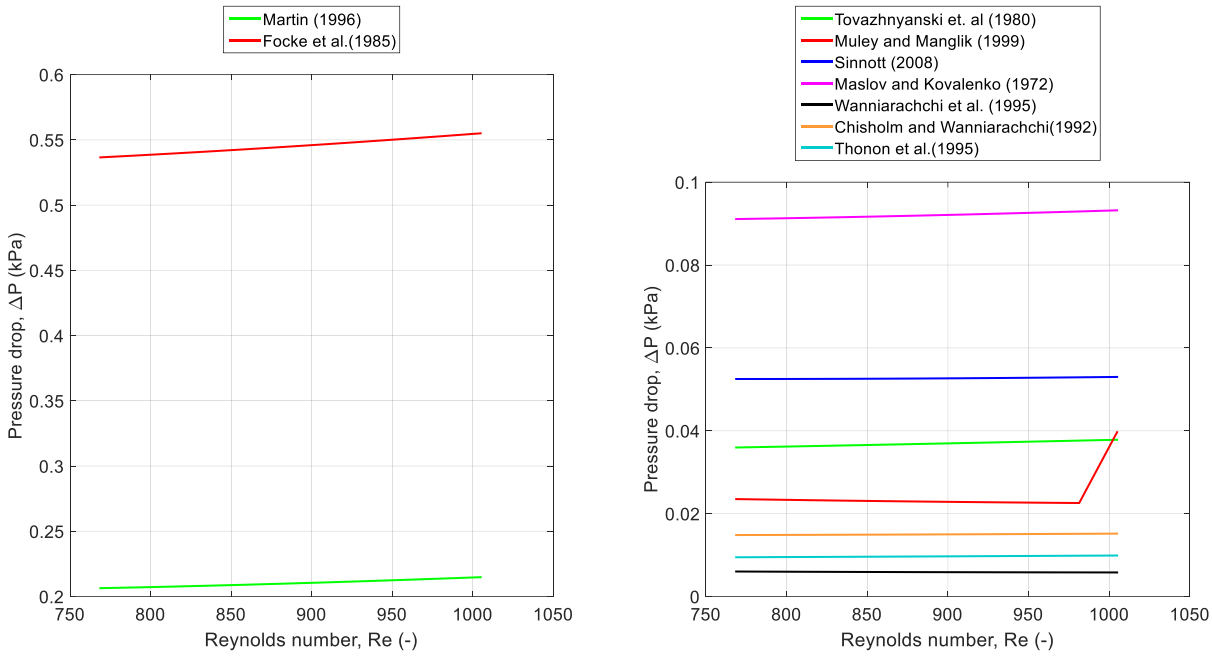

(c)

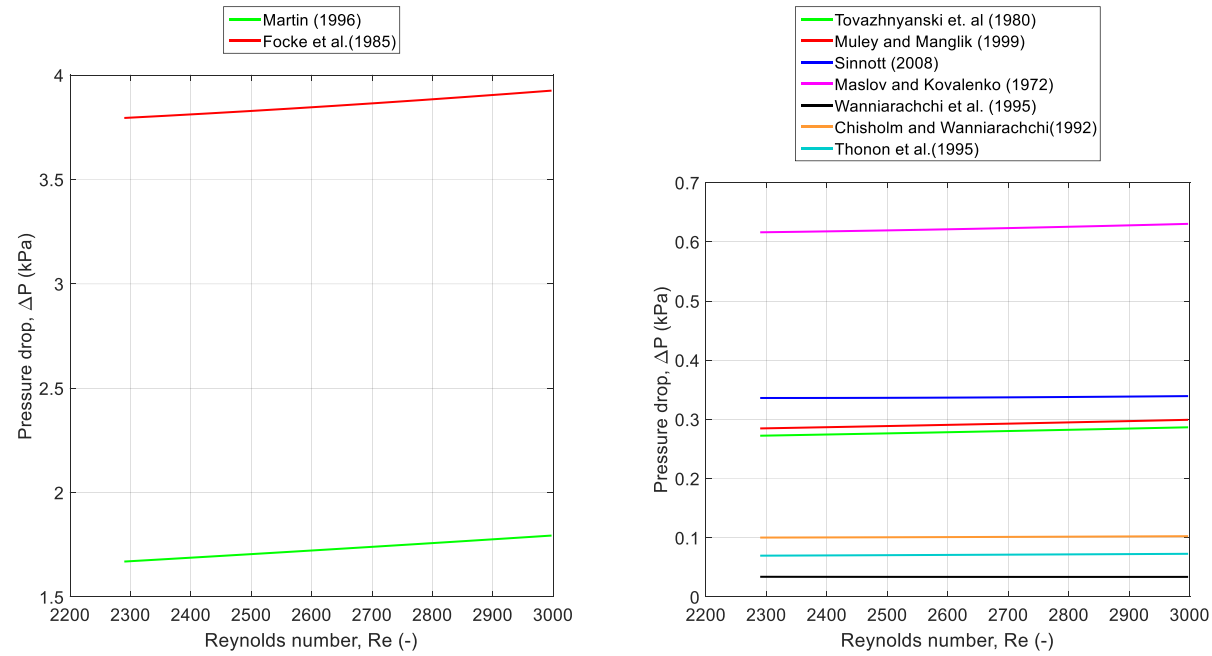

(d)

Fig. 4.9. Overview of single phase pressure drop predictions for R1234ze with (a) Re=240, (b) Re=500, (c) Re=1000 and (d) Re=3000.

Chapter 5. Conclusions

To sum up the abovementioned results, in this chapter, some tables will be presented, indicating a general conclusion for the calculations made for each scenario in Chapter 3 and Chapter 4. The tables provide information on the scale of predict for each case and each correlation.

5.1. Heat transfer coefficient

The tables for the heat transfer coefficient were created by using the default conditions mentioned on each of the sub- chapters of Chapter 3, with the use of R245ca. It was estimated that a well predicted value for the heat transfer coefficient for the evaporation and the condensation case is in the region of 3000 to 5000 W/m^2K, and for the single phase heat transfer in the region of 800 to 1500 W/m^2K. Based on these conditions the following tables were made:

Table 5-1 Evaporation heat transfer coefficient scale of predict

Reference	Range of application	Test range	Slope	Scale of Predict	Reynolds increase effect	Use of R1234ze	Use of Cyclopen
Yan and Lin (1999) [13]	$2000 < \mathrm{Re_{eq}} < 10000$	$Re_{eq} = 104 \div 152$ $\rightarrow out\ of\ range$	↘	Slight over-prediction	Low effect	↘ Slight over-prediction	↘ Slight over-prediction
Hsieh and Lin (2002) [14]	$50 < \mathrm{G} < 125$ $8.5 < \mathrm{q_{flux}} < 30$	$G = 6.62 \rightarrow out\ of\ range$ $q_{flux} = 44.9 \div 49.3$ $\rightarrow out\ of\ range$	↗	Over-prediction	Increase	↗ Over-prediction	↗ Over-prediction
Han et. al (2003) [15]	$13 < \mathrm{G} < 34$ $2.5 < \mathrm{q_{flux}} < 8.5$	$G = 6.62 \rightarrow out\ of\ range$ $q_{flux} = 44.9 \div 49.3$ $\rightarrow out\ of\ range$	↘	Well predicted	Increase	↘ Well predicted	↘ Well predicted
Kim et. al (2007) [16]	$600 < \mathrm{Re} < 2{,}300$ $40 \leq \mathrm{G} \leq 80$	$Re = 157.7$ $\rightarrow out\ of\ range$ $G = 6.62 \rightarrow out\ of\ range$	↘	Well predicted	Increase	↘ Slight under-prediction	↘ Well predicted
Longo et. al (2015) [18]	$5.7 < \mathrm{G} < 125$ $2.7 < \mathrm{q_{flux}} < 36.5$	$G = 6.62 \rightarrow in\ range$ $q_{flux} = 44.9 \div 49.3$ $\rightarrow out\ of\ range$	→	Over-prediction	Low effect	→ Over-prediction	→ Well predicted
Palmer et. al (2000) [17]	$13 < \mathrm{Re_{eq}} < 230$ $1.6 \leq \mathrm{G} \leq 19$ $1.3 \leq \mathrm{q_{flux}} \leq 8.3$	$G = 6.62 \rightarrow in\ range$ $q_{flux} = 44.9 \div 49.3$ $\rightarrow out\ of\ range$ $Re_{eq} = 104 \div 152$ $\rightarrow in\ range$	↘↘	Well predicted $(0.25 \leq x \leq 0.55)$	Increase	↘↘ Under-prediction $(0.25 \leq x \leq 0.55)$	↘↘ Well predicted $(0.25 \leq x \leq 0.55)$

Kim and Park (2003) [19]	$45 \leq \mathrm{G} \leq 55$ $4 \leq \mathrm{q_{flux}} \leq 8$	$G = 6.62 \rightarrow out\ of\ range$ $q_{flux} = 44.9 \div 49.3$ $\rightarrow out\ of\ range$	↗	Slight over-prediction	Decrease	↗ Well predicted	↗ Over-prediction
Ayub (2003) [20]	$4000 \leq \mathrm{Re} \leq 16000$, US units	$Re = 157.7$ $\rightarrow out\ of\ range$	→	Over-prediction	Increase	→ Over- prediction	→ Over-prediction
Arima et. al (2010) [21]	$40 < \mathrm{Re} < 3600$ $7.4 \leq \mathrm{G} \leq 15$ $15.4 \leq \mathrm{q_{flux}} \leq 24.5$	$G = 6.62$ $\rightarrow slightly\ out\ of\ range$ $q_{flux} = 44.9 \div 49.3$ $\rightarrow out\ of\ range$ $Re = 157.7 \rightarrow in\ range$	↗↘	Under-prediction	Low effect	↗↘ Under-prediction	↗↘ Under-prediction
Khan and Chyu (2010) and Khan et. al (2014) [22, 23]	$500 < \mathrm{Re} < 2500$ $5.5 < \mathrm{G} < 27$ $20 \leq \mathrm{q_{flux}} \leq 70$ $1225 < \mathrm{Re_{eq}} < 3000$	$G = 6.62 \rightarrow in\ range$ $q_{flux} = 44.9 \div 49.3$ $\rightarrow in\ range$ $Re = 157.7$ $\rightarrow out\ of\ range$ $Re_{eq} = 104 \div 152$ $\rightarrow out\ of\ range$	→	Well predicted	Low effect	→ Slight under-prediction	→ Well predicted
Taboas et. al (2012) [24]	$70 \leq \mathrm{G} \leq 140$ $20 \leq \mathrm{q_{flux}} \leq 50$	$G = 6.62 \rightarrow out\ of\ range$ $q_{flux} = 44.9 \div 49.3$ $\rightarrow in\ range$	→	Under-prediction	Low effect	→ Under-prediction	→ Under-prediction
Huang et. al (2012) [25]	$5.6 \leq \mathrm{G} \leq 52.3$ $1.8 \leq \mathrm{q_{flux}} \leq 6.9$	$G = 6.62 \rightarrow in\ range$ $q_{flux} = 44.9 \div 49.3$ $\rightarrow out\ of\ range$	↗	Over-prediction	Slight increase	↗ Over- prediction	↗ Over-prediction
Lee et. al (2014) [26]	$14.5 \leq \mathrm{G} \leq 33.6$ $15 \leq \mathrm{q_{flux}} \leq 30$	$G = 6.62 \rightarrow out\ of\ range$ $q_{flux} = 44.9 \div 49.3$ $\rightarrow out\ of\ range$	↘	Well predicted ($x \leq 0.8$)	Low effect	↘ Slight under-prediction($x \leq 0.8$)	↘ Well predicted ($x \leq 0.8$)

Almalfi et. al (2016) [27]	N/A	N/A	↗	Slight over-prediction	Increase	↗ Well predicted	↗ Slight over-prediction
Koyama et. al (2014) [28]	N/A	N/A	↗↘	Well predicted	Increase	↗↘ Slight under-prediction	↗↘ Well predicted
Vakili-Farahani et. al (2014) [29]	$10 \leq G \leq 85$ $0.1 \leq q_{flux} \leq 4.2$	$G = 6.62 \rightarrow out\ of\ range$ $q_{flux} = 44.9 \div 49.3$ $\rightarrow out\ of\ range$	↗	Over-prediction	Increase	↗ Slight over-prediction	↗ Over-prediction

Table 5-2 Condensation heat transfer coefficient scale of predict

Reference	Range of application	Test range	Slope	Scale of Predict	Reynolds increase effect	Use of R1234ze	Use of Cyclopen
Shah (1979) (modified) [30]	N/A	N/A	↗	Under-prediction	Increase	↗ Under-prediction	↗ Under-prediction
Yan et. al (1999) [31]	$500 < Re_{eq} < 1{,}000$ $60 \leq G \leq 120$	$Re_{eq} = 500 \div 1800$ $\rightarrow mostly\ in\ range$ $G = 17.84 \rightarrow out\ of\ range$	↗	Well predicted	Increase	↗ Slight under-prediction	↗ Well predicted
Thonon and Bontemps (2002) [32]	$100 < Re_{eq} < 2{,}000$	$Re_{eq} = 500 \div 1800$ $\rightarrow in\ range$	↘↘	Well predicted ($x > 0.4$)	Low effect	↘↘ Well predicted ($x > 0.2$)	↘↘ Well predicted ($x > 0.4$)
Han et. al (2003) [33]	$10 < G < 35$ $4.7 < q < 5.3$	$G = 17.84 \rightarrow in\ range$ $q = 17.3 \div 37$ $\rightarrow out\ of\ range$	↗	Slight under-prediction	Low effect	↗ Slight under-prediction	↗ Slight under-prediction
Longo et. al (2014,2015) [34, 35]	N/A	N/A	↗	Well predicted	Low effect ($Re \leq 1000$) Increase (Turbulent region)	↗ Well predicted	Piecewise function Well predicted
Palmer et. al (2000) [17]	$13 < Re_{eq} < 230$ $1.6 \leq G \leq 19$ $1.3 \leq q \leq 8.3$	$Re_{eq} = 500 \div 1800$ $\rightarrow out\ of\ range$ $G = 17.84 \rightarrow in\ range$ $q = 17.3 \div 37$ $\rightarrow\ out\ of\ range$	→	Under-prediction	Slight increase	→ Under-prediction	→ Under-prediction

Kuo et. al (2005) [36]	$50 \leq G \leq 150$ $10 \leq q$	$G = 17.84 \rightarrow out\ of\ range$ $q = 17.3 \div 37 \rightarrow in\ range$	↗	Well predicted	Increase	↗ Over-prediction	↗ Over-prediction
Mancin et. al (2012) [37]	$15 \leq G \leq 40$	$G = 17.84 \rightarrow in\ range$	N/A	N/A	N/A	N/A	↗↗ Over-prediction
Zhang et. al (2019) [38]	$16 \leq G \leq 90$ $4 \leq q \leq 57.4$	$G = 17.84 \rightarrow in\ range$ $q = 17.3 \div 37 \rightarrow in\ range$	↗	Over- prediction	Increase	↗ Over-prediction	↗ Over-prediction
Wang and Zhao (1993) [39]	N/A	N/A	↗	Under-prediction	Increase	↗ Under-prediction	↗ Under-prediction
Winkelmann (2010) [40]	$0.07 < Co < 0.28$ $6.9 \leq q \leq 51$	$Co = 0.01 \div 1.12$ $\rightarrow mostly\ out\ of\ range$ $q = 17.3 \div 37 \rightarrow in\ range$	↗↗	Over- prediction	Low effect	↗↗ Well predicted $(x < 0.5)$	↗↗ Over-prediction
Shon et. al (2018) [41]	$13 \leq G \leq 23.8$ $2.5 \leq q \leq 4.5$	$G = 17.84 \rightarrow in\ range$ $q = 17.3 \div 37$ $\rightarrow out\ of\ range$	↗	Well predicted	Increase	↗ Well predicted	↗ Slight over-prediction
Jokar et. al (2006) [42]	N/A	N/A	↗	Under-prediction	Increase	↗ Under-prediction	↗ Under-prediction
Shi et. al (2010) [43]	$22 \leq G \leq 65$ $11.5 \leq q \leq 35$	$G = 17.84 \rightarrow in\ range$ $q = 17.3 \div 37 \rightarrow in\ range$	↗↗	Well predicted $(x < 0.7)$	Increase	↗↗ Well predicted $(x < 0.9)$	↗↗ Well predicted $(x < 0.5)$

Soontarapiromsook et al. (2018) [44]	$61 \leq G \leq 89$ $5 \leq q \leq 15$	$G = 17.84 \rightarrow out\ of\ range$ $q = 17.3 \div 37$ $\rightarrow out\ of\ range$	↗	Over- prediction	Increase	↗ Slight under-prediction	↗ Over-prediction

Table 5-3 Single phase heat transfer coefficient scale of predict

Reference	Range of application	Test range	Slope	Scale of Predict	Reynolds increase effect	Use of R1234ze	Use of Cyclopen
Focke (1985) [45]	N/A	N/A	↗	Slight under-prediction	Increase	↗ Slight under-prediction	↗ Well predicted
Chisholm (1992) [46]	$1{,}000 < Re < 40{,}000$	$Re = 192 \rightarrow out\ of\ range$	↗	Slight under-prediction	Increase	→ Slight under-prediction	↗ Slight under-prediction
Walraven (2013) [48]	N/A	N/A	→ Piecewise	Under-prediction	Increase	↘ Piecewise Under-prediction	→ Piecewise Under-prediction
Yan and Lin (1999) [13]	N/A	N/A	↗ Piecewise	Under-prediction	Increase	→ Piecewise Under-prediction	↗ Piecewise Under-prediction
Donowski (2000) [49]	$Re \geq 200$	$Re = 192$ $\rightarrow slighlty\ out\ of\ range$	↗	Under-prediction	Increase	↗ Under-prediction	↗ Slight under-prediction
Chisholm and Wanniarachchi (1991) [50]	$Re > 1000$	$Re = 192 \rightarrow out\ of\ range$	↗	Slight under-prediction	Increase	→ Slight under-prediction	↗ Well predicted
Kim (1999) [51]	N/A	N/A	↗	Under-prediction	Increase	→ Under-prediction	↗ Under-prediction

Wanniarachchi (1995) [52]	N/A	N/A	→ Piecewise	Under-prediction	Increase	→ Piecewise Under-prediction	→ Piecewise Under-prediction
Talik et. al (1995) [54]	$1{,}450 \leq Re \leq 11{,}460$ $2.5 \leq Pr \leq 5.0$	$Re = 192 \rightarrow out\ of\ range$ $Pr = 3.72 \rightarrow in\ range$	↗	Under-prediction	Increase	↗ Under-prediction	↗ Under-prediction
Han et. al (2003) [15]	$2{,}000 \leq Re$ $2 \leq Pr \leq 6$	$Re = 192 \rightarrow out\ of\ range$ $Pr = 3.72 \rightarrow in\ range$	↗	Under-prediction	Increase	→ Under-prediction	↗ Under-prediction
Khan et. al (2014) [23]	$500 \leq Re \leq 2{,}500$ $3.5 \leq Pr \leq 6.5$	$Re = 192 \rightarrow out\ of\ range$ $Pr = 3.72 \rightarrow in\ range$	→ Piecewise	Under-prediction	Increase	→ Piecewise Under-prediction	→ Piecewise Slight under-prediction
Hayes et. al (2011) [55]	N/A	N/A	↗ Piecewise	Well predicted	Increase	→ Piecewise Well predicted	↗ Piecewise Well predicted
Maslov and Kovalenko (1972) [56]	$50 < Re < 20{,}000$	$Re = 192 \rightarrow in\ range$	→	Under-prediction	Increase	→ Under-prediction	→ Under-prediction
Longo and Gasparella (2007) [57]	$350 < Re < 1{,}100$ $5 < Pr < 10$	$Re = 192 \rightarrow out\ of\ range$ $Pr = 3.72$ $\rightarrow out\ of\ range$	↗	Under-prediction	Increase	↗ Under-prediction	↗ Slight under-prediction
Okada et. al (1972) [58]	$400 < Re < 15{,}000$	$Re = 192 \rightarrow out\ of\ range$	→	Under-prediction	Increase	→ Under-prediction	→ Under-prediction

5.2. Pressure drop

The tables for the pressure drop were, as mentioned in Chapter 5.1, created by using the default conditions mentioned on each of the sub- chapters of Chapter 3, with the use of R245ca. It was estimated that a well predicted value for the pressure drop for the evaporation case is in the region of 0.03 to 0.1 kPa, for the condensation case in the region of 1 to 4 kPa, and for the single phase heat transfer in the region of 0.02 to 0.07 kPa. Based on these conditions the following tables were made:

Table 5-4 Evaporation pressure drop scale of predict

Reference	Range of application	Test range	Slope	Scale of Predict	Reynolds increase effect	Use of R1234ze	Use of Cyclopen
Yan and Lin (1999) [13]	N/A	N/A	↘	Over- prediction	Increase	↘ Over- prediction	↘ Over- prediction
Hsieh and Lin (2002) [14]	N/A	N/A	↘	Over- prediction	Increase	↘ Over- prediction	↘ Over- prediction
Han et. al (2003) [15]	$13 < G < 34$ $2.5 < q < 8.5$	$G = 6.62 \rightarrow out\ of\ range$ $q_{flux} = 44.9 \div 49.3$ $\rightarrow out\ of\ range$	↘	Well predicted	Increase	↘ Well predicted	↘ Well predicted
Ayub (2003) [20]	$4000 \leq Re \leq 16000, US\ units$	$Re = 157.7$ $\rightarrow out\ of\ range$	↘	Well predicted	Increase	↘ Well predicted	↘ Well predicted
Khan and Chyu (2010) and Khan et. al (2014) [22, 23]	$500 < Re < 2500$ $5.5 < G < 27$ $20 \leq q_{flux} \leq 70$ $3.5 < Pr < 61225 < Re_{eq} < 3000$	$Re = 157.7$ $\rightarrow out\ of\ range$ $G = 6.62 \rightarrow in\ range$ $q_{flux} = 44.9 \div 49.3$ $\rightarrow in\ range$ $Pr = 3.64 \rightarrow in\ range$ $Re_{eq} = 104 \div 152$ $\rightarrow out\ of\ range$	↘	Over- prediction	Increase	↘ Over- prediction	↘ Over- prediction

Huang et. al (2012) [25]	$5.6 \leq G \leq 52.3$ $1.8 \leq q_{flux} \leq 6.9$	$G = 6.62 \rightarrow in\ range$ $q_{flux} = 44.9 \div 49.3$ $\rightarrow out\ of\ range$	↘	Over- prediction	Increase	↘ Over- prediction	↘ Over-prediction
Lee et. al (2014) [26]	$14.5 \leq G \leq 33.6$ $15 \leq q_{flux} \leq 30$	$G = 6.62 \rightarrow out\ of\ range$ $q_{flux} = 44.9 \div 49.3$ $\rightarrow out\ of\ range$	↘	Under-prediction	Low effet	↘ Under-prediction	↘ Under-prediction
Almalfi et. al (2016) [27]	N/A	N/A	↘	Over- prediction	Increase	↘ Over- prediction	↘ Over-prediction

Table 5-5 Condensation pressure drop scale of predict

Reference	Range of application	Test range	Slope	Scale of Predict	Reynolds increase effect	Use of R1234ze	Use of Cyclopen
Yan et al. (1999) [31]	$500 < Re < 1{,}000$ $60 \leq G \leq 120$	$Re = 179$ $\rightarrow out\ of\ range$ $G = 17.84$ $\rightarrow out\ of\ range$	↗	Under-prediction	Slight increase	↗ Under-prediction	↗ Under-prediction
Han et al. (2003b) [33]	$10 < G < 35$ $4.7 < q < 5.3$	$G = 17.84 \rightarrow in\ range$ $q = 17.3 \div 37$ $\rightarrow out\ of\ range$	↘	Under-prediction	Low effect	↘ Under-prediction	↘ Under-prediction
Kuo et. al (2005) [36]	$50 \leq G \leq 150$ $10 \leq q \leq 20$	$G = 17.84$ $\rightarrow out\ of\ range$ $q = 17.3 \div 37$ $\rightarrow mostly\ out\ of\ range$	↗	Slight over-prediction	Increase	↗ Slight under-prediction	↗ Slight over-prediction
Shi et. al (2010) [43]	$22 \leq G \leq 65$ $11.5 \leq q \leq 35$	$G = 17.84$ $\rightarrow out\ of\ range$ $q = 17.3 \div 37$ $\rightarrow mostly\ in\ range$	→	Under-prediction	Low effect	→ Under-prediction	→ Under-prediction
Zhang et. al (2019) [38]	$16 \leq G \leq 90$ $4 \leq q \leq 57.4$	$G = 17.84 \rightarrow in\ range$ $q = 17.3 \div 37$ $\rightarrow in\ range$	↗	Well predicted	Increase	↗ Slight under-prediction	↗ Slight over-prediction
Shon et. al (2018) [41]	$13 \leq G \leq 23.8$ $2.5 \leq q \leq 4.5$	$G = 17.84 \rightarrow in\ range$ $q = 17.3 \div 37$ $\rightarrow out\ of\ range$	↗	Well predicted	Increase	↗ Under-prediction	↗ Slight over-prediction
Soontarapiromsook et al. (2018) [44]	$61 \leq G \leq 89$ $5 \leq q \leq 15$	$G = 17.84$ $\rightarrow out\ of\ range$ $q = 17.3 \div 37$ $\rightarrow out\ of\ range$	↗	Slight over-prediction	Increase	↗ Slight under-prediction	↗ Slight over-prediction

Jokar et. al (2006) [42]	N/A	N/A	↘	Over- prediction	Increase	↘ Well predicted	↘ Over-prediction
Hayes et. al (2012) [59]	$2 \leq G \leq 45$ $2.5 \leq q \leq 15.7$	$G = 17.84 \rightarrow in\ range$ $q = 17.3 \div 37$ $\rightarrow out\ of\ range$	↗	Over- prediction	Increase	↗ Slight under-prediction	↗ Over-prediction

Table 5-6 Single phase heat transfer pressure drop scale of predict

Reference	Range of application	Test range	Slope	Scale of Predict	Reynolds increase effect	Use of R1234ze	Use of Cyclopen
Focke et al. (1985) [45]	$90 < Re < 16{,}000$	$Re = 125 \div 169 \rightarrow in\ range$	↗	Well predicted	Increase	↗ Well predicted	→ Well predicted
Chisholm and Wanniarachchi (1992) [46]	$1{,}000 < Re < 40{,}000$	$Re = 125 \div 169 \rightarrow out\ of\ range$	→	Under-prediction	Increase	→ Under-prediction	→ Under-prediction
Thonon et al. (1995) [60]	N/A	N/A	→	Under-prediction	Increase	→ Under-prediction	→ Under-prediction
Martin(1996) [61]	N/A	N/A	↘	Well predicted	Increase	↘ Well predicted	↘ Well predicted
Tovazhnyanski et. al (1980) [62]	$2{,}000 < Re < 25{,}000$	$Re = 125 \div 169 \rightarrow out\ of\ range$	→	Under-prediction	Increase	→ Under-prediction	→ Under-prediction
Muley and Manglik (1999) [63]	N/A	N/A	↘	Under-prediction	Increase	↘ Under-prediction	↘ Under-prediction
Sinnott (2008) [64]	$Re \geq 3{,}000$	$Re = 125 \div 169 \rightarrow out\ of\ range$	→	Under-prediction	Increase	→ Under-prediction	→ Under-prediction
Maslov and Kovalenko (1972) [56]	$50 < Re < 20{,}000$	$Re = 125 \div 169 \rightarrow in\ range$	→	Under-prediction	Increase	→ Under-prediction	→ Slight under-prediction
Wanniarachchi et al. (1995) [52]	$1 < Re < 10{,}000$	$Re = 125 \div 169 \rightarrow in\ range$	↘	Under-prediction	Increase	↘ Under-prediction	↘ Under-prediction

5.3. Future work

Due to the lack of time many scenarios were not taken into consideration, but can be analyzed in other studies depending on future needs and new proposals. Some ideas worth looking into are the following:

- Using different fluids in the evaporation, condensation or single phase heat transfer case. For example fluids that are rarely used in each situation and are worth a deeper behavior analysis.
- Researching to find new correlations and include them in a similar analysis to compare them with the already tested correlations.
- Using a different type of heat exchanger, such as a shell and tube heat exchanger, to calculate the corresponding results with the use of the same correlations and conditions.
- Considering larger Reynolds number regions, and calculating the equivalent results for $Re < 100$, or $Re > 5000$.
- Investigating the scenario of supercritical flows.
- Using different script conditions such as initial temperatures, therefore alternating the pinch point in each case.

References

1. Som, S.K., *Introduction to heat transfer*. 2008, New Delhi: PHI Learning.
2. Thulukkanam, K., *Heat Exchanger Design Handbook, Second Edition*. 2013: Taylor & Francis.
3. Milani Shirvan, K., M. Mamourian, and J. Abolfazli Esfahani, *Experimental investigation on thermal performance and economic analysis of cosine wave tube structure in a shell and tube heat exchanger.* Energy Conversion and Management, 2018. **175**: p. 86-98.
4. Cartelle Barros, J.J., et al., *Sustainability optimisation of shell and tube heat exchanger, using a new integrated methodology.* Journal of Cleaner Production, 2018. **200**: p. 552-567.
5. Pandey, P.K., et al., *Heat Transfer Analysis of Shell and Tube Heat Exchanger using Al2O3/SiC Nanofluid.* European Journal of Advances in Engineering and Technology, 2017. **4**(8): p. 608-616.
6. Keshavarzian, S., et al., *Fuel saving due to pinch analysis and heat recovery in a petrochemical company*. 2015.
7. Guo, Y., et al., *Modeling of plate heat exchanger based on sensitivity analysis and model updating.* Chemical Engineering Research and Design, 2018. **138**: p. 418-432.
8. Lin, Z.-M., et al., *Characteristics of the Absolute Vorticity Flux along the Main Flow Direction on the Cross Section of the Channel Formed by Oval Tube Bank Fins.* Numerical Heat Transfer, Part A: Applications, 2010. **57**(9): p. 666-690.
9. Ahmadi, P., H. Hajabdollahi, and I. Dincer, *Cost and entropy generation minimization of a cross-flow plate fin heat exchanger using multi-objective genetic algorithm.* Journal of heat transfer, 2011. **133**(2): p. 021801.
10. Qasem, N.A.A. and S.M. Zubair, *Compact and microchannel heat exchangers: A comprehensive review of air-side friction factor and heat transfer correlations.* Energy Conversion and Management, 2018. **173**: p. 555-601.
11. Kwon, B., et al., *High power density air-cooled microchannel heat exchanger.* International Journal of Heat and Mass Transfer, 2018. **118**: p. 1276-1283.
12. Han, Y., et al., *A review of development of micro-channel heat exchanger applied in air-conditioning system.* Energy Procedia, 2012. **14**: p. 148-153.
13. Yan, Y.Y. and T.F. Lin, *Evaporation Heat Transfer and Pressure Drop of Refrigerant R-134a in a Plate Heat Exchanger.* Journal of Heat Transfer, 1999. **121**(1): p. 118-127.
14. Hsieh, Y.Y. and T.F. Lin, *Saturated flow boiling heat transfer and pressure drop of refrigerant R-410A in a vertical plate heat exchanger.* International Journal of Heat and Mass Transfer, 2002. **45**(5): p. 1033-1044.
15. Han, D.-H., K.-J. Lee, and Y.-H. Kim, *Experiments on the characteristics of evaporation of R410A in brazed plate heat exchangers with different geometric configurations.* Applied Thermal Engineering, 2003. **23**(10): p. 1209-1225.
16. Kim, I.-K., et al., *Experimental study on R-410a evaporation heat transfer characteristics in oblong shell and plate heat exchanger.* Heat transfer engineering, 2007. **28**(7): p. 633-639.
17. Palmer, S.C., W.V. Payne, and P.A. Domanski, *Evaporation and condensation heat transfer performance of flammable refrigerants in a brazed plate heat exchanger*. 2000: Citeseer.
18. Longo, G.A., et al., *A new model for refrigerant boiling inside Brazed Plate Heat Exchangers (BPHEs).* International Journal of Heat and Mass Transfer, 2015. **91**: p. 144-149.

19. Kim, S.J., et al. *Experimental study on R-134a evaporation heat transfer characteristics in plate and shell heat exchanger*. in *Proceedings of the 4th International Symposium on HVAC*. 2003.
20. Ayub, Z.H., *Plate Heat Exchanger Literature Survey and New Heat Transfer and Pressure Drop Correlations for Refrigerant Evaporators.* Heat Transfer Engineering, 2003. **24**(5): p. 3-16.
21. Arima, H., et al., *Local boiling heat transfer characteristics of ammonia in a vertical plate evaporator.* International Journal of Refrigeration, 2010. **33**(2): p. 359-370.
22. Khan, M. and M. Chyu, *Evaporation in Flooded Corrugated Plate Heat Exchangers with Ammonia and Ammonia/Miscible Oil, RP-1352.* American Society of Heating, Refrigerating and Air-Conditioning Engineers, Inc., Atlanta, GA, USA, 2010.
23. Khan, M.S., et al., *Evaporation heat transfer and pressure drop of ammonia in a mixed configuration chevron plate heat exchanger.* International Journal of Refrigeration, 2014. **41**: p. 92-102.
24. Táboas, F., et al., *Assessment of boiling heat transfer and pressure drop correlations of ammonia/water mixture in a plate heat exchanger.* International Journal of Refrigeration, 2012. **35**(3): p. 633-644.
25. Huang, J., T.J. Sheer, and M. Bailey-McEwan, *Heat transfer and pressure drop in plate heat exchanger refrigerant evaporators.* International Journal of Refrigeration, 2012. **35**(2): p. 325-335.
26. Lee, E., H. Kang, and Y. Kim, *Flow boiling heat transfer and pressure drop of water in a plate heat exchanger with corrugated channels at low mass flux conditions.* International Journal of Heat and Mass Transfer, 2014. **77**: p. 37-45.
27. Amalfi, R.L., F. Vakili-Farahani, and J.R. Thome, *Flow boiling and frictional pressure gradients in plate heat exchangers. Part 2: Comparison of literature methods to database and new prediction methods.* International Journal of Refrigeration, 2016. **61**: p. 185-203.
28. Koyama, K., et al., *Experimental study on thermal characteristics of ammonia flow boiling in a plate evaporator at low mass flux.* International Journal of Refrigeration, 2014. **38**: p. 227-235.
29. Vakili-Farahani, F., R. Amalfi, and J.R. Thome, *TWO-PHASE FLOW OF R245FA IN A 1MM CORRUGATION DEPTH PLATE HEAT EXCHANGER– PART II: FLOW BOILING HEAT TRANSFER.* Interfacial Phenomena and Heat Transfer, 2014. **2**(4).
30. Shah, M.M., *A general correlation for heat transfer during film condensation inside pipes.* International Journal of Heat and Mass Transfer, 1979. **22**(4): p. 547-556.
31. Yan, Y.-Y., H.-C. Lio, and T.-F. Lin, *Condensation heat transfer and pressure drop of refrigerant R-134a in a plate heat exchanger.* International Journal of Heat and Mass Transfer, 1999. **42**(6): p. 993-1006.
32. Thonon, B. and A. Bontemps, *Condensation of Pure and Mixture of Hydrocarbons in a Compact Heat Exchanger: Experiments and Modelling.* Heat Transfer Engineering, 2002. **23**(6): p. 3-17.
33. Han, D.H., K.J. Lee, and Y.H. Kim, *The characteristics of condensation in brazed plate heat exchangers with different chevron angles.* Journal of the Korean Physical Society, 2003. **43**(1): p. 66-73.
34. Longo, G., G. Righetti, and C. Zilio. *A New Model for Refrigeration Condensation Inside a Brazed Plate Heat Exchanger (BPHE)*. in *Proceedings of the 15th International Heat Transfer Conference, IHTC*. 2014.
35. Longo, G.A., G. Righetti, and C. Zilio, *A new computational procedure for refrigerant condensation inside herringbone-type Brazed Plate Heat Exchangers.* International Journal of Heat and Mass Transfer, 2015. **82**: p. 530-536.

36. Kuo, W.S., et al., *Condensation heat transfer and pressure drop of refrigerant R-410A flow in a vertical plate heat exchanger.* International Journal of Heat and Mass Transfer, 2005. **48**(25): p. 5205-5220.
37. Mancin, S., D. Del Col, and L. Rossetto, *Condensation of superheated vapour of R410A and R407C inside plate heat exchangers: Experimental results and simulation procedure.* International Journal of Refrigeration, 2012. **35**(7): p. 2003-2013.
38. Zhang, J., et al., *Condensation heat transfer and pressure drop characteristics of R134a, R1234ze(E), R245fa and R1233zd(E) in a plate heat exchanger.* International Journal of Heat and Mass Transfer, 2019. **128**: p. 136-149.
39. Wang, Z.-Z. and Z.-N. Zhao, *Analysis of Performance of Steam Condensation Heat Transfer and Pressure Drop in Plate Condensers.* Heat Transfer Engineering, 1993. **14**(4): p. 32-41.
40. Winkelmann, D., *Condensation of pure refrigerants and their zeotropic mixtures in plate heat exchangers*. 2010: Deutscher Kälte-und Klimatechnischer Verein.
41. Shon, B.H., et al., *Characteristics on condensation heat transfer and pressure drop for a low GWP refrigerant in brazed plate heat exchanger.* International Journal of Heat and Mass Transfer, 2018. **122**: p. 1272-1282.
42. Jokar, A., M.H. Hosni, and S.J. Eckels, *Dimensional analysis on the evaporation and condensation of refrigerant R-134a in minichannel plate heat exchangers.* Applied Thermal Engineering, 2006. **26**(17): p. 2287-2300.
43. Shi, Z.Y., et al., *Experimental investigation on condensation heat transfer and pressure drop of R134a in a plate heat exchanger.* Heat and Mass Transfer, 2010. **46**(10): p. 1177-1185.
44. Soontarapiromsook, J., et al., *Effect of surface roughness on the condensation of R-134a in vertical chevron gasketed plate heat exchangers.* Experimental Thermal and Fluid Science, 2018. **91**: p. 54-63.
45. Focke, W.W., J. Zachariades, and I. Olivier, *The effect of the corrugation inclination angle on the thermohydraulic performance of plate heat exchangers.* International Journal of Heat and Mass Transfer, 1985. **28**(8): p. 1469-1479.
46. Chisholm, D. and A. Wanniarachchi, *Maldistribution in single-pass mixed-channel plate heat exchangers.* ASME, NEW YORK, NY(USA). 1992. **201**: p. 95-99.
47. Bogaert, R. and A. Böles, *GLOBAL PERFORMANCE OF A PROTOTYPE BRAZED PLATE HEAT EXCHANGER IN A LARGE REYNOLDS NUMBER RANGE.* Experimental Heat Transfer, 1995. **8**(4): p. 293-311.
48. Walraven, D., B. Laenen, and W. D'haeseleer. *Optimum configuration of plate-type heat exchangers for the use in ORCs for low-temperature geothermal heat sources*. in *Proceedings of the European Geothermal Congress 2013*. 2013.
49. Donowski, V.D. and S.G. Kandlikar. *Correlating evaporation heat transfer coefficient of refrigerant R-134a in a plate heat exchanger*. in *Engineering Foundation Conference on Pool and Flow Boiling, Alaska*. 2000.
50. Chisholm, D. and A. Wanniarachchi. *Layout of plate heat exchangers*. in *ASME/JSME Thermal Engineering Proceedings*. 1991. ASME New York.
51. Kim, Y., *An experimental study on evaporation heat transfer characteristics and pressure drop in plate heat exchanger.* Diss. MS thesis, Yonsei University, 1999.
52. Wanniarachchi, A., et al., *Approximate correlations for chevron-type plate heat exchangers*. 1995, American Society of Mechanical Engineers, New York, NY (United States).
53. Muley, A. and R. Manglik, *Experimental study of turbulent flow heat transfer and pressure drop in a plate heat exchanger with chevron plates.* Journal of heat transfer, 1999. **121**(1): p. 110-117.

54. Talik, A.C., et al., *Heat transfer and pressure drop characteristics of a plate heat exchanger using a propylene-glycol/water mixture as the working fluid*. Vol. 314. 1995.
55. Hayes, N., A. Jokar, and Z.H. Ayub, *Study of carbon dioxide condensation in chevron plate exchangers; heat transfer analysis.* International Journal of Heat and Mass Transfer, 2011. **54**(5): p. 1121-1131.
56. Maslov, A. and L. Kovalenko, *Hydraulic resistance and heat transfer in plate heat exchangers.* Molochnaya Promyshlennost, 1972. **10**: p. 20-22.
57. Longo, G. and A. Gasparella, *Refrigerant R134a vaporisation heat transfer and pressure drop inside a small brazed plate heat exchanger.* International journal of refrigeration, 2007. **30**(5): p. 821-830.
58. Okada, K., et al., *Design and heat transfer characteristics of new plate heat exchanger.* Heat Transfer Japanese Research, 1972. **1**(1): p. 90-95.
59. Hayes, N., A. Jokar, and Z.H. Ayub, *Study of carbon dioxide condensation in chevron plate exchangers; pressure drop analysis.* International Journal of Heat and Mass Transfer, 2012. **55**(11): p. 2916-2925.
60. Thonon, B., R. Vidil, and C. Marvillet, *Recent research and developments in plate heat exchangers.* Journal of Enhanced Heat Transfer, 1995. **2**(1-2).
61. Martin, H., *A theoretical approach to predict the performance of chevron-type plate heat exchangers.* Chemical Engineering and Processing: Process Intensification, 1996. **35**(4): p. 301-310.
62. Tovazhnyanski, L., P. Kapustenko, and V. Tsibulnik, *Heat transfer and hydraulic resistance in channels of plate heat exchangers.* Energetika, 1980. **9**: p. 123-125.
63. Muley, A., R. Manglik, and H. Metwally, *Enhanced heat transfer characteristics of viscous liquid flows in a chevron plate heat exchanger.* Journal of Heat Transfer, 1999. **121**(4): p. 1011-1017.
64. Sinnott, R.K., *Chemical engineering design*. Vol. 6. 2014: Elsevier.